Durham E-Theses

The scattering of baby Skyrmions off potential obstructions, in a Landau-Lifshitz model

Jonathan Collins

How to cite:

Collins, Jonathan (2009) The scattering of baby Skyrmions off potential obstructions, in a Landau-Lifshitz model. Doctoral thesis, Durham University.

The scattering of baby Skyrmions off potential obstructions, in a Landau-Lifshitz model

Jonathan Collins

A Thesis presented for the degree of

Doctor of Philosophy

Centre for Particle Theory

Department of Mathematical Sciences

University of Durham

England

May 2009

Dedicated to

Mam, Dad, Jen and Kate.

Couldn't have done it with out you.

The scattering of baby Skyrmions off potential obstructions, in a Landau-Lifshitz model

Jonathan Collins

Submitted for the degree of Doctor of Philosophy

May 2009

Abstract

The dynamics of baby skyrmions of the (2+1) new baby Skyrme model, in a Landau-Lifshitz model, was studied in the presence of various potential obstructions of varying geometries. The potential obstructions were created by introducing a localised inhomogeneity in the new baby Skyrme model's potential coefficient. The size and shape of the potential obstruction was varied and two systems were investigated, namely the symmetric and asymmetric systems

In the symmetric system the trajectory of the baby skyrmions, as they traverse the barrier, was deformed from the normal circular trajectory, during which time the skyrmions sped up. For critical values of the barrier height, the baby skyrmions no longer formed a bound state and were free to separate. In the case of a potential hole, the baby skyrmions no longer formed a bound state and moved asymptotically along the edge of the hole.

In the asymmetric barrier system the baby skyrmions behaved the same as the skyrmions of the symmetric obstructions. Away from the obstruction the baby skyrmions orbited the boundary of the system. In the potential hole system the bound skyrmions moved along the edge of the hole. For critical values of the hole depth, the bound state between the skyrmions was broken, resulting in one of the skyrmions remaining stationary and the other traversing the edge of the hole.

During our investigations into this system it was found that the definition of the angular momentum must be modified to ensure overall conservation. It was shown how these modifications arise and how they are calculated.

Declaration

The work in this thesis is based on research carried out at the Centre for Particle Theory group, the Department of Mathematical Sciences, England. No part of this thesis has been submitted elsewhere for any other degree or qualification and it all my own work unless referenced to the contrary in the text.

Chapter's 1 and 2 contain background material used to motivate our investigations. Although Chapter 3 presents background material on the numerical methods I used, it contains work done by myself in constructing the baby skyrmion configurations. Chapter's 4 and 5 present the novel work done during my research. The work in Chapter 4 was published jointly with my supervisor Wojtek Zakrzewski in [7]. The contents of Chapter 5 will appear in a publication at a later date.

Acknowledgements

that this whole four years was built on, especially the last year of it.

Contents

List of Figures

List of Tables

Chapter 1

Introduction

Solitons are localised finite energy solutions possessing the unique property that two solitons emerge unchanged after scattering, apart from a change in relative phase. Solitons are classical solutions to an integrable non-linear partial differential equation. An integrable system, or simply the idea of integrability, can be difficult to define precisely. Hitchin et al [13] have a reasonable definition of the idea: An integrable differential equation, or set of them, are those in which there exist an infinite number of conservation laws, explicit solutions and for which the system possess some element of algebraic geometry. Integrable systems usually occur in (1+1) dimensions, examples of such are the KdV equation or the Sine-Gordon model. Higher dimensional models which are integrable are difficult to find, although some do exist, such as the KP equation. Finding other systems where soliton solutions exist, as defined previously, is difficult. However there exists another type of soliton, a topological soliton, whose stability is due to the topological aspect of the system. In many cases this topological stability prevents any of the solutions from decaying to a trivial one but we shall see that is not always true. The topological non-trivial nature of such solutions is usually characterised by a conserved integer, Q, the topological charge. In most Lagrangian field theories, conserved quantities such as linear or angular momentum, arise as a Noether charge due to the invariance of the action under some symmetry. The conserved charge due to the topological aspect of the model does not arise in this manner. In many models this conserved charge results from the boundary conditions placed upon the system by imposing that the fields

lie on a non-trivial target manifold and from the structure of the vacuum manifold of the model. However, there exist some topological solitons whose stability arises in a different manner.

Topological solitons arise in many physically interesting systems. The first topological solitons to appear and probably one of the most important, are Skyrmions. Skyrmions first surfaced in the work of Skyrme [32] during his investigations into the Yukawa model, a model consisting of spin-$\frac{1}{2}$ nucleons, whose interactions are mediated by pions. Skyrme's insight was to reconsider the system so that it included a term which allowed topologically non-trivial solutions to exist. These solutions, when quantised, resembled the spin-$\frac{1}{2}$ states that could be considered as nucleons. Topological solitons are also prevalent in condensed matter systems. They originally appeared as the vortex solutions in the Ginzburg-Landau theory of superconductors, before the emergence of the BCS theory.

Topological soliton solutions exist in other condensed matter systems, notably magnetic systems. Topological solitons can occur in a variety of different forms in magnetic systems, appearing in ferromagnetic or anti-ferromagnetic materials. The most well known examples of these are the familiar; domain walls, spin waves and magnetic bubbles. A magnetic domain wall is a kink-like solution that interpolates between two domains of the material. Magnetic bubbles have a different structure altogether. They have some very unique and interesting properties and can be produced experimentally by subjecting a ferromagnetic material to a pulsed magnetic field. In the applied field the ferromagnetic domains of the material are squeezed. If a field of large enough magnitude is applied over a sufficient length of time the magnetic domains of the system collapse, leaving behind a material which is uniformly magnetised in the direction of the applied field. This process is not instantaneous or uniform. As the domains tend to align with the applied field, the pulsing of certain materials results in the pinching of the domain walls into a cylindrical domain called a magnetic bubble. Since they were once considered as an alternative form of memory storage, they have been studied intensively in experiments on particular ferromagnetic materials [4], [22]. The dynamics of magnetic bubbles in a ferromagnetic or an anti-ferromagnetic medium are largely different. Theoretical research

on both materials has led to the curious fact that both of these different systems are in some way related to the $O(3)$ σ-model, which shall be introduced later in this chapter. Komineas et al [15] show explicitly that the continuum dynamics of the anti-ferromagnetic system, with an easy axis anisotropy, is given by the $O(3)$ σ-model equation of motion and magnetic bubble solutions have been studied in this system [16], [15].

In the ferromagnetic system the motion of a magnetic bubble is described by the Landau-Lifshitz equation. The Landau-Lifshitz equation determines the motion of the magnetization vector, $\underline{M}$, of a classical ferromagnet and is given by :

$$\frac{\partial \underline{M}}{\partial t} = \underline{M} \times -\frac{\delta E}{\delta \underline{M}}, \tag{1.1}$$

where E is the static energy functional of the system. This system also has a constraint upon it, such that the magnetization is a unit vector, $\underline{M}^2 = 1$. The physical properties of the ferromagnet are determined by the behaviour of the spins of the electrons in the material. The physical basis for the Landau-Lifshitz equation is the processional motion of the electron spin of the ferromagnet around the effective field $-\frac{\delta E}{\delta \underline{M}}$. This model was proposed by Landau and Lifshitz in 1935, along with properties of the energy of the system which arise due to the spin-spin interactions. The link between magnetic bubble solutions, in the ferromagnetic system, and the $O(3)$ σ-model is not as explicit as the anti-ferromagnetic system.

To obtain the direct link between magnetic bubble solutions and the $O(3)$ σ-model, the $O(3)$ σ-model must be first introduced. In the next section we do this by considering a simple Lagrangian and showing that the existence of topological soliton solutions can be determined, if particular conditions are imposed on the Lagrangian and its solutions.

1.1 Derrick's Theorem and finite energy solutions

Consider the Lagrangian, $\mathcal{L}$, in $(d+1)$ dimensions for a triplet of scalar fields $\underline{\phi}(\underline{x}, t) = \{\phi_i(\underline{x}, t); i = 1, 2, 3\}$:

$$\mathcal{L} = \frac{1}{2}\partial_\mu \underline{\phi} \cdot \partial^\mu \underline{\phi} - V(\underline{\phi}). \tag{1.2}$$

The Lagrangian consists of a kinetic term and a potential term, $V(\underline{\phi})$. We shall examine whether or not non-trivial, static, finite energy solutions exist in this generic model. A static solution to (1.2) obeys:

$$\nabla^2 \underline{\phi} = -\frac{\partial V}{\partial \underline{\phi}}, \tag{1.3}$$

where ∇^2 is the Laplacian in d dimensions. This equation results from the condition that the field configuration, $\underline{\phi}$, is an extremum of the static energy functional, $E[\underline{\phi}]$, for (1.2) which is given by:

$$E[\underline{\phi}] = \int_{\mathbb{R}^d} d^d x \left[\frac{1}{2} \partial_i \underline{\phi} \cdot \partial_i \underline{\phi} + V(\underline{\phi}) \right], \tag{1.4}$$

or that $\delta E = 0$. We shall assume the existence of a static solution, $\underline{\phi}(\underline{x})$, to (1.3). If a rescaling of the space coordinates by λ is performed, such that $\underline{x} \to \lambda \underline{x}$, there now exists a 1-parameter family of field configurations, $\underline{\phi}^\lambda(\underline{x}) = \underline{\phi}(\lambda \underline{x})$. The behaviour of the static energy functional under this rescaling can be understood by considering the derivative of the rescaled field configuration $\underline{\phi}^\lambda(\underline{x})$:

$$\partial_\mu \underline{\phi} \to \partial_\mu \underline{\phi}^\lambda(\underline{x}),$$
$$\partial_\mu(\underline{\phi}^\lambda(\underline{x})) = \lambda \partial_\mu(\underline{\phi}(\lambda \underline{x})).$$

Under this rescaling the static energy functional $E[\underline{\phi}]$ transforms to:

$$\begin{aligned}
E[\underline{\phi}^\lambda(\underline{x})] &= \int_{\mathbb{R}^d} d^d x \left[\frac{1}{2} \partial_i \underline{\phi}^\lambda(\underline{x}) \cdot \partial_i \underline{\phi}^\lambda(\underline{x}) + V(\underline{\phi}^\lambda(\underline{x})) \right] \\
&= \int_{\mathbb{R}^d} d^d x \lambda^{-d} \left[\frac{\lambda^2}{2} \partial_i \underline{\phi}(\lambda \underline{x}) \cdot \partial_i \underline{\phi}(\lambda \underline{x}) + V(\underline{\phi}(\lambda \underline{x})) \right] \qquad (1.5) \\
&= \lambda^{2-d} K[\underline{\phi}(\lambda \underline{x})] + \lambda^{-d} P[\underline{\phi}(\lambda \underline{x})],
\end{aligned}$$

where $K[\underline{\phi}(\lambda \underline{x})]$ and $P[\underline{\phi}(\lambda \underline{x})]$ are the integrals of the respective kinetic and potential energy components over $\mathbb{R}^d$. If $\underline{\phi}(\underline{x})$ is an extremum of $E[\underline{\phi}]$ it implies $\underline{\phi}^\lambda(\underline{x})$ is a stationary point of $E[\underline{\phi}^\lambda(\underline{x})]$, such that:

$$\frac{d}{d\lambda} E[\underline{\phi}^\lambda(\underline{x})] = (2-d)\lambda^{2-d-1} K[\underline{\phi}(\lambda \underline{x})] - d\lambda^{-d-1} P[\underline{\phi}(\lambda \underline{x})]. \tag{1.6}$$

The theorem by Derrick [8] tells us that static non-trivial solutions exist for models that when subjected to a coordinate rescaling, the rescaled solutions extremise the

energy functional. It was already assumed that $\lambda = 1$ is a static solution and therefore extremises $E[\underline{\phi}^\lambda(\underline{x})]$. If we set $\lambda = 1$ in (1.6), with $\frac{d}{d\lambda}E[\underline{\phi}^\lambda(\underline{x})] = 0$, it implies:

$$(2 - d)K[\underline{\phi}] = dP[\underline{\phi}]. \tag{1.7}$$

Equation (1.7) is a virial relationship between the potential and kinetic energies. Both $P[\underline{\phi}]$ and $K[\underline{\phi}]$ are non-negative functions and therefore for $d \geq 3$ there cannot exist static solutions $\underline{\phi}(\underline{x})$ which when subjected to a rescaling are an extremum of (1.5). If $d = 1$, (1.7) is not violated and non-trivial static solutions can exist. These solutions are the kink solutions found in the sine-Gordon or ϕ^4 models. However, if we seek non-trivial static solutions in $d = 2$, in order to satisfy the scaling arguments of Derrick, there must be no potential term, $V(\underline{\phi})$, and only the kinetic term remains in the Lagrangian (1.2). In all of the following considerations we shall work in $(2+1)$ dimensions.

To obtain a finite energy, non-trivial, static solution in $d = 2$, it is necessary to examine the conditions imposed on the system, for such solutions to exist. The Lagrangian (1.2), modified by the previous considerations based on Derrick's Theorem, is given by:

$$\mathcal{L} = \frac{1}{2}\partial_\mu\underline{\phi} \cdot \partial^\mu\underline{\phi}, \tag{1.8}$$

with a static energy functional:

$$E[\underline{\phi}] = \frac{1}{2}\int_{\mathbb{R}^2} d^2x\, \partial_i\underline{\phi} \cdot \partial_i\underline{\phi}. \tag{1.9}$$

Consider the simplest finite energy solution, $E = 0$. In order for $E = 0$, we require $\partial_i\underline{\phi} = 0$ everywhere and thus $\underline{\phi} = \underline{\phi}^0$, where $\underline{\phi}^0$ is space independent. Since $\underline{\phi}^0$ can point in any direction in space, there exists a family of solutions which are related through an $O(3)$ rotation. Next consider a non-zero but finite energy solution. If such solutions are to exist then it is necessary that $\partial_i\underline{\phi} \to 0$ at infinity. This can be restated in terms of the polar variables as, $r|\nabla\underline{\phi}| \to 0$ as $r \to \infty$, such that at infinity $\nabla\underline{\phi}^\infty = 0$ and $\underline{\phi}^\infty \to \underline{\phi}^0$. This limit can be reached by going in any direction, such that the boundary points of $\underline{\phi}$ constitute the circle at infinity. The finite energy condition imposed on the field, implies $\underline{\phi}$ now takes values in the extended plane, $\mathbb{R}^2 \cup \{\infty\}$. Topologically the extended plane is equivalent to the two sphere, S^2.

The finite energy condition results in a one point compactification of the real plane, $\mathbb{R}^2$, into the topologically non-trivial two sphere:

$$\mathbb{R}^2 \cup \{\infty\} \simeq S^2,$$

where the circle at infinity is mapped to the North pole of the sphere.

1.1.1 Topologically stable solutions

In $(2+1)$ dimensions the static field configuration, $\underline{\phi}$, is a map: $\underline{\phi} : \mathbb{R}^2 \to \mathbb{R}^3$. Suppose we impose a constraint upon the fields of the model:

$$\underline{\phi} \cdot \underline{\phi} = \phi_1^2 + \phi_2^2 + \phi_3^2 = 1, \tag{1.10}$$

where the dot product is in the internal space of the fields. The constraint (1.10) imposes that the target space of the map is now non-trivial and is given by the two sphere. The field configuration, $\underline{\phi}$, is now a map:

$$\underline{\phi} : \mathbb{R}^2 \to S^2.$$

In the previous section it was shown that the finite energy condition compactifies the real plane $\mathbb{R}^2$ providing a non-trivial domain of the map S^2. Therefore all static, finite energy, non-trivial solutions of (1.8), along with the constraint (1.10), are field configurations which map between the two spheres:

$$\underline{\phi} : S^2 \to S^2. \tag{1.11}$$

These field configurations can be grouped into different homotopy classes. All elements within each homotopy class can be continuously deformed into each other. Elements of different homotopy classes cannot be deformed into each other. The set of all homotopy classes forms a group. Each different homotopy class is defined by the winding number, or topological charge, $Q \in \mathbb{Z}$, of the map (1.11). The topological charge, Q, is a consequence of the non-trivial homotopy group associated with $\underline{\phi} : S^2 \to S^2$, which is given by $\pi_2(S^2) = \mathbb{Z}$. The topological charge for this non-trivial homotopy group is given by:

$$Q = \frac{1}{8\pi} \int_{\mathbb{R}^2} d^2x \, \epsilon_{ij} \underline{\phi} \cdot (\partial_j \underline{\phi} \times \partial_i \underline{\phi}), \tag{1.12}$$

where ϵ_{ij} is the totally anti-symmetric tensor in two dimensions ($\epsilon_{11} = \epsilon_{22} = 0$ and $\epsilon_{12} = -\epsilon_{21} = 1$) and Q integrates over the topological charge density, q, which is given by:

$$q = \epsilon_{ij}\underline{\phi} \cdot (\partial_j\underline{\phi} \times \partial_i\underline{\phi}). \tag{1.13}$$

Therefore each of these field configurations, associated with each different Q, are topologically stable, since solutions corresponding to different values of Q cannot be deformed into each other.

The model constituting the Lagrangian (1.8) and the constraint (1.10) is known as the $O(3)$ σ-model. The equations of motion for the $O(3)$ σ-model are derived from the following action S, where we have introduced the Lagrange multiplier, λ, to incorporate the constraint on the fields:

$$S[\underline{\phi}] = \int dt \int d^2x \left[\frac{1}{2}\partial_\mu\underline{\phi} \cdot \partial^\mu\underline{\phi} + \lambda(\underline{\phi}^2 - 1)\right].$$

The static equations of motion of such a system are given by:

$$\nabla^2\underline{\phi} - (\underline{\phi} \cdot \nabla^2\underline{\phi})\underline{\phi} = 0. \tag{1.14}$$

By comparison with (1.3) for $V(\underline{\phi}) = 0$, it is evident the introduction of the constraint (1.10) results in a non-trivial differential equation. The constraint also provides a topological stability for any solutions which satisfy Derrick's Theorem and the finite energy condition. These finite energy, static field configurations are the topological solitons of the model. The $O(3)$ σ-model, in its present form, possesses an analytic solution. These topological solitons are called σ-model lumps. A lower bound on the energy of any such topological soliton solution can be obtained by considering the following inequality:

$$(\partial_i\underline{\phi} \pm \epsilon_{ij}\underline{\phi} \times \partial_j\underline{\phi}) \cdot (\partial_i\underline{\phi} \pm \epsilon_{ik}\underline{\phi} \times \partial_k\underline{\phi}) \geq 0. \tag{1.15}$$

It can be shown through expansion and the use of some vector identities that the integral of (1.15) over $\mathbb{R}^2$ can be written as the inequality:

$$E \geq 4\pi|Q|. \tag{1.16}$$

This provides a lower bound on the energy for a lump solution. The bound is saturated for solutions which satisfy:

$$\partial_i\underline{\phi} \pm \epsilon_{ij}\underline{\phi} \times \partial_j\underline{\phi} = 0. \tag{1.17}$$

This is known as the Bogomolny equation. Thus if solutions which saturate the bound (1.16) were sought, we need only consider finding field configurations which are solutions to (1.17). Finding solutions to (1.17) is easier since it is a first order differential equation, as opposed to (1.14) which is of second order and therefore more difficult to solve. For an in-depth overview of the $O(3)$ σ-model and its solutions see [31], [21] or [36].

The $O(3)$ σ-model is conformally invariant which results in a size instability of the lump solution. Since the energy does not depend explicitly on the lump size, any lump solution that is perturbed can change its size without changing its energy. Although this size instability has not been analytically proven there have been numerical studies confirming the existence of the instability [20].

1.1.2 Stabilising solutions

In the absence of any stabilising terms the energy of the $O(3)$ σ-model is scale invariant and the previously explained size instability exists. Therefore to study the lump solutions in two dimensions, the solutions must be stabilised against such instabilities. The σ-model lumps can be stabilised in a number of ways:

- The scale invariance of the system can be broken by the addition of scale-dependent terms.

- A time-dependent solution can be introduced into the system, although the solutions are not quite the same as the lump solutions.

Breaking the scale invariance

In previous sections it was shown that the inclusion of a potential term, $V(\underline{\phi})$, into (1.8), in two dimensions, according to Derrick's Theorem, requires such a potential term to be zero for the existence of non-trivial static solutions. Therefore an additional potential term, V_S, must be included such that both of these potential terms scale in different ways, breaking the conformal invariance of the pure $O(3)$ σ-model. The simplest method of doing this is to include terms which are, in general, functions of the field's derivative raised to a power. Hence the two potential terms

V_S and V, which are general functions of the derivative of the field raised to some power p, are added to (1.8). If $p = 0$ then the potential terms V_S or V are simple functions of the field $V(\underline{\phi})$, $V_S(\underline{\phi})$. Introducing both of these potentials into (1.8) provides a new Lagrangian of the form:

$$\mathcal{L} = \frac{1}{2}\partial_\mu\underline{\phi} \cdot \partial^\mu\underline{\phi} - V\left(\left\{\partial_\mu\underline{\phi}\right\}^m\right) - V_S\left(\left\{\partial_\mu\underline{\phi}\right\}^n\right), \tag{1.18}$$

where both of the potential terms scale in different ways and we are free to choose their form. The two potential terms $V_S\left(\left\{\partial_\mu\underline{\phi}\right\}^n\right)$ and $V\left(\left\{\partial_\mu\underline{\phi}\right\}^m\right)$ when subjected to the rescaling $\underline{x} \to \lambda\underline{x}$, transform as:

$$V\left(\left\{\partial_\mu\underline{\phi}^\lambda(\underline{x})\right\}^m\right) \quad \to \quad \lambda^m V\left(\left\{\partial_\mu\underline{\phi}(\lambda\underline{x})\right\}^m\right),$$
$$V_S\left(\left\{\partial_\mu\underline{\phi}^\lambda(\underline{x})\right\}^n\right) \quad \to \quad \lambda^n V_S\left(\left\{\partial_\mu\underline{\phi}(\lambda\underline{x})\right\}^n\right).$$

After applying Derrick's Theorem, using similar arguments as section (1.1), the following relationship between the different energy components is obtained :

$$(2 - m)V[\underline{\phi}] = (n - 2)V_S[\underline{\phi}]. \tag{1.19}$$

Since both energies $V[\underline{\phi}], V_S[\underline{\phi}] > 0$, this places conditions on the integers, (m, n), such that $n \geq 2$ and $m \leq 2$. If the different possible pairs (m, n) are examined, the types of potentials that are required to break the scale invariance of the pure σ-model term can be seen. It is clear for any pairs (m, n) when $n = 2$ or $m = 2$, the pure σ-model is recovered. Since $n \geq 2$, there are therefore many pairs (m, n) that break the scale invariance of the system. Let us examine the first four of the available pairs of integers (m, n) which include $(0, 3), (0, 4), (1, 3)$ and $(1, 4)$. A potential V that scales as $m = 0$ or $m = 1$ implies potentials of the form:

$$m = 0 \quad : \quad V(\underline{\phi}),$$
$$m = 1 \quad : \quad V(\partial_\mu\underline{\phi}).$$

or when $n = 3$ or 4:

$$n = 3 \quad : \quad V_S((\partial_\mu\underline{\phi})^3),$$
$$n = 4 \quad : \quad V_S((\partial_\mu\underline{\phi})^4).$$

In all of the preceding analysis, the breaking of the scale invariance in accordance with Derrick's Theorem was the primary concern, when considering the existence of stable topological soliton solutions. However, it has not yet been considered whether any of the terms that could be included into (1.8), conform to the normal conditions one imposes upon constructing a physically sensible Lagrangian. Lorentz invariance is a required property of such a Lagrangian. Imposing Lorentz invariance on the first set of available potential choices, results in only one pair remaining: $(0, 4)$. The $n = 3$ or $m = 1$ potentials, if allowed, would not be Lorentz invariant. Lorentz invariant potentials with $n = 6, 8..$ are also available since they do not violate the condition placed upon n. However, the use of these terms would result in the inclusion of a term with a time derivative which is greater than second order. The potential for $n = 4$ is therefore the only Lorentz invariant potential which satisfies the conditions placed upon it by Derrick's Theorem, and crucially, results in terms of no more than second order derivative in time. This imposes that $V(\underline{\phi})$ can only be a simple function of the field or one of its components and that $V_S(\underline{\phi})$ must be a function quartic in its derivative of the field, such that it scales as λ^4. The simplest choice of such a Lorentz invariant potential is the Skyrme potential:

$$V_S(\underline{\phi}) = \frac{1}{4}[(\partial_\mu \underline{\phi} \cdot \partial^\mu \underline{\phi})^2 - (\partial_\mu \underline{\phi} \cdot \partial_\nu \underline{\phi})(\partial^\mu \underline{\phi} \cdot \partial^\nu \underline{\phi})]. \tag{1.20}$$

The inclusion of (1.20) and a potential $V(\underline{\phi})$ into (1.8) produces what is known as the baby Skyrme model since it is a (2+1) dimensional analogue of the full (3+1) Skyrme model. The potential term, $V(\underline{\phi})$, is not uniquely defined and there exist many different baby Skyrme models corresponding to different choices of $V(\underline{\phi})$. The most commonly studied baby Skyrme models will be discussed in the next chapter.

There are other ways to stabilise the σ-model by the introduction of scale dependent terms. There has been some recent work on the stabilisation of the lump solutions by the use of vector mesons [11]. It is shown in [11] that the vector meson system reduces to the baby Skyrme model in a certain limit of the model. The resulting skyrmion and multi-skyrmion structures of the vector meson model look remarkably similar to the multi-skyrmion structures of the baby skyrme model; see the work of Weidig [35].

Time dependent solutions

The σ-model lump solutions can also be stabilised by using a time dependent solution. Leese [18] has shown the introduction of scale dependent terms is not required to stabilise the lump solutions, if a time-dependent solution is constructed. Leese examined the following system:

$$\mathcal{L} = \frac{1}{2}\partial_\mu\underline{\phi} \cdot \partial^\mu\underline{\phi} - \frac{1}{2}\alpha^2(1 - \phi_3^2). \tag{1.21}$$

As $\alpha \to 0$, (1.21) reduces to the usual σ-model system. If α is finite in $d = 2$, according to Derrick's Theorem no static non-trivial solutions can exist. To avoid this Leese proposed solutions of the form:

$$W(z, t) = W_0 e^{\pm i\alpha t}, \tag{1.22}$$

where W is the stereographic projection variable, defined in chapter 3 and z is the complex coordinate $z = x + iy$. A Bogomolny bound argument can be performed, resulting in a lower bound on the energy:

$$E = 2\pi|Q| + |\alpha N|. \tag{1.23}$$

This bound contains two conserved charges: A topological charge, Q, and also a non-topological charge, N. The non-topological charge arises as a conserved Noether charge due to the $U(1)$ symmetry. These solutions are called Q-lumps since they are related to Q-balls; see [6]. A Q-ball is a class of non-topological soliton solution occurring in models which possess a continuous unbroken symmetry. The Q-ball energy is fixed with time but there exists an internal rotation. Q-lump and σ-model lump solutions both occur for arbitrary width. However, as seen before, the lump solutions tend to expand or contract, while Q-lump solutions do not possess this instability. A Q-lump solution of slightly larger size has a slightly larger energy. The conservation of the non-topological charge prevents the Q-lump collapsing on itself.

1.2 Ferromagnets and solitons

There is a rather nice connection between the solutions of the $O(3)$ σ-model and the Landau-Lifshitz equation (1.1). It was stated previously that the continuum dynamics of ferromagnets (or anti-ferromagnets) is in some way related to the $O(3)$ σ-model. The equation describing the isotropic ferromagnet in (2+1) dimensions is given by:

$$\frac{\partial \underline{\phi}}{\partial t} = \underline{\phi} \times -\frac{\delta E}{\delta \underline{\phi}},$$ (1.24)

where we have changed the magnetization vector $\underline{M}$ to our previously defined scalar field $\underline{\phi}$. There still exists the constraint $\underline{\phi}^2 = 1$ and E is the static energy functional of the system given by:

$$E = \frac{1}{2} \int_{\mathbb{R}^2} d^2x \, \partial_i \underline{\phi} \cdot \partial_i \underline{\phi},$$ (1.25)

which is the corresponding exchange energy of the ferromagnet. If we assume that $\underline{\phi} = \underline{\phi}_s$ is a static solution to (1.24) then $\frac{\partial \underline{\phi}}{\partial t} = \frac{\partial \underline{\phi}_s}{\partial t} = 0$. Therefore (1.24) can be written:

$$\underline{\phi}_s \times \nabla^2 \underline{\phi}_s = 0$$ (1.26)

This is only true if $\underline{\phi}_s$ is parallel to $\nabla^2 \underline{\phi}_s$ or if $\nabla^2 \underline{\phi}_s = k\underline{\phi}_s$. If we use the constraint equation, $\underline{\phi}^2 = 1$, it can be shown that $k = \underline{\phi}_s \cdot \nabla^2 \underline{\phi}_s$, such that the equation now becomes:

$$\nabla^2 \underline{\phi}_s - k\underline{\phi}_s = \nabla^2 \underline{\phi}_s - (\underline{\phi}_s \cdot \nabla^2 \underline{\phi}_s)\underline{\phi}_s = 0.$$ (1.27)

This is the equation of motion for a static solution to the $O(3)$ σ-model, (1.14). Therefore any static solution of the $O(3)$ σ-model is a static solution to the Landau-Lifshitz equation. This provides a direct link between the topological soliton solutions of the $O(3)$ σ-model and the magnetic bubble solutions described by the Landau-Lifshitz equation. In (2+1) dimensions the $O(3)$ sigma model must be stabilised, producing the baby Skyrme model. Baby skyrmion solutions are solutions to a modified $O(3)$ σ-model and therefore are a static solution to the Landau-Lifshitz equation. This connection between baby skyrmions and magnetic bubbles has provided many different avenues for research, both experimentally and theoretically. Much research has been done on magnetic bubbles represented by baby skyrmion solutions, both analytically [26] and using numerical methods [30], [29]. Some of

this work [30], [29] has examined the dynamics of two interacting bubbles in the presence of an applied field. Other work has tried to gather theoretical evidence of the experimentally observed 'golden rule' of bubble dynamics (see [22]). This relates the topological charge, Q, and the deflection angle the bubble makes in the applied field, δ, along with various other quantities. In [26] the authors sought to explicitly reformulate the conservation laws of the Landau-Lifshitz equation, to aid a theoretical understanding of the motion of two interacting bubbles. Their analysis has provided a better understanding of the conservation laws of the system and has shown a link between the dynamics of magnetic bubbles and the underlying topological structure. The conservation laws of the Landau-Lifshitz equation, as formulated in [26], play a crucial role in our investigations and shall be presented in the next section.

1.2.1 Conservation laws

Analysis of the dynamics of magnetic bubbles or topological soliton solutions in Landau-Lifshitz model has been greatly simplified by the work of Papanicolaou and Tomaras [26], who constructed unambiguous conservation laws for the system governed by (1.24). In their work they found that the important quantity was the topological charge density q, (1.13): The conservation laws are constructed from the moments of q. They involve:

$$l = \frac{1}{2}\int_{\mathbb{R}^2} d^2x\, \underline{x}^2 q, \tag{1.28}$$

$$m = \int_{\mathbb{R}^2} d^2x(\phi_3 - 1), \tag{1.29}$$

$$J = l + m, \tag{1.30}$$

where l is the orbital angular momentum, m is the total magnetization in the third direction and J is the total angular momentum. The conservation laws for the system were constructed by examining the time evolution of q:

$$\dot{q} = -\epsilon_{ij}\partial_i\partial_k\sigma_{jk}, \tag{1.31}$$

where $\partial_k\sigma_{jk}$ can be written in terms of the energy functional E:

$$\partial_k\sigma_{jk} = \left(\frac{\delta E}{\delta\underline{\phi}} \cdot \partial_j\underline{\phi}\right). \tag{1.32}$$

Taking an explicit time derivative of (1.28) gives:

$$l = \frac{1}{2} \int_{\mathbb{R}^2} d^2x \, \underline{x}^2 \dot{q}. \tag{1.33}$$

The guiding centre coordinate $\underline{R}$ of the baby skyrmion is defined as the first moment of the topological charge density q:

$$\underline{R} = \frac{1}{4\pi Q} \int_{\mathbb{R}^2} d^2x \, \underline{x} q. \tag{1.34}$$

We can also consider the mean squared radius r of the baby skyrmions, defined by:

$$r^2 = \frac{1}{4\pi Q} \int_{\mathbb{R}^2} d^2x \, \left(\underline{x} - \underline{R}\right)^2 q. \tag{1.35}$$

One can expand out (1.35) to find a relationship between the mean squared radius of the baby skyrmions and l:

$$r^2 = \frac{l}{2\pi Q} - \underline{R}^2. \tag{1.36}$$

This relationship between l, r and R can be beneficial to the understanding of the dynamics described in later sections.

Chapter 2

Baby Skyrmions

In the previous chapter it was demonstrated that static solutions to the $O(3)$ σ-model are static solutions to the Landau-Lifshitz model. The Landau-Lifshitz model described the dynamics of extended structures, called magnetic bubbles, which appear in ferromagnetic materials. In our work we shall be investigating the behaviour of magnetic bubble solutions in (2+1) dimensions, described by the $O(3)$ σ-model solutions, in a Landau-Lifshitz equation. In two dimensions the solutions of the $O(3)$ σ-model have to be stabilised by the introduction of scale dependent terms, resulting in the construction of the baby Skyrme model. Baby Skyrme models are not specified by a particular Lagrangian due to the freedom allowed in choosing the potential term, $V(\underline{\phi})$, in accordance with Derrick's theorem. The only condition placed upon these different potentials is that they must stabilise the lump solutions of the scale invariant pure $O(3)$ σ-model in (2+1) dimensions. Choosing different potentials produces differing models with various properties. In the following chapter we shall discuss these various baby Skyrme models and explain any differences between them. Baby skyrmion solutions of the new baby Skyrme model, for a general topological charge Q, are constructed using the hedgehog anzatz. Our investigations concern the interaction between two singly charged baby skyrmions in the Landau-Lifshitz model. We therefore require a field configuration that reflects two baby skyrmions separated by a finite distance d. This is best done using a superposition variable, known as the stereographic projection variable, W, which utilises the topology of the field configurations.

2.1 Baby Skyrme models

Baby Skyrme models exist for a variety of different potentials, $V(\underline{\phi})$. A general Lagrangian for the baby Skyrme model can be written as:

$$\mathcal{L} = \frac{1}{2}\gamma_1 \partial_\mu \underline{\phi} \cdot \partial^\mu \underline{\phi} - \frac{1}{4}\gamma_2[(\partial_\mu \underline{\phi} \cdot \partial^\mu \underline{\phi})^2 - (\partial_\mu \underline{\phi} \cdot \partial_\nu \underline{\phi})(\partial^\mu \underline{\phi} \cdot \partial^\nu \underline{\phi})] - V(\underline{\phi}), \quad (2.1)$$

which has static energy density $\mathcal{E}$ given by:

$$\mathcal{E} = \frac{1}{2}\gamma_1 \partial_i \underline{\phi} \cdot \partial_i \underline{\phi} + \frac{1}{4}\gamma_2[(\partial_i \underline{\phi} \cdot \partial_i \underline{\phi})^2 - (\partial_i \underline{\phi} \cdot \partial_j \underline{\phi})(\partial_i \underline{\phi} \cdot \partial_j \underline{\phi})] + V(\underline{\phi}), \quad (2.2)$$

where the coefficients γ_1, γ_2 are positive constants. Each of the different models, corresponding to choices of the various potentials, has differing properties. The models differ in their ability to possess analytic solutions or in their multi-skyrmion structure. They can also differ in their vacuum structure. While some possess just a single vacuum, others have multiple vacua. Some of the baby Skyrme models have been previously studied because of their relationship to physical reality and others because of their underlying mathematical structure. A few of these models have been studied and discussed in the context of Landau-Lifshitz dynamics. In the following sections we shall give an overview of each different model and its properties. The interactions between the baby skyrmions of each model plays a crucial role in the observed dynamics in Landau-Lifshitz systems. The skyrmions' ability to form a bound state, whether multi-skyrmion states exist and whether such states are stable, form other important parts of our discussion.

2.1.1 Holomorphic model

The first baby Skyrme model to be investigated was the holomorphic model, which is given by a potential of the form:

$$V(\underline{\phi}) = \frac{1}{2}\gamma_3(1 - \phi_3)^4, \quad (2.3)$$

where the coefficient γ_3 is a positive constant. It was first studied by Leese et al [20] and Sutcliffe [34], since it possesses an analytic solution for the charge one baby skyrmion in a model which breaks the scale invariance of the $O(3)$ σ-model. The

analytic solution can be constructed once the equations of motion are written in terms of the stereographic variable W. Here it was noted that a potential of the form of (2.3) would permit an analytic solution. The solution can be written as $W = \lambda(x + iy)$. The size of the baby skyrmion is given by λ which is related to γ_2 and γ_3 of the model. The baby skyrmion solutions for this potential are polynomially localised. The holomorphic model has unstable multi-skyrmion solutions. The multi-skyrmions are unstable because the force between the baby skyrmions is strongly repulsive and they do not form bound states.

2.1.2 Old baby Skyrme model

The old baby Skyrme model's potential form first emerged during studies of the full Skyrme model since it provided a mass term for the pion field. It is defined by the following potential:

$$V(\underline{\phi}) = \frac{1}{2}\gamma_3(1 - \phi_3).$$ (2.4)

This model has only recently been referred to as the 'old' baby Skyrme model to distinguish it from a different model studied more recently referred to as the 'new' baby Skyrme model. There are no analytic solutions for this model and the baby skyrmion solutions have to be computed numerically. The differential equation governing the baby skyrmion solutions shows that the solutions are exponentially localised. The model possesses only a single vacuum $\phi_3 = 1$. The centre of a skyrmion in this system is defined by the point $\phi_3 = -1$. Examining the value of the potential term at this point, $V(\phi_3 = -1) \neq 0$ suggests there exists an energetic argument implying the baby skyrmions would prefer not to be on top of each other. This is in fact the case and there is repulsion between baby skyrmions that are close together. The dynamics and the bound states of the baby skyrmions in this model have been well studied by Piette et al [24] and [25]. The structure of the bound state, formed by the multi-skyrmion solutions, organise themselves into pairs or triplets of bound baby skyrmions. These crystal-like structures were thought to be the minimal energy configurations for a set of baby skyrmions. However, recent work [10] has shown there exists a slightly lower energy configuration which consists of a chain of baby skyrmions.

2.1.3 New baby Skyrme model

The new baby skyrme model is defined by the following potential:

$$V(\underline{\phi}) = \frac{1}{2}\gamma_3(1 - \phi_3^2). \tag{2.5}$$

It has only been recently studied after its introduction by Kudryavtsev et al [14] since it was a baby Skyrme model which possessed multiple vacua $\phi_3 = \pm 1$, differing from the 'old' baby Skyrme model which possessed just a single vacuum state, $\phi_3 = 1$. This model is similar to the old baby Skyrme model, also requiring numerical techniques to obtain a solution. The old and new baby Skyrme models behave similarly for large r since the baby skyrmion solutions of both models are exponentially localised. The two models differ only for small r. The value of the field at $r = 0$ implies $\phi_3 = -1$, thus $V(\phi_3 = -1) = 0$. It is therefore clear that there is no energetic cost for two baby skyrmions to lie 'on top' of each other. The multi-skyrmion structures of the new baby Skyrme model have been examined by Weidig [35] and show that the lowest energy stable multi-skyrmion structures correspond to many baby skyrmions lying on top of each other. The multi-skyrmion states look like ring configurations and take a radially symmetric form. The new baby Skyrme model is the particular model which we shall be studying further.

There have been other attempts at introducing new potential terms into the generic baby Skyrme model Lagrangian (2.1), which contain more exotic multiple vacua. Eslami et al [9] considered various different potential terms similar to the old and new models but which also included the additional vacuum value of $\phi_3 = 0$.

The behaviour of baby skyrmion solutions from two of the models has been investigated in a Landau-Lifshitz model. The holomorphic model was the first of the baby Skyrme models to be studied in this context by Papanicolaou et al in [30]. A two baby skyrmion configuration was formulated as an anzatz and used as an initial condition to the Landau-Lifshitz equation. In [30] it was shown that the two baby skyrmions orbited around each other along deformed circular trajectories. In addition to the three terms constituting the Lagrangian of the holomorphic baby Skyrme model, their work also included a local magneto-static field. This local magneto-static field caused the non-conservation of the orbital angular momentum,

l, and the total magnetization in the third direction, m, all defined in the previous chapter. However the total angular momentum $J = l + m$ was well conserved in time. The authors of [30] attributed the non-conservation of l and m to the non-symmetric structure of σ_{ij} due to the presence of the magneto-static field. The new baby Skyrme model has also been studied in relation to the Landau-Lifshitz model by Papanicolaou et al [29]. Here it was found that two baby skyrmions orbited each other on a circular trajectory modified by a Larmor procession due to the magnetic field. The total angular momentum $J = l + m$ was well conserved in time but its constituent components l and m were not. The arguments for the non-conservation of l and m in this model are identical to the arguments for the non-conservation of l and m in the holomorphic model.

2.2 Baby skyrmion solutions

In all of the previously defined models we wish that any topological soliton solutions we obtain will be a minimal energy configuration. In general, baby skyrmion solutions have to be computed numerically but to do so we require an anzatz for the field configuration. In some variational problems the configuration which extremises the energy functional also has maximal symmetry. The anzatz we choose is the one which is also invariant under the maximal symmetry group that leaves the energy functional of the system invariant. In choosing such a configuration, the principle of symmetric criticality (developed by Coleman and Palais) [23], informs us it is only necessary to solve the resulting variational problem to find the minimal energy configuration. For a discussion and brief proof see [21], pp 99. Therefore possessing an assumed anzatz for the field configuration, the theorem allows us to insert this field configuration into the energy functional of the system and to integrate over any superfluous variables. The resulting energy functional, when minimised, will possess the same solutions as if the anzatz was inserted into the equations of motion for the full theory. In the case of baby Skyrme models the anzatz that is used is known as the hedgehog anzatz. It is called this since it produces radially symmetric solutions. The hedgehog anzatz used in the baby Skyrme model is a simplified version

of the anzatz employed when constructing the skyrmion solutions of the full nuclear Skyrme model. The hedgehog anzatz for the field configuration of a charge Q baby skyrmion is given by:

$$\underline{\phi} = (\cos(Q\theta)\sin(f(r)), \sin(Q\theta)\sin(f(r)), \cos(f(r))), \qquad (2.6)$$

where $f(r)$ is the profile function satisfying certain boundary conditions, θ is the polar angle and Q is the topological charge. The only unknown quantity is the profile function $f(r)$ and with it obtained, a charge Q baby skyrmion of the new baby Skyrme model can be constructed.

The minimal energy configurations of the new baby Skyrme model can be constructed using the method previously outlined. Therefore by inserting the hedgehog anzatz into (2.2), with $V(\underline{\phi})$ given by (2.5), and integrating over $\mathbb{R}^2$ produces an energy functional, $E[f(r)]$, of the form:

$$E[f(r)] = \pi \int_0^\infty \left(\gamma_1 \left(f'^2 + \frac{Q^2 \sin^2 f}{r^2} \right) + \gamma_2 \frac{f'^2 \sin^2 f}{r^2} + \frac{\gamma_3}{2} \sin^2 f \right) r\, dr. \qquad (2.7)$$

With some rearranging, the Euler-Lagrange equations for the functional $E[f(r)]$ are calculated to be:

$$f'' \left(\gamma_1 r + \frac{\gamma_2 Q^2 \sin^2 f}{r} \right) + f' \left(\gamma_1 - \frac{\gamma_2 Q^2 \sin^2 f}{r^2} \right)$$
$$+ f'^2 \left(\frac{\gamma_2 Q^2 \sin f \cos f}{r} \right) - \frac{\gamma_1 Q^2 \sin f \cos f}{r} - \gamma_3 r \sin f \cos f = 0. \qquad (2.8)$$

This equation can be rearranged into the form $f'' = h(r, f, f')$, which is a second order ordinary differential equation and must be solved numerically to obtain the profile function, $f(r)$, of the new baby Skyrme model.

2.2.1 Profile function boundary conditions

Solving (2.8) numerically requires information about $f(r)$ on the boundaries of the system. The finite energy condition placed upon the topological soliton solutions requires at infinity $f(\infty) = 0$. This boundary condition on $f(r)$ ensures the finite energy condition and provides the topological stability for the baby skyrmion solutions. The boundary condition also imposes that the vacuum state for the new

baby Skyrme model is $\underline{\phi} = (0, 0, 1)$. The value of the profile function at the origin is also required in order to integrate (2.8) numerically. The boundary condition at this point can be found by calculating the topological charge, Q, written in term of the hedgehog anzatz. Recall the definition of the topological charge Q:

$$Q = \frac{1}{4\pi} \int_{\mathbb{R}^2} d^2x \, \frac{1}{2} \epsilon_{ij} \underline{\phi} \cdot (\partial_j \underline{\phi} \times \partial_i \underline{\phi}). \qquad (2.9)$$

Inserting the hedgehog anzatz (2.6) into (2.9) gives:

$$
\begin{aligned}
Q &= \frac{1}{4\pi} \int_{\mathbb{R}^2} d^2x \, q = \frac{1}{4\pi} \int_0^{2\pi} d\theta \int_0^\infty r \, dr \, q \\
&= -\frac{Q}{2} \int_0^\infty df \sin f \\
&= \frac{Q}{2} \left[\cos(f(\infty)) - \cos(f(0)) \right].
\end{aligned}
\qquad (2.10)
$$

We have already imposed the boundary condition on the profile function at infinity $f(\infty) = 0$, for the fields to tend to a constant at infinity. Therefore for the value of Q to be consistent it requires the profile function at the origin to be $f(0) = \pi$. The two boundary conditions on the profile function $f(0) = \pi$ and $f(\infty) = 0$ are all that is required to determine the numerical solution of the profile function.

2.2.2 Asymptotics of $f'' = h(r, f, f')$

Consider the two limiting cases of the differential equation (2.8); for large values of r and for $r = 0$. In the case when $r >> 1$ the boundary condition placed upon the profile function, $f(\infty) = 0$, requires that for large values of r the profile function is small. In such cases the differential equation reduces to :

$$f'' + \frac{f'}{r} - f \left[\frac{Q^2}{r^2} + \gamma_3 \right] = 0. \qquad (2.11)$$

The solutions of this differential equation are Bessel's functions of the first kind and take the form:

$$f(r) \simeq \frac{1}{\sqrt{\gamma_3 r}} exp(-\gamma_3 r). \qquad (2.12)$$

The profile function near the origin can be approximated by, $f(r) \simeq \pi + A_m r^m$, where A_m is an arbitrary constant dependent upon the value of m. Inserting this approximate solution into the full differential equation (2.8), obtains $Q = m$. The

profile function near the origin can therefore be approximated by: $f(r) \simeq \pi + A_Q r^Q$ for $r << 1$.

2.3 Initial field configuration

In Chapter 1 it was shown that the finite energy condition placed upon the topological soliton solutions places a boundary condition on the fields at infinity. This condition resulted in the compactification of the $\mathbb{R}^2$ plane into the topologically equivalent $S^2 \simeq \mathbb{R}^2 \bigcup \{\infty\}$. At times it is more convenient to deal with a single variable as opposed to the three scalar fields (ϕ_1, ϕ_2, ϕ_3). This is particularly pertinent when constructing a superposition of topological soliton solutions. In such cases the field $\underline{\phi}$ can be used as a single variable W, known as the stereographic projection variable. A stereographic projection is a projection of the unit sphere, S^2, onto the complex plane. In this new variable the point at infinity is mapped to the north pole of the sphere. W can be defined as:

$$
\begin{aligned}
W &= \frac{\phi_1 + i\phi_2}{1 + \phi_3}, \\
\phi_1 &= \frac{W + W^*}{1 + |W|^2}, \\
\phi_2 &= \frac{1}{i}\frac{W - W^*}{1 + |W|^2}, \\
\phi_3 &= \frac{1 - |W|^2}{1 + |W|^2},
\end{aligned}
\tag{2.13}
$$

where W^* denotes the complex conjugate of W. The previous discussion of the boundary condition placed upon the fields at infinity, can be restated as: $\underline{\phi}(\infty) = (0, 0, 1)$. This condition results in the stereographic projection variable $W \to 0$ as we approach the boundary. Conversely, the baby skyrmion centre is the point where $\underline{\phi} = (0, 0, -1)$ resulting in the divergence of W at the centre of the baby skyrmions. It is in this W formalism that the construction of the initial configuration can be easily computed. The stereographic variable W can be rewritten in terms of the hedgehog anzatz variables $f(r)$ and θ:

$$
W = \tan(\frac{f(r)}{2})e^{i\theta}.
\tag{2.14}
$$

Suppose we wish to construct an N baby skyrmion solution. The work of Weidig [35] on the new baby Skyrme model has shown that for $N > 1$, the minimal energy configurations are the ring configurations. The hedgehog anzatz produces the minimal energy configurations for a given topological charge Q in the new baby Skyrme model. We are interested in producing a minimal energy configuration for two baby skyrmions of the new baby Skyrme model, where the skyrmion centres are separated by a finite distance d. This configuration can be constructed by taking a superposition of singly charged baby skyrmion solutions in the W formalism. Given a set of N singly charged baby skyrmions, $\{\underline{\phi}^1, \underline{\phi}^2, \underline{\phi}^3, ..., \underline{\phi}^N\}$, a N baby skyrmion configuration is therefore given by:

$$W_N = \sum_{k=1}^{N} W_k(\underline{x} - \underline{x}_k), \qquad (2.15)$$

where $\underline{x}_k$ denotes the position of the centre of the kth baby skyrmion. A N baby skyrmion configuration can be numerically constructed by using (2.13), (2.14) and (2.15), for any number of baby skyrmions N.

Chapter 3

Numerical Methods

Physical systems are governed by the equations of motion, which are ordinary or partial differential equations of varying orders. In general, the problems of interest to most theoretical physicists involve differential equations which are difficult, or impossible, to solve analytically. They may also involve very complicated initial conditions, all of which require the system considered to be solved numerically. Obtaining a solution to these problems involves the numerical integration of the equations of motion, which must be considered carefully. Numerical accuracy is of paramount importance but we must also consider the time required to achieve such an accuracy. It is sometimes better to forsake numerical accuracy to allow the simulation to progress in a reasonable amount of time.

In our investigations the complexity of the problem requires us to use numerical methods. In this chapter we shall discuss all the numerical methods used to study the system of interest which shall include:

- The discretisation of the problem to allow for computer simulations.

- Obtaining the initial field configuration of a two baby skyrmion configuration separated by a distance d.

- The numerical integration of the Landau-Lifshitz equation.

- Imposing the S^2 constraint and approximating the baby skyrmions position on the lattice.

3.1 Fields discretisation

To perform numerical simulations of the equations of motion subject to the initial conditions, the continuum problem must be translated to aid the application of numerical methods. The field, $\underline{\phi}$, is subjected to lie on a square lattice of spacing width h. The discretisation of the fields is crucial to performing the simulations. The field, $\underline{\phi}$, in this purely two dimensional problem becomes a function of the lattice variables (i, j):

$$\underline{\phi} = \big(\phi_1(x, y), \phi_2(x, y), \phi_3(x, y)\big) \rightarrow \big(\phi_1(x_i, y_j), \phi_2(x_i, y_j), \phi_3(x_i, y_j),$$

where $\phi_k(x_i, y_j)$ is the field ϕ_k at the $(i, j)^{th}$ point. The various different derivatives of the field at each lattice point are computed using finite differences. The field's derivative, computed at the point (i, j), can be approximated in many ways. Any of the respective backward, forward or central difference formulae can be used:

$$
\begin{aligned}
\frac{\partial \phi_k}{\partial x}(i, j) &= \frac{\phi_k(x_i, y_j) - \phi_k(x_i - h, y_j)}{h}, \\
\frac{\partial \phi_k}{\partial x}(i, j) &= \frac{\phi_k(x_i + h, y_j) - \phi_k(x_i, y_j)}{h}, \\
\frac{\partial \phi_k}{\partial x}(i, j) &= \frac{\phi_k(x_i + h, y_j) - \phi_k(x_i - h, y_j)}{2h}.
\end{aligned}
$$

Each different approximation has its own benefits. The forward and backward difference formulae have an associated error $\mathcal{O}(h)$ and are very useful for the calculation of the derivative on the boundary. If the lattice spacing is sufficiently small then the errors for the forward and backward difference formulae would be within reasonable tolerances. In practical simulations the problem with choosing a small lattice spacing is it requires the use of a large number of lattice points, greatly reducing the speed of the simulation. The central difference formula has an error $\mathcal{O}(h^2)$ and is therefore a more accurate method for calculating the derivatives, for a larger value of h. The central difference approximation of the 2nd order derivative on the lattice is given by the following:

$$\frac{\partial^2 \phi_k}{\partial x^2}(i, j) = \frac{\phi_k(x_i + h, y_j) - 2\phi_k(x_i, y_j) + \phi_k(x_i - h, y_j)}{h^2},$$

and has error $\mathcal{O}(h^3)$. The mixed derivative term $\frac{\partial^2 \phi_k}{\partial x \partial y}(i,j)$ can be written as:

$$
\begin{aligned}
\frac{\partial^2 \phi_k}{\partial x \partial y}(i,j) \;=\; & \frac{\phi_k(x_i + h, y_j + h) + \phi_k(x_i - h, y_j - h)}{4h^2} \\
& \frac{-\phi_k(x_i + h, y_j - h) - \phi_k(x_i - h, y_j + h)}{4h^2}.
\end{aligned}
$$

It is possible to refine the accuracy of this discretisation to higher orders. This involves including information about the field values at lattices sites around the point of interest, in addition to the sites either side. This method improves the accuracy of the calculation, although it involves a few more calculations per derivative term, which costs computing time. One can also use more sophisticated expressions for the numerical calculation of the two dimensional Laplacian $\nabla^2 \underline{\phi}$. Once again this requires more information at the cost of more calculations. In all of our simulations we decided not to exploit such higher order, more accurate terms and have decided that the terms and expressions given above would suffice for the numerical accuracy we required.

3.2 Numerical integration

Most of the important equations in mathematical physics are first or second order differential equations. The difficulty numerically integrating a second order equation can be overcome by reducing the system to a set of two coupled first order equations. If the differential equation of interest is given by:

$$
\frac{d^2 f(x)}{dx^2} = H(x, f(x), \frac{df(x)}{dx}),
$$

then by setting $g(x) = \frac{df(x)}{dx}$, the above system is now reduced to the two differential equations:

$$
\begin{aligned}
g(x) &= \frac{df(x)}{dx}, \\
\frac{dg(x)}{dx} &= H(x, f(x), g(x)).
\end{aligned}
$$

There are a variety of different methods available to integrate the above system of equations. Each one of these different methods can be more suitable than one of the other methods, depending on the problem, due for example to their accuracy

or the ease of implementation. Here we shall discuss the Runge-Kutta method for integrating such a set of equations and show how it arises. For simplicity we shall discuss integrating a first order differential equation of the form:

$$\frac{dy(x)}{dx} = f(x, y).$$

Firstly, consider the Taylor expansion of the function $y(x)$ a small distance h away:

$$y(x + h) = y(x) + hy'(x) + \frac{h^2}{2!}y''(x) + \mathcal{O}(h^3).$$

Since $y'(x) = f(x, y)$ we can rewrite the second derivative as:

$$\begin{aligned} y''(x) &= f_x(x, y) + f_y(x, y)y'(x) \\ &= f_x(x, y) + f_y(x, y)f(x, y). \end{aligned}$$

Using this we can write the Taylor expansion as:

$$y(x + h) = y(x) + hf(x, y) + \frac{h^2}{2!}\left[f_x(x, y) + f_y(x, y)f(x, y)\right] + \mathcal{O}(h^3).$$

The Runge-Kutta method assumes that the correct value of the slope, over the step size, can be written as a linear combination of the function $f(x, y)$, evaluated at certain points along the interval. The second order Runge-Kutta method approximates $y(x + h)$ by:

$$y(x + h) = y(x) + Ahf_o + Bhf_1, \tag{3.1}$$

where the functions f_0, f_1 are given by:

$$\begin{aligned} f_0 &= f(x, y), \\ f_1 &= f(x + Ph, y + Rhf_0), \end{aligned}$$

written in terms of the undetermined constants A, B, P and R.

We can Taylor expand f_1:

$$y(x + h) = f(x, y) + Phf_x(x, y) + Phf_y(x, y) + \mathcal{O}(h^2).$$

Inserting this Taylor expansion into the Runge-Kutta equation (3.1):

$$\begin{aligned} y(x + h) &= y(x) + Ahf(x, y) + Bh\left[f(x, y) + Phf_x(x, y) + Phf_y(x, y)\right] \\ &= y(x) + (A + B)hf(x, y) + PBh^2 f_x(x, y) \\ &\quad + BRh^2 f_y(x, y)f(x, y) + \mathcal{O}(h^3). \end{aligned}$$

If the Taylor expansion and the Runge-Kutta formula are to agree to second order, then there are conditions placed upon the constants such that $A + B = 1$ and $PB = BR = \frac{1}{2}$. There are three equations with four unknowns. We can choose $A = 0$ and $B = 1$ such that $P = R = \frac{1}{2}$. This choice of constants produces the second order Runge-Kutta method:

$$y(x + h) = y(x) + hf\left(x + \frac{h}{2}, y + \frac{h}{2}f(x, y)\right). \tag{3.2}$$

The above process can be repeated to obtain a fourth order method. The fourth order Runge-Kutta method to integrate $y'(x) = f(x, y)$ is given by a set of 5 equations:

$$
\begin{aligned}
y(x + h) &= y(x) + \frac{1}{6}(k_1 + 2k_2 + 2k_3 + k_4) + \mathcal{O}(h^5), \tag{3.3} \\
k_1 &= hf(x, y), \\
k_2 &= hf(x + \frac{h}{2}, y + \frac{1}{2}k_1), \\
k_3 &= hf(x + \frac{h}{2}, y + \frac{1}{2}k_2), \\
k_4 &= hf(x + h, y + k_3).
\end{aligned}
$$

The Runge-Kutta fourth order method is the most popular method of integrating a differential equation. This is due to its accuracy and that it requires only five function evaluations per step interval, which also makes it computationally efficient.

3.2.1   Coupled differential equations

The Landau-Lifshitz equation of motion is a set of three coupled partial differential equations:

$$
\begin{aligned}
\frac{\partial \phi_1}{\partial t} &= f_1(\phi_1, \phi_2, \phi_3), \\
\frac{\partial \phi_2}{\partial t} &= f_2(\phi_1, \phi_2, \phi_3), \\
\frac{\partial \phi_3}{\partial t} &= f_3(\phi_1, \phi_2, \phi_3).
\end{aligned}
$$

The Runge-Kutta algorithm, extended to deal with coupled differential equations, involves the sum of four complicated functions:

$$\phi_i^{n+1} = \phi_i^n + \frac{k}{6}(a_{i,n} + 2b_{i,n} + 2c_{i,n} + d_{i,n}), \tag{3.4}$$

where the functions $a_{i,n}, b_{i,n}, c_{i,n}$ and $d_{i,n}$ depend on the functions f_i given by:

$$
\begin{aligned}
a_{i,n} &= f_i(\phi_1^n, \phi_2^n, \phi_3^n), \\
b_{i,n} &= f_i(\phi_1^n + \frac{k}{2}a_{1,n}, \phi_2^n + \frac{k}{2}a_{2,n}, \phi_3^n + \frac{k}{2}a_{3,n}), \\
c_{i,n} &= f_i(\phi_1^n + \frac{k}{2}b_{1,n}, \phi_2^n + \frac{k}{2}b_{2,n}, \phi_3^n + \frac{k}{2}b_{3,n}), \\
d_{i,n} &= f_i(\phi_1^n + kc_{1,n}, \phi_2^n + kc_{2,n}, \phi_3^n + kc_{3,n}),
\end{aligned}
$$

and the index i corresponds to the component of the field, $\underline{\phi}$, and n to the iteration step.

3.3 Numerical techniques

In this section some of the numerical techniques that are specific to our system of interest shall be discussed. The differential equation governing the dynamics of the baby skyrmion solution is subject to a constraint upon the fields. This constraint is an integral component of the system and must be considered carefully. Obtaining a numerical solution to the differential equation governing the behaviour of the profile function requires utilising the shooting method. Although this method is conceptually easy to understand, the differential equation itself provides its own difficulties to be overcome, notably the singularity at the origin. Much of our later analysis relies on the knowledge of the position of the baby skyrmions during the simulations. The idea of the 'position' of a baby skyrmion is discussed and it is shown how we improve upon the accuracy of the baby skyrmions location, using Lagrange interpolation.

3.3.1 Imposing the S^2 constraint

The constraint on the target space of the fields, $\underline{\phi} \cdot \underline{\phi} = 1$, gives rise to the topological aspects of the field configurations. It is important that this constraint is observed during the simulations. Generally the field configurations, constructed in the manner that is described in a later section, will observe this constraint in the continuum limit. Unfortunately the discretised version of this system of equations does not. The numerical errors tend to propagate through the system, eventually leading to

the fields no longer satisfying the constraint. There are many different numerical techniques that could be implemented to ensure the constraint is observed during the simulations. Piette et al [28] performed numerical simulations on a baby Skyrme model using a variety of different numerical techniques. These different techniques were used to impose that the solutions lay on the two sphere. They found that all of the different methods gave reliable results and we shall employ one of them. In order to preserve the constraint we therefore impose that the fields at every time step are projected back onto the unit sphere such that:

$$\underline{\phi} \rightarrow \frac{\underline{\phi}}{\sqrt{\underline{\phi} \cdot \underline{\phi}}}.$$

During our initial investigations this projection technique was examined to see how effective it was in our system. To do this we evaluated the following function: $\lambda = 1 - \underline{\phi} \cdot \underline{\phi}$, during the simulations. The function λ would therefore inform us how the numerical errors due to the discretisation of the fields, pushed the fields off the unit sphere. During the simulations, it was observed that for the usual time step and lattice parameters $\lambda < 10^{-6}$. Therefore the results that followed from using the projection scheme could be considered reliable.

3.3.2 Shooting method

The differential equation governing the profile function of a baby skyrmion from the new baby Skyrme model, (2.8), can be written in the form:

$$
\begin{aligned}
f'' &= h(r, f, f'), \qquad (3.5) \\
h(r, f, f') &= \left(\frac{Q^2 \gamma_1 \sin f \cos f + \gamma_3 r^2 \cos f \sin f}{\gamma_1 r^2 + Q^2 \gamma_2 \sin^2 f} \right) \\
&\quad - \left(\frac{\gamma_1 r^2 + Q^2 \gamma_2 r f' \sin f \cos f - Q^2 \gamma_2 \sin^2 f}{\gamma_1 r^3 + Q^2 \gamma_2 r \sin^2 f} \right) f',
\end{aligned}
$$

subject to the boundary conditions:

$$f(0) = \pi, \ f(\infty) = 0.$$

The profile function of a baby skyrmion of charge Q close to the origin can be approximated by:

$$f(r) \simeq \pi + A_Q r^Q, \qquad (3.6)$$

where A_Q is an arbitrary constant. To solve (3.5) the second order differential equation is reduced to two coupled first order differential equations. Let $g = \frac{df}{dr}$, substituting this into (3.5) gives:

$$\begin{aligned} \frac{dg}{dr} &= h(r, f, g) \\ g &= \frac{df}{dr} \end{aligned} \tag{3.7}$$

It is noted that the differential equation (3.5) possess a $\frac{1}{r}$ singularity. The singularity can be avoided numerically by utilising the information about the profile function close to the origin. The profile function $f(r)$ close to $r = 0$ can be approximated from (3.6) and then used as the initial data for the numerical integration. The set of differential equations (3.7) now becomes:

$$\begin{aligned} \frac{dg}{dr} &= h(r, f, g) \\ g &= QA_Q r^{Q-1}. \end{aligned} \tag{3.8}$$

Initial condition problems are in general much easier to solve. Once the initial condition is specified, the system undergoes its evolution accordingly. Here the difficulty computing $f(r)$ is the boundary conditions. The boundary conditions are specified at the two endpoints of the system. Differential equations involving such boundary conditions are referred to as two-point boundary problems. To solve this system the shooting method must be utilised. In the following section, we shall illustrate how the shooting method is used to solve (3.5) for $Q = 1$.

Shooting method algorithm

In the realistic case of computing the profile function, the end point cannot be taken to infinity. The profile functions for baby skyrmions of this potential decay exponentially and for this system $f(r) \sim 0$ for $r \simeq 10$. There is no need to calculate $f(r)$ for a large distance and the standard value used is $r = 30$. The profile function's value at the endpoint in this revised system is denoted $f(N)$. In a general shooting method, the endpoint boundary condition is $f(N) = \beta$. The system to be solved,

written in terms of all the new variables, is given by:

$$g' = h(r, f, g),$$
$$g = A_1,$$
$$f(0) = \pi \qquad f(N) = \beta,$$

where in the system of interest $\beta = 0$. The differential equation for $f(r)$ is solved using this choice of A_1, by the 4th order Runge-Kutta method. After the profile function is obtained, $f(N, A_1)$ is examined for the given A_1. In general $f(N, A_1) \neq \beta$. Thus we can define a function $P(A_1) = f(N, A_1) - \beta$. When $P(A_1) = 0$ the chosen value of A_1 results in the matching of the boundary conditions at the end point and the correct profile function is obtained. If this is not true, then A_1 must be chosen again until it is satisfied. Thus the shooting method algorithm finds the root of $P(A_1)$. In our simulations the bisection method was used to find the root of $P(A_1)$. One would think that such a primitive method would be slow to converge compared to the more sophisticated root finding algorithms. In actual fact, for this differential equation, the more sophisticated methods such as Newton-Raphson or secant, are not a good choice. Due to the nature of the differential equation, it was found that both of these methods failed to converge on the root and the bisection method was by far the best option for finding the root of $P(A_1)$. The bisection algorithm is outlined in the following section.

Bisection algorithm

- Choose two values of A_1: A_1^o, A_1^p such that:

$$f(N, A_1^o)f(N, A_1^p) < 0,$$

therefore there exists a root on the interval $[A_1^o, A_1^P]$

- Evaluate:

$$A_1^n = \frac{A_1^o + A_1^p}{2}.$$

recalculate $f(N, A_1^n)$

- If $f(N, A_1^n) = 0$: root found

- Otherwise if

$$f(N, A_1^n)f(N, A_1^p) < 0,$$

then $A_1^o = A_1^n$

- Otherwise $A_1^p = A_1^n$

This algorithm is performed until a sufficient precision is obtained for a given N. The numerical precision required is dependent upon the coefficients γ_i and the topological charge Q. The higher the charge and the lower the values of the γ_i's, the greater the number of decimal places needed for the same accuracy. Fig. 3.1 shows a plot of the numerical solution to (3.5) using the shooting method for various values of the coefficient γ_2 with $\gamma_{1,3} = 1$ for a $Q = 1$ baby skyrmion.
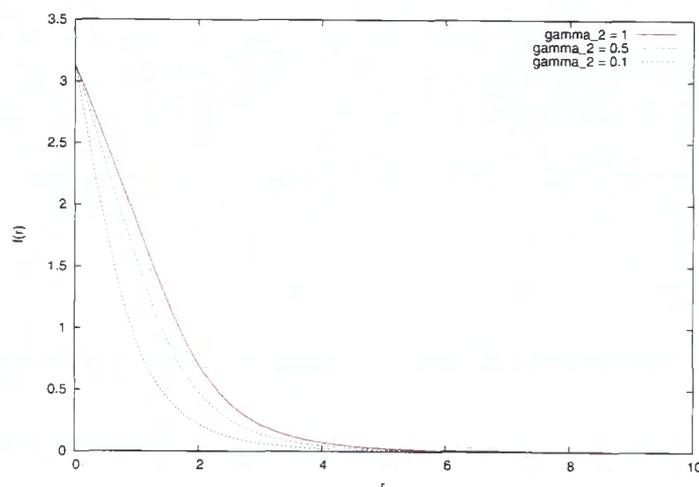
Figure 3.1: The profile function, $f(r)$, of a baby skyrmion of the new baby Skyrme model, for various values of the coefficient $\gamma_2 = 1, 0.5, 0.1$.

3.3.3 Skyrmion position

In previous chapters the extended nature of baby skyrmions was alluded to. How we interpret the results of our problem relies on knowledge of the baby skyrmions trajectory. In order to plot the trajectory of an extended object, the function or

parameter that will describe the trajectory of a baby skyrmion needs to be considered carefully. The most natural parameter is the centre of the object. In the model of interest there are two ways of defining the baby skyrmions centre. One such definition of the centre of the baby skyrmion is the point where $\phi_3 = -1$. Alternatively, one can consider the maximum of the topological charge density, $q(x, y)$, as the centre of the baby skyrmion. It has been shown in previous work [30], that both of these definitions are valid and both reproduce similar trajectories. Here the maximum of the topological charge density is used as a measure of the baby skyrmion position during the simulations. The simulations have been performed on a two dimensional lattice and therefore it is conceivable that the position of the maximum of the topological charge density could lie off the lattice. To find the exact position of the baby skyrmion centre, the region around the maximum of $q(x, y)$ on the lattice sites, $q(i, j)$, is approximated by two quadratic functions in each of the x, y directions. Lagrange interpolation between points either side of the maximum can be used to find the quadratic in each direction. The coordinate of the baby skyrmion centre lies at the maximum of the quadratics in each direction.

The location of the maximum on the lattice and the points either side of the maximum are denoted (x_1, y_1), (x_0, y_0) and (x_2, y_2) respectively. The quadratics in each direction are denoted $g(x)$ and $g(y)$ and therefore the centre of the skyrmion lies at $(g(x)_{max}, g(y)_{max})$. Given the set of points (x_i, y_i), a quadratic through each point in each direction can be constructed. An nth order polynomial, $P(x)$, can be constructed from $(n + 1)$ points x_k given knowledge of the functional points $f(x_k)$:

$$P(x) = \sum_{k=0}^{n} f(x_k) \Big(\prod_{i=0; i \neq k}^{n} \frac{x - x_i}{x_k - x_i} \Big), \qquad (3.9)$$

where x_i, x_k and $f(x_k)$ are the points to be interpolated through. The quadratics interpolating through these points can be written:

$$g(x) = \sum_{k=0}^{2} f(x_k) \Big(\prod_{i=0; i \neq k}^{2} \frac{x - x_i}{x_k - x_i} \Big),$$

$$g(y) = \sum_{k=0}^{2} f(y_k) \Big(\prod_{i=0; i \neq k}^{2} \frac{y - y_i}{y_k - y_i} \Big).$$

It can be shown that the maximum of $g(x)$ exists and is given by:

$$g(x)_{max} = \frac{1}{2}\frac{P_x}{P_{x^2}},$$ (3.10)

where P_x and P_{x^2} are written in terms of x_i and $f(x_i)$:

$$P_x = f(x_0)\frac{(x_1 + x_2)}{(x_0 - x_1)(x_0 - x_2)} - f(x_1)\frac{(x_0 + x_2)}{(x_0 - x_1)(x_1 - x_2)} + f(x_2)\frac{(x_0 + x_1)}{(x_0 - x_2)(x_1 - x_2)},$$

$$P_{x^2} = \frac{f(x_0)}{(x_0 - x_1)(x_0 - x_2)} - \frac{f(x_1)}{(x_0 - x_1)(x_1 - x_2)} + \frac{f(x_2)}{(x_0 - x_2)(x_1 - x_2)}.$$

There also exists a corresponding formula for $g(y)_{max}$.

3.4 Baby skyrmion configuration

The use of the hedgehog anzatz as a means of dimensional reduction to the one dimensional first order nonlinear ordinary differential equation for the profile function $f(r)$, allows the construction of the field configuration from this anzatz. The construction of a two baby skyrmion configuration requires us to superimpose the two $Q = 1$ baby skyrmion solutions of the new baby Skyrme model. This superposition is greatly simplified if performed in terms of the stereographic variable W, defined in Chapter 2. There it was noted that a N baby skyrmion configuration can be constructed from (2.13), (2.14) and (2.15).

The aim of the W-superposition method is to construct an initial field configuration comprising two single charged baby skyrmions, separated by a finite distance d. The field configuration of such a system in terms of W is just the superposition of two different W's, W_1 and W_2. Within the W formalism another degree of freedom is allowed. A relative phase, α, between the two baby skyrmions can be introduced, when the initial field configuration of two baby skyrmions is constructed. This relative phase determines whether the interaction is attractive or repulsive. The relative phase plays a crucial role in the scattering process between the baby skyrmions in a Landau-Lifshitz model. To construct the desired baby skyrmion configuration,

including this relative phase, consider the following anzatz for $W_{N=2}$:

$$W_{N=2} = W_1 - W_2 e^{i\alpha}, \tag{3.11}$$

$$W_1 = \tan(\frac{f(r_1)}{2})e^{i\theta_1},$$

$$W_2 = \tan(\frac{f(r_2)}{2})e^{i\theta_2},$$

where (r_i, θ_i) are the coordinates of the baby skyrmions centre. From (2.13) the initial two baby skyrmion field configuration can be written in terms of α:

$$\phi_1 = \frac{2\tan\left(\frac{f(r_1)}{2}\right)\cos(\theta_1) - 2\tan\left(\frac{f(r_2)}{2}\right)\cos(\theta_2 + \alpha)}{1 + \tan^2\left(\frac{f(r_1)}{2}\right) + \tan^2\left(\frac{f(r_2)}{2}\right) - 2\tan\left(\frac{f(r_1)}{2}\right)\tan\left(\frac{f(r_2)}{2}\right)\cos(\Delta\theta + \alpha)},$$

$$\phi_2 = \frac{2\tan\left(\frac{f(r_1)}{2}\right)\sin(\theta_1) - 2\tan\left(\frac{f(r_2)}{2}\right)\sin(\theta_2 + \alpha)}{1 + \tan^2\left(\frac{f(r_1)}{2}\right) + \tan^2\left(\frac{f(r_2)}{2}\right) - 2\tan\left(\frac{f(r_1)}{2}\right)\tan\left(\frac{f(r_2)}{2}\right)\cos(\Delta\theta + \alpha)}, \tag{3.12}$$

$$\phi_3 = \frac{1 - \tan^2\left(\frac{f(r_1)}{2}\right) - \tan^2\left(\frac{f(r_2)}{2}\right) + 2\tan\left(\frac{f(r_1)}{2}\right)\tan\left(\frac{f(r_2)}{2}\right)\cos(\Delta\theta + \alpha)}{1 + \tan^2\left(\frac{f(r_1)}{2}\right) + \tan^2\left(\frac{f(r_2)}{2}\right) - 2\tan\left(\frac{f(r_1)}{2}\right)\tan\left(\frac{f(r_2)}{2}\right)\cos(\Delta\theta + \alpha)},$$

where $\Delta\theta = \theta_1 - \theta_2$. The two baby skyrmion configuration has been constructed using the W-superposition, for various values of α and the baby skyrmion separation, d. The total energy and topological charge were calculated for each such configuration. The interaction energy between the baby skyrmions for a given value of α can be defined as:

$$U(d, \alpha) = E_2(\alpha) - 2E_1, \tag{3.13}$$

where $E_2(\alpha)$ is the energy of the two baby skyrmion configuration for a given value of α and E_1 is the energy of a single baby skyrmion.

Fig. 3.2 shows plots of $U(d)$ for $\alpha = 0, \pi, \frac{\pi}{2}$, for two different values of γ_2. It can be seen from both these plots that the lowest energy configuration, for baby skyrmions that are close enough to interact, occurs for $\alpha = 0$. This is known as the attractive channel. In this channel the baby skyrmions form a bound state. The channel for which $\alpha = \pi$ is the totally repulsive channel. In this channel the baby skyrmions do not form a bound state. The formation of a bound state is not unique to $\alpha = 0$. There exist other values of α in which a bound state between the two baby skyrmions can exist although $\alpha = 0$ is the most tightly bound.
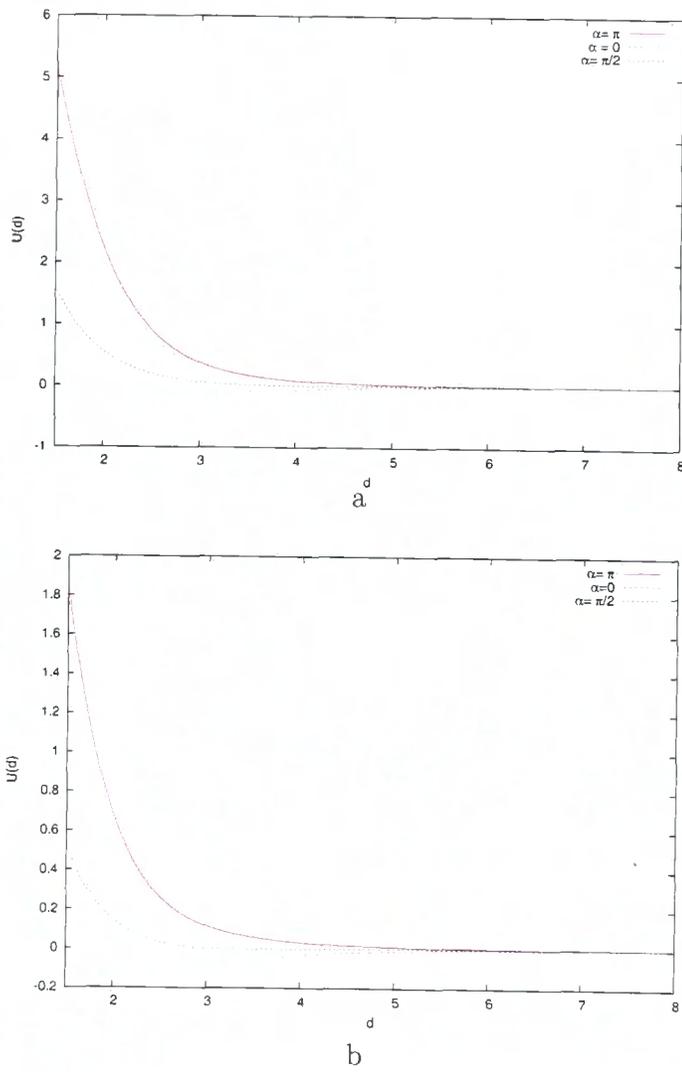
Figure 3.2: Plot of the interaction energy, $U(d)$, as a function of the baby skyrmion separation, d, for different values of the relative phase, α, and the Skyrme term coefficient γ_2: a) 1 b) 0.5.
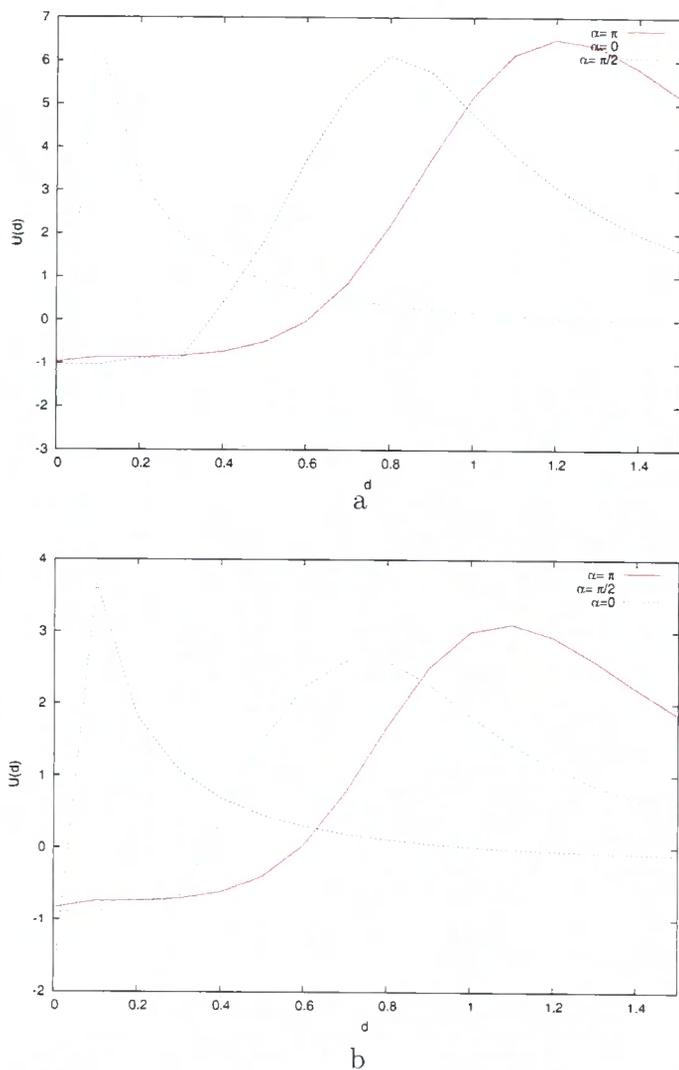
Figure 3.3: Plot of the interaction energy, $U(d)$, as a function of the baby skyrmion separation, d, for different values of the relative phase, α, and the Skyrme term coefficient γ_2: a) 1 b) 0.5. The plot ranges over $0 < d < 1.5$, where the numerical curiosities become apparent.
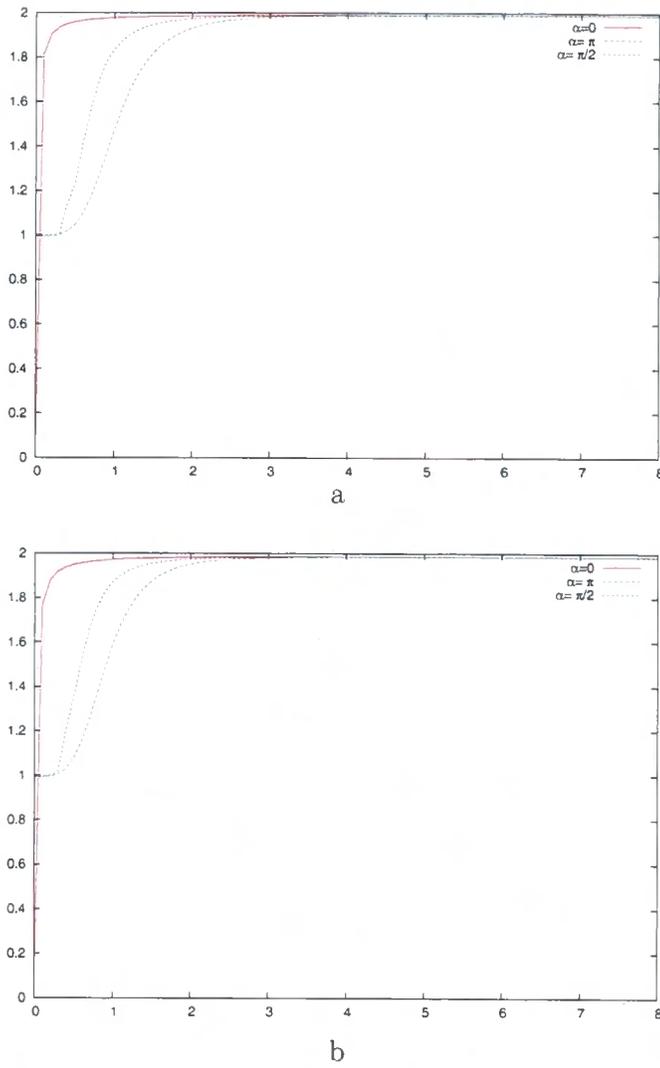
Figure 3.4: Plot of the topological charge, Q, as a function of the baby skyrmion separation, d, for different values of the relative phase, α, and the Skyrme term coefficient γ_2: a) 1 b) 0.5.

The two further plots of the interaction energy in Fig. 3.3 are plotted over the unseen region, $0 < d < 1.5$, not shown in the plots of Fig. 3.2. This region was not shown in these plots because it gave a misleading representation of the interaction energy between the baby skyrmions over such values of d. In Fig. 3.3 it appears that other values of d allow for the formation of a bound state. This is a numerical artifact. A plot of the topological charge $Q(d)$ for each of the plots in Fig. 3.4, shows for $\alpha = 0$ the topological charge initially starts at $Q = 0$ and quickly increases to the correct value of $Q = 2$, within numerical tolerances. Plots for the other values of α show that $Q = 1$ initially. This is simply incorrect. The topological charge is a conserved quantity and there exists a problem in the computer calculation of the field configuration for small values of d. This problem can be examined further by considering the field configuration (3.12) for $r_1 \simeq r_2 = \hat{r}$. The set of equations then become:

$$
\begin{aligned}
\phi_1 &= \frac{2\tan\left(\frac{f(\hat{r})}{2}\right)[\cos(\theta_1) - \cos(\theta_2 + \alpha)]}{1 + 2\tan^2\left(\frac{f(\hat{r})}{2}\right)[1 - \cos(\Delta\theta + \alpha)]}, \\
\phi_2 &= \frac{2\tan\left(\frac{f(\hat{r})}{2}\right)[\sin(\theta_1) - \sin(\theta_2 + \alpha)]}{1 + 2\tan^2\left(\frac{f(\hat{r})}{2}\right)[1 - \cos(\Delta\theta + \alpha)]}, \\
\phi_3 &= \frac{1 - 2\tan^2\left(\frac{f(\hat{r})}{2}\right)[1 - \cos(\Delta\theta + \alpha)]}{1 + 2\tan^2\left(\frac{f(\hat{r})}{2}\right)[1 - \cos(\Delta\theta + \alpha)]}.
\end{aligned}
\tag{3.14}
$$

The field configuration in this limit resembles that of a $Q = 1$ baby skyrmion. The core of the problem, illustrated in Fig. 3.4, is the computer's calculation of $\tan\left(\frac{f(\hat{r})}{2}\right)$ which is divergent at the origin, since $f(\hat{r}) = \pi$. The computer therefore has difficulty distinguishing this configuration from a single baby skyrmion and hence the topological charge initially starts out around $Q = 1$ when $\alpha \neq 0$. This example serves to illustrate that the W-superposition, in this context, is only valid when the baby skyrmions are well separated. When the baby skyrmions are close enough to overlap, the superposition procedure does not produce the correct ring configurations associated with the $Q = 2$ baby skyrmion of the new baby Skyrme model. In our work the superposition procedure was used to produce an initial field configuration of two well separated baby skyrmions. This configuration is then used as an initial condition in a gradient flow simulation to allow the field configuration to relax into its lowest energy state. The configuration formed once the baby skyrmions

had completely relaxed, was the ring configuration of the $Q = 2$ baby skyrmion of the new baby Skyrme model.

3.4.1 Gradient flow

The numerical method known as gradient flow allows field configurations to relax into their lowest energy state, a desired quantity when investigating topological soliton solutions. The gradient flow equation simply relates the time derivative of the fields to the direction of minimal energy flow:

$$\frac{\partial \underline{\phi}}{\partial t} = -\kappa \frac{\delta E}{\delta \underline{\phi}} + k\underline{\phi}, \tag{3.15}$$

where the constraint $\underline{\phi} \cdot \underline{\phi} = 1$ was imposed by including a term proportional to $\underline{\phi}$. Dotting $\underline{\phi}$ on both sides and using $\underline{\phi} \cdot \frac{\partial \underline{\phi}}{\partial t} = 0$:

$$k = \kappa \underline{\phi} \cdot \frac{\delta E}{\delta \underline{\phi}}. \tag{3.16}$$

Thus:

$$\frac{\partial \underline{\phi}}{\partial t} = \kappa \left[\underline{\phi} \left(\underline{\phi} \cdot \frac{\delta E}{\delta \underline{\phi}} \right) - \frac{\delta E}{\delta \underline{\phi}} \right]. \tag{3.17}$$

The above system can be expanded out to give:

$$
\begin{aligned}
\frac{\partial \underline{\phi}}{\partial t} &= \kappa \underline{f}, \\
\underline{f} &= \gamma_1 \left[-\underline{\phi}\,\underline{\phi} \cdot \nabla^2 \underline{\phi} + \nabla^2 \underline{\phi} \right] + \gamma_3 \left[-\underline{\phi}\phi_3^2 + \phi_3 \cdot (0,0,1) \right] \\
&+ \gamma_2 \Big\{ \partial_x \left(\partial_y \underline{\phi} \cdot \partial_y \underline{\phi} \right) \left[\partial_x \underline{\phi} - \underline{\phi}\,\underline{\phi} \cdot \partial_x \underline{\phi} \right] + \partial_y \left(\partial_x \underline{\phi} \cdot \partial_y \underline{\phi} \right) \left[\partial_y \underline{\phi} - \underline{\phi}\,\underline{\phi} \cdot \partial_y \underline{\phi} \right] \\
&+ \left(\partial_y \underline{\phi} \cdot \partial_y \underline{\phi} \right) \left[\partial_{xx} \underline{\phi} - \underline{\phi}\,\underline{\phi} \cdot \partial_{xx} \underline{\phi} \right] + \left(\partial_x \underline{\phi} \cdot \partial_x \underline{\phi} \right) \left[\partial_{yy} \underline{\phi} - \underline{\phi}\,\underline{\phi} \cdot \partial_{yy} \underline{\phi} \right] \\
&- 2 \left(\partial_x \underline{\phi} \cdot \partial_y \underline{\phi} \right) \left[\partial_{xy} \underline{\phi} - \underline{\phi}\,\underline{\phi} \cdot \partial_{xy} \underline{\phi} \right] - \partial_x \left(\partial_x \underline{\phi} \cdot \partial_y \underline{\phi} \right) \left[\partial_y \underline{\phi} - \underline{\phi}\,\underline{\phi} \cdot \partial_y \underline{\phi} \right] \\
&- \partial_y \left(\partial_x \underline{\phi} \cdot \partial_y \underline{\phi} \right) \left[\partial_x \underline{\phi} - \underline{\phi}\,\underline{\phi} \cdot \partial_x \underline{\phi} \right] \Big\}.
\end{aligned}
$$

Gradient flow simulation

The required configuration of two baby skyrmions of the new baby Skyrme model, whose centres (x_i, y_i) are separated by a distance d, is obtained by using a field configuration, generated by the W-superposition method, as an initial condition to the above gradient flow equation. The two-dimensional space was discretised as

described in a previous section using a grid of size 251×251 points with a lattice spacing $dx = 0.1$. The numerical integration of the gradient flow equations was performed using the 4th order Runge-Kutta method with time step $dt = 0.001$ using a fixed boundary condition of $\underline{\phi} = (0, 0, 1)$. The coefficients appearing in the gradient flow equation were set to: $\kappa = \gamma_i = 1$. The baby skyrmions were initially at a separation of $d = 8$, where the skyrmions centres were at the points $(0, \pm 4)$. This configuration, generated by the W-superposition method, was allowed to relax under gradient flow. The resulting field configurations from the gradient flow simulation are classified according to the distance of separation, d, between the centres of the baby skyrmion. Figs. 3.5 shows the energy density and energy density contours for a baby skyrmion configuration of the new baby Skyrme model, after the gradient flow simulation. In the contour plot of Fig. 3.5 the vertical axis represents the y coordinate, while the horizontal axis the x coordinate. The boundary of the grid is the points where $x, y = \pm 12.5$ and has been cut off from this plot to better illustrate the configuration's contours.
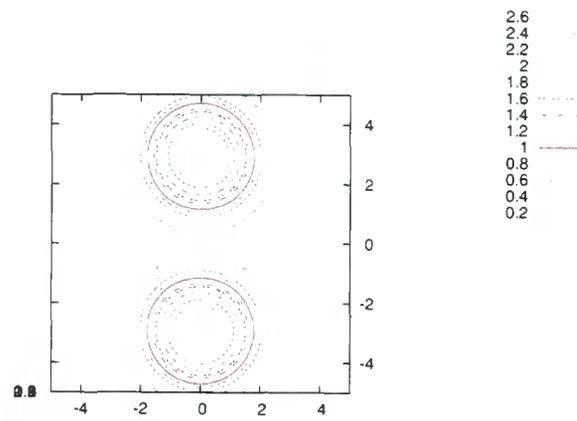
Figure 3.5: Plot of the energy density and the energy density contours for a two baby skyrmion configuration after gradient flow.

3.5   Numerical procedures

In the next chapter we shall present and discuss the results of our investigations which was done by performing numerical simulations. Here we shall summarise the values of the various constants used in the discretisation and the numerical integration of the equations of motion:

- The fields were placed on a lattice of 251 × 251, with a lattice spacing $dx = 0.1$ and therefore the boundary in all plots of the baby skyrmions trajectory corresponds to the points when $x, y = \pm 12.5$.

- The numerical integration of the three coupled differential equations comprising the Landau-Lifshitz equation was performed using a 4th order Runge-Kutta method with a time step of $dt = 0.001$.

- The various integrals calculated during the simulations were performed using a two-dimensional Simpson's rule.

- The baby skyrmions in all of the simulations are initially placed at $(0, \pm d/2)$ in the upper and lower semi-planes, where d is the distance of separation between the baby skyrmion centres (x_i, y_i).

- We shall frequently refer to the two baby skyrmions of the configuration as either the upper or lower baby skyrmion. The upper baby skyrmion is the baby skyrmion whose centre is initially located at $(0, d/2)$ and the lower baby skyrmion is the one whose centre is initially located at $(0, -d/2)$.

- In all of the simulations the coefficients γ_i have been set to unity, unless stated otherwise.

- The value of the fields $\underline{\phi}$ on the boundary are fixed at the vacuum value $\underline{\phi} = (0, 0, 1)$.

During the presentation of the results in the next two chapters and the subsequent analysis, we shall refer to the simulations of the skyrmion configurations on

the accompanying Cd. In the appendix the different parameters of each simulation are presented in a table and any additional information required about these simulations is given there.

Chapter 4

Symmetric Potential Obstruction

The scattering of particles off potential holes and barriers in classical and quantum mechanical systems are seemingly different. In a classical system, if the particle has sufficient energy it can traverse a barrier; if it does not, it gets reflected. When it encounters a hole it speeds up as it passes over the hole and is always transmitted. In both cases the particle is either transmitted or reflected. In quantum mechanical scattering the particle can be reflected and transmitted for either a barrier or a hole but these events occur with a certain probability which is dependent on the particle's energy and on the size of the barrier or hole. Our investigations concern the scattering properties of a baby skyrmion configuration, resulting from the new baby Skyrme model, in a magnetic system, whose motion is then governed by the Landau-Lifshitz equation. Topological solitons are, of course, classical objects. However, they describe extended objects and, as shown in [5], some of their properties resemble those of quantum systems. There has been much work recently on the scattering behaviour of topological solitons off potential obstructions. Speight [33] has recently investigated the scattering of a magnetic bubble solution in a anti-ferromagnetic system, where the continuum dynamical equation resembles a second order relativistic wave equation. Al-Awali et al [1], [2], [3] have considered the scattering of various topological and non-topological solitons off potential holes an barriers. Both of these system have shown that the scattering of topological soliton off holes or barriers exhibit some interesting results. Hence in the following two chapters we shall study this problem further, concentrating on systems whose dy-

46

namics are described by the Landau-Lifshitz equation and examining the behaviour of a baby skyrmion configuration, as constructed in the previous chapter, in the presence of various potential obstructions.

We start by reminding ourselves of the Lagrangian for the (2+1) new baby Skyrme model, discussed in Chapter 1 and the Landau-Lifshitz equation which shall govern the dynamics of the baby skyrmion solutions in our investigations:

$$\mathcal{L} = \frac{1}{2}\partial_\mu\underline{\phi} \cdot \partial^\mu\underline{\phi} - \frac{1}{4}[(\partial_\mu\underline{\phi} \cdot \partial^\mu\underline{\phi})^2 - (\partial_\mu\underline{\phi} \cdot \partial_\nu\underline{\phi})(\partial^\mu\underline{\phi} \cdot \partial^\nu\underline{\phi})] - \frac{1}{2}(1 - \phi_3^2), \quad (4.1)$$

The Landau-Lifshitz equation and its constraint is given by:

$$\frac{\partial\underline{\phi}}{\partial t} = \underline{\phi} \times -\frac{\delta E}{\delta\underline{\phi}}, \quad \underline{\phi}^2 = 1,$$

where E is the energy functional written as:

$$E = \int_{\mathbb{R}^2} d^2x \mathcal{E},$$

and $\mathcal{E}$ is the static energy density given by:

$$\mathcal{E} = \frac{1}{2}\partial_i\underline{\phi} \cdot \partial_i\underline{\phi} + \frac{1}{4}[(\partial_i\underline{\phi} \cdot \partial_i\underline{\phi})^2 - (\partial_i\underline{\phi} \cdot \partial_j\underline{\phi})(\partial_i\underline{\phi} \cdot \partial_j\underline{\phi})] + \frac{1}{2}(1 - \phi_3^2).$$

Thus we can write down $-\frac{\delta E}{\delta\underline{\phi}}$:

$$-\frac{\delta E}{\delta\underline{\phi}} = \nabla^2\underline{\phi} + \phi_3 \cdot (0, 0, 1)$$
$$+ \frac{1}{2}\{2\partial_i[(\partial_j\underline{\phi} \cdot \partial_j\underline{\phi})\partial_i\underline{\phi}] - \partial_i[(\partial_i\underline{\phi} \cdot \partial_j\underline{\phi})\partial_j\underline{\phi}] - \partial_j[(\partial_i\underline{\phi} \cdot \partial_j\underline{\phi})\partial_i\underline{\phi}]\}.$$

In the following sections we shall explain how the potential obstructions are introduced into the system and discuss the scattering properties of the baby skyrmion configuration off the potential obstructions, initially examining the dynamics when there are no obstructions. From now on, for simplicity, we shall refer to baby skyrmions as simply skyrmions.

4.1 Simple obstruction

In our construction of the potential obstructions we adopt a similar approach to [5] and introduce a term into the Lagrangian (4.1) which vanishes in the vacuum state

$\phi_3 = +1$. The obstructions need to be introduced in this manner so the tails of the skyrmions are not changed by the obstruction. Therefore, the additional potential term $V_{obs}(\phi_3)$ is added to the new baby Skyrme Lagrangian and is identical to the potential in (4.1) but localised to a finite region of space:

$$\mathcal{L}_{new} = \mathcal{L}_{old} + V_{obs}(\phi_3),$$

where:

$$V_{obs}(\phi) = \frac{1}{2}\Gamma(1 - \phi_3^2). \tag{4.2}$$

Γ can be either positive or negative. The Lagrangian of (4.1), by the introduction of this additional potential, is changed such that the potential coefficient now depends on the space coordinates. The introduction of this term, implies that the static part of (4.1) can be rewritten as:

$$\mathcal{L} = \frac{1}{2}\partial_i\underline{\phi} \cdot \partial_i\underline{\phi} - \frac{1}{4}[(\partial_i\underline{\phi} \cdot \partial_i\underline{\phi})^2 - (\partial_i\underline{\phi} \cdot \partial_j\underline{\phi})(\partial_i\underline{\phi} \cdot \partial_j\underline{\phi})] - \frac{1}{2}\gamma_3(x,y)(1 - \phi_3^2), \tag{4.3}$$

where the potential term coefficient γ_3 is now a function of the coordinates (x,y) and the static part of (4.1) is only considered as imposed by the Landau-Lifshitz equation. This inhomogeneity is localised to a finite region of space and can be written in terms of Heaviside functions which are defined by:

$$\Theta(\alpha) = \begin{cases} 0, & \alpha < 0 \\ 1, & \alpha \geq 0. \end{cases}$$

Therefore the potential we shall be investigating can be written as:

$$\gamma_3(x,y) = 1 + \Gamma\left[\Theta(y + y_0) - \Theta(y - y_0)\right], \tag{4.4}$$

where $y_0 = b/2$, b is the width of the obstruction and Γ is the height or depth of the obstruction. The sign of Γ determines whether the potential obstruction is a hole or a barrier. When $\Gamma > 0$, the obstruction is a barrier. Conversely when $\Gamma < 0$ the obstruction is a hole. In our study we look at the differences of dynamics due to holes and barriers, which shall be discussed in the following sections.

4.1.1 Skyrmion scattering off potential obstructions

To fully understand the dynamics of a skyrmion configuration interacting with a potential obstruction, we initially examined the behaviour of the configuration in the absence of any obstructions i.e. $\Gamma = 0$. Fig. 4.1 shows the trajectory of the upper skyrmion of a $d = 6$ two-skyrmion configuration with $\Gamma = 0$. The skyrmions' centre is initially located at $(0, \pm 3)$. The skyrmions orbit anti-clockwise around the configuration's centre $(0, 0)$. The trajectories of each skyrmion lie along a circle of radius $r \simeq 3$. Their position undergoes mild oscillations during the simulation. The total energy and angular momentum, $J = l + m$, are conserved with time. Additionally, each individual angular momentum component l and m is also conserved. The time scale for one period is 700 secs. The motion of two interacting skyrmions in a Landau-Lifshitz system is well understood. In [26], Papanicolaou and Tomaras, when discussing the trajectory of the skyrmions, make an analogy between this system and the Hall motion of two electrons. This analogy is made because of an underlying structure of the conservation laws in the Landau-Lifshitz model, which is not required when discussing the scattering behaviour of skyrmions off potential obstructions. A simulation of the skyrmions in this system with $\Gamma = 0$ and $d = 6$ can be seen on the accompanying Cd.

4.1.2 Potential hole

In the absence of all obstructions the skyrmions execute a circular path around their centre. Fig. 4.3 shows the trajectories of the upper and lower skyrmion of a $d = 6$ two-skyrmion configuration encountering a potential hole for different values of Γ and for $b = 1$. In all plots the skyrmions initially try to execute the trajectory of Fig. 4.1 but are deflected. They move asymptotically along the axis of the hole at an approximately constant value, y_{max}. It is clear from Fig. 4.3 that the larger the $|\Gamma|$, the larger the value of y_{max}. The skyrmions of Fig. 4.3a are able to get 'closer' to the hole than the skyrmions of Fig. 4.3b or Fig. 4.3c.

Fig. 4.2 shows the trajectories of only the upper skyrmions interacting with the potential hole for various values of Γ when $b = 3$. Comparing this plot with those
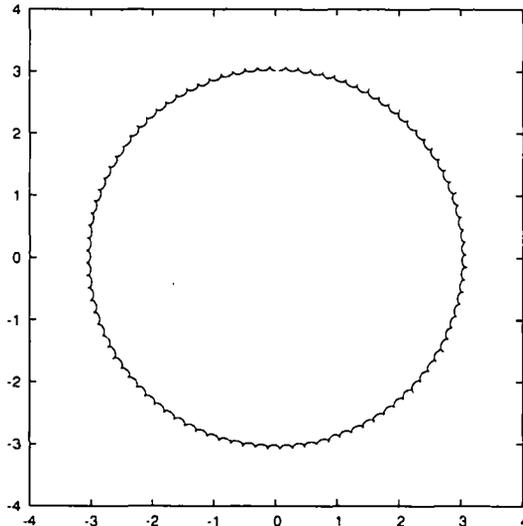
Figure 4.1: Trajectory of the upper skyrmion in the absence of any obstruction for a $d = 6$ two-skyrmion configuration, where the horizontal axis represents the x coordinate and the vertical axis the y coordinate.

in Fig. 4.3 one sees the effect of a larger b. The larger the b the larger the y_{max} for a given Γ. The skyrmions' tail can feel the hole earlier in a system of larger b, than in a system of smaller b. The same dependence of y_{max} on Γ is evident in Fig. 4.2. In Fig. 4.2 the skyrmion trajectories of $\Gamma = -0.25, -0.5$ are seen to be reflected by the boundary. The skyrmions in the lower plane execute similar trajectories. A simulation of the skyrmions in this system with $\Gamma = -0.25$, $b = 2$ and $d = 6$ can be seen on the accompanying Cd.

To explain the observed behavior of skyrmions when encountering a hole, which may at first sight, appear as non-classical, we need to examine the binding energies of the configuration. If the energy of the two-skyrmion configuration in the presence of a hole is denoted by E_2 and E_1 is the energy of a single skyrmion placed at the same position as one of the skyrmions in E_2, then the binding, or the interaction energy, is given by:

$$E_B = E_2 - 2E_1. \tag{4.5}$$

In the system with $b = 1$, $\Gamma = -0.25$ we have $E_2 = 2.1206/8\pi$ and $E_1 = 1.0685/8\pi$.
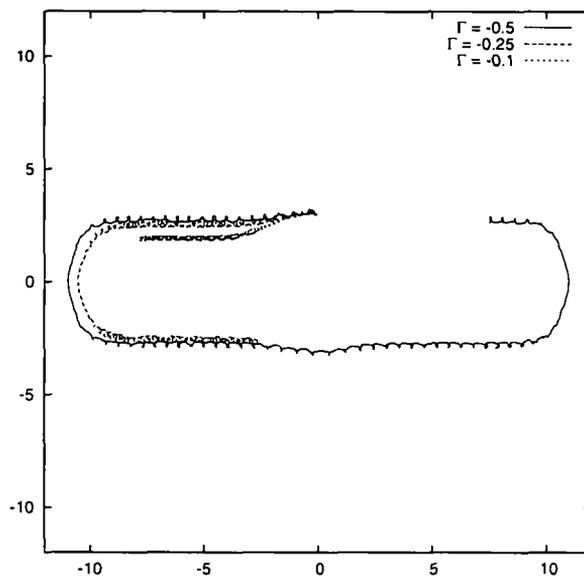
Figure 4.2: Plot of the trajectories of the upper skyrmion in a system with a potential hole of width b=3 for various values of Γ, where the horizontal axis represents the x coordinate and the vertical axis the y coordinate.

Figure 4.3: Plots of the trajectories of the upper and lower skyrmions for a $d = 6$ skyrmion configuration interacting with a potential hole of width $b = 1$ for various values of Γ: a) $\Gamma = -0.1$, b) $\Gamma = -0.25$, c) $\Gamma = -0.5$, where the horizontal axis represents the x coordinate and the vertical axis the y coordinate.

The binding energy of the two skyrmions in this system is thus $E_B = -0.0174/8\pi$, which is negative. Thus initially the skyrmions behave as if they are still in a bound state and try to execute the usual circular motion about their centre. If we examine the plot of the trajectory in Fig. 4.3, we see that as the skyrmions approach the hole, they reach a point where they separate and behave as two unbound skyrmions. Considering the definition of E_1, we can compute the energy of the single skyrmion as a function of the distance from the hole. Initially the skyrmion is at a distance $D = 3$ from the centre of a $b = 1$ hole and the binding energy is $E_B = -0.0174/8\pi$. If $D = 2$, the binding energy is reduced to $E_B = -0.005/8\pi$ and if the skyrmion is brought closer, at $D = 1$ then $E_B = +0.0152/8\pi$. So, as the skyrmions approach the hole the binding energy of the configuration is modified such that they no longer form a bound state and are able to separate. It is clear from plots of the trajectory, that the skyrmions, for a smaller value of $|\Gamma|$, are able to get closer to the hole than those of larger values of $|\Gamma|$. The skyrmions are able to get closer in these systems because the binding energies of the skyrmions do not reach the critical value until the skyrmions get closer to the hole. In the system of larger value of $|\Gamma|$ the hole modifies the binding energy earlier and thus the system reaches its critical value before the skyrmions can get as close as those for the smaller $|\Gamma|$.

4.1.3 Potential barrier

Next we have studied several cases of the scattering of the same $d = 6$ two-skyrmion configuration off potential barriers. Fig. 4.4 shows the trajectories of the upper and lower skyrmions of a two-skyrmion configuration, scattering off a potential barrier of width $b = 2$, for various values of Γ. It can be seen in each plot that the skyrmions are deflected as they traverse the barrier. This deflection always occurs in the direction of the centre of the configuration and hence the normal circular path is deformed as the skyrmions overcome the barrier. Trajectories for a smaller barrier width show a sharper deflection than those with larger b. Since the skyrmions are extended objects, when they are traversing the barrier they feel the barrier the most at the middle point. It is then only natural that the maximum point of deviation from the normal circular path will be at this point. Comparing trajectories of the same Γ

but with different values of b, we note that the skyrmions in the system with the larger value of b have more time to adjust to the barrier once they are 'on' top of it and therefore their path is not as sharp as for a smaller b. The larger value of b 'smooths' out the sharpening effects seen in the system with a smaller value of b's. More interestingly, during this deviation the skyrmions speed up as they traverse the barrier. In Figs. 4.4a and 4.4b the times taken for the skyrmion centre to reach the edge of the barrier are 110 secs and 140 secs respectively but the times taken for the centre to traverse the full width of the barrier are only 25 secs and 12.5 secs. A simulation of the skyrmions in this system with $\Gamma = 0.25$, $b = 2$ and $d = 6$ can be seen on the accompanying Cd.

The deflection and speeding up of the skyrmions can be explained by remembering how the skyrmions are constructed. As explained in Chapter 3, the two-skyrmion configuration was constructed such that the skyrmions were in the attractive channel. When they encounter a barrier, the energy of their configuration increases. The skyrmions counteract this increase due to the barrier by reducing their separation distance, d. This is clear by considering the energies of the configuration away from the barrier with $d = 6$. The energy of such a configuration is $E = 2.1277/8\pi$. If the same configuration was then placed on the barrier with $\Gamma = 0.2$, the energy becomes $E = 2.2271/8\pi$. Thus any increase in the potential energy due to the barrier must be compensated by a reduction in d. The energy increase of the system would be at its greatest when the skyrmions are in the middle of the barrier, hence the biggest deflection is seen at this point. Due to this quick adjustment of d, the skyrmions speed up as they traverse the barrier.

Another interesting feature of the scattering on a barrier is the 'transition dynamics' shown in Fig. 4.5. These plots show the transition to a state in which the skyrmions do not traverse the barrier and instead move away from each other. The transition to such a state is shown through the variation in the potential coefficient Γ for a fixed value of the barrier width $b = 3$. Similar plots could also have been obtained by choosing a fixed value of $\Gamma \simeq 0.25$ and increasing the barrier width b from $b = 2$ to $b = 3$. This effect is due to the binding energies of the skyrmion configuration. Using the previous definition of the binding energy (4.5) and its constituent
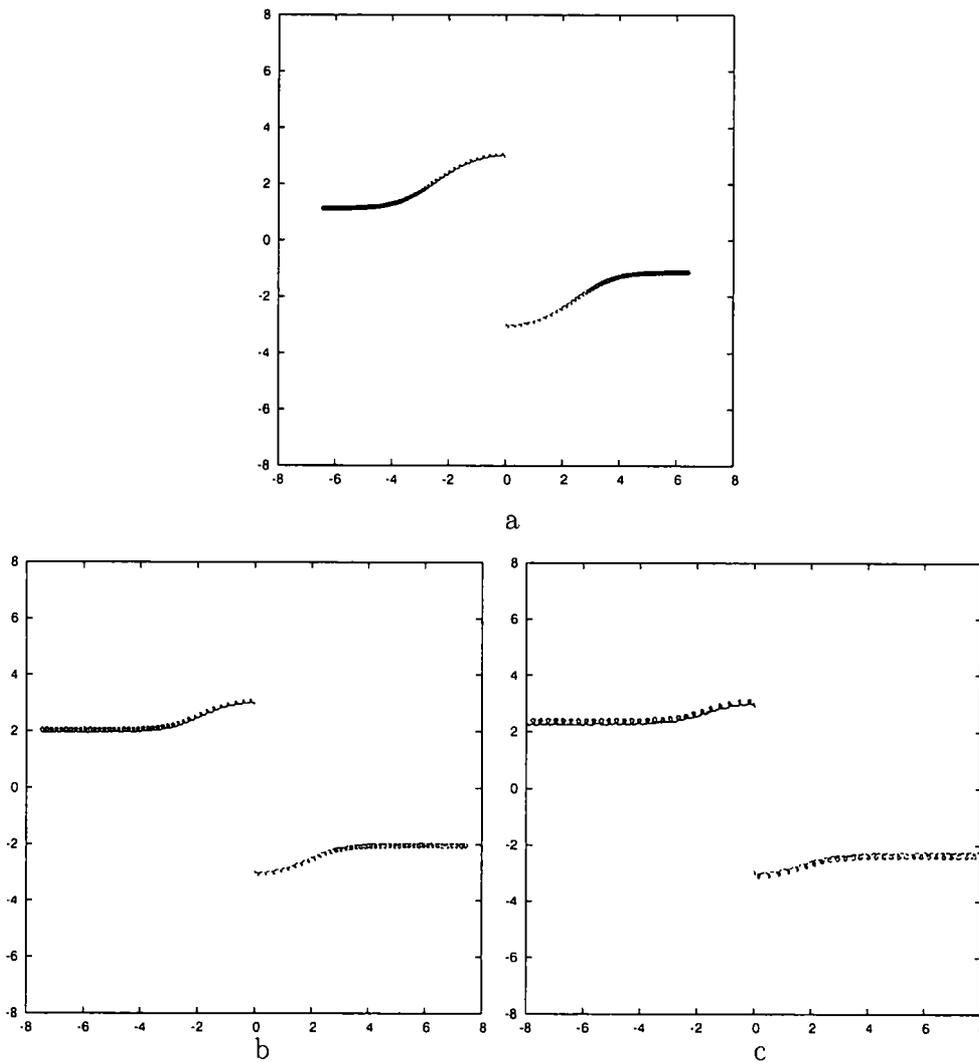
Figure 4.4: Plots of the trajectories of the upper and lower skyrmions for a $d = 6$ skyrmion configuration interacting with a potential barrier of width $b = 2$ for various values of Γ: a) $\Gamma = 0.1$, b) $\Gamma = 0.25$, c) $\Gamma = 0.3$, where the horizontal axis represents the x coordinate and the vertical axis the y coordinate.

Figure 4.5: Plots of the trajectories of the upper and lower skyrmions for a $d = 6$ skyrmion configuration interacting with a potential barrier of width $b = 3$ for various values of Γ: a) $\Gamma = 0.10$, b) $\Gamma = 0.15$, c) $\Gamma = 0.20$, d) $\Gamma = 0.25$, where the horizontal axis represents the x coordinate and the vertical axis the y coordinate.

parts, one can examine the binding energies in the barrier system. In a system with $b = 2$ and $\Gamma = 0.1$, $E_2 = 2.1317/8\pi$ and $E_1 = 1.0723/8\pi$ therefore $E_B = -0.0087/8\pi$ so the skyrmions are still bound. In $b = 2$ and $\Gamma = 0.3$, $E_2 = 2.1397/8\pi$ and $E_1 = 1.0730/8\pi$ therefore $E_B = -0.0063/8\pi$ and the skyrmions are still bound although a bit more loosely than for the smaller value of Γ. Next consider the state where the skyrmions separate from each other i.e. for $b = 3$ and $\Gamma = 0.25$. Then $E_2 = 2.1482/8\pi$ and $E_1 = 1.0767/8\pi$ and therefore, $E_B = -0.0052/8\pi$. The trajectory clearly shows that the skyrmions, for these values of b and Γ, behave as if they are unbound. Thus there appears to exist a threshold value of E_B in the barrier system, according to our definition of E_B, which determines whether the skyrmions are bound or unbound. This threshold value is b dependent but is approximately around $E_B = -0.005/8\pi$. We believe that this threshold is associated with the 'tails' of the skyrmions.

When two skyrmions are well separated they interact through their tails. In the new baby skyrme model the skyrmions are exponentially localised. In Chapter 2 it was shown that for large r the profile function can be approximated by:

$$f(r) \simeq \frac{1}{\sqrt{r}} exp(r). \tag{4.6}$$

The localisation of the profile function for a skyrmion is governed by the potential term coefficient, γ_3. The potential obstructions were introduced as inhomogeneities in γ_3's value. In the barrier system γ_3 takes the value of $1 + \Gamma$ on the barrier. On the barrier the asymptotic value of the profile function is modified:

$$\begin{aligned} \gamma_3 &\to 1 + \Gamma, \\ f(r) &\simeq \frac{1}{\sqrt{(1 + \Gamma)r}} exp\left(-(1 + \Gamma)r\right). \end{aligned} \tag{4.7}$$

As the skyrmion tail penetrates the region, it becomes attenuated by the potential obstruction. The width of the barrier causes the tail to be attenuated earlier for a larger value of b than for a smaller one. If, as we have assumed, the appreciable interaction of two well separated skyrmions is due to the tail-tail interaction between them, then if these tails are attenuated the interaction must also be reduced. Thus there must exist a value of Γ, the size of the attenuation of the tail in the obstruction,

for which the appreciable interaction of the skyrmions' tail is no longer sufficient for the skyrmions to undergo their usual dynamics. If there exists a critical value for Γ, then there must exist a critical value of E_B. Thus the threshold value of the binding energy corresponds to the particular values of b and Γ for which the tail-tail interaction of the skyrmions is no longer sufficient to cause the usual circular motion and the skyrmions can separate off from each other.

In this asymptotic state the skyrmions get deflected away from the barrier. There are some interesting consequences of the skyrmion behaviour in this state. The direction of motion of the skyrmion, in the asymptotic state, is at an an angle, α, relative to edge of the barrier. When the skyrmions are in this asymptotic state, as the value of Γ is increased the angle $\alpha \to 0$ in the limit for sufficiently large Γ. This right angle deflection of skyrmions off potential barriers is identical to the skyrmion hitting the boundary of the system. Thus the skyrmions can not distinguish between a large potential barrier and the fixed boundary of the system. The behaviour of the skyrmions in a potential barrier system is reminiscent of an identical skyrmion system's interaction with a potential hole. Here, however, the skyrmions move along the edge of the barrier and the boundary of the system, as seen in Fig. 4.6. In the hole system the skyrmions move only along the edge.
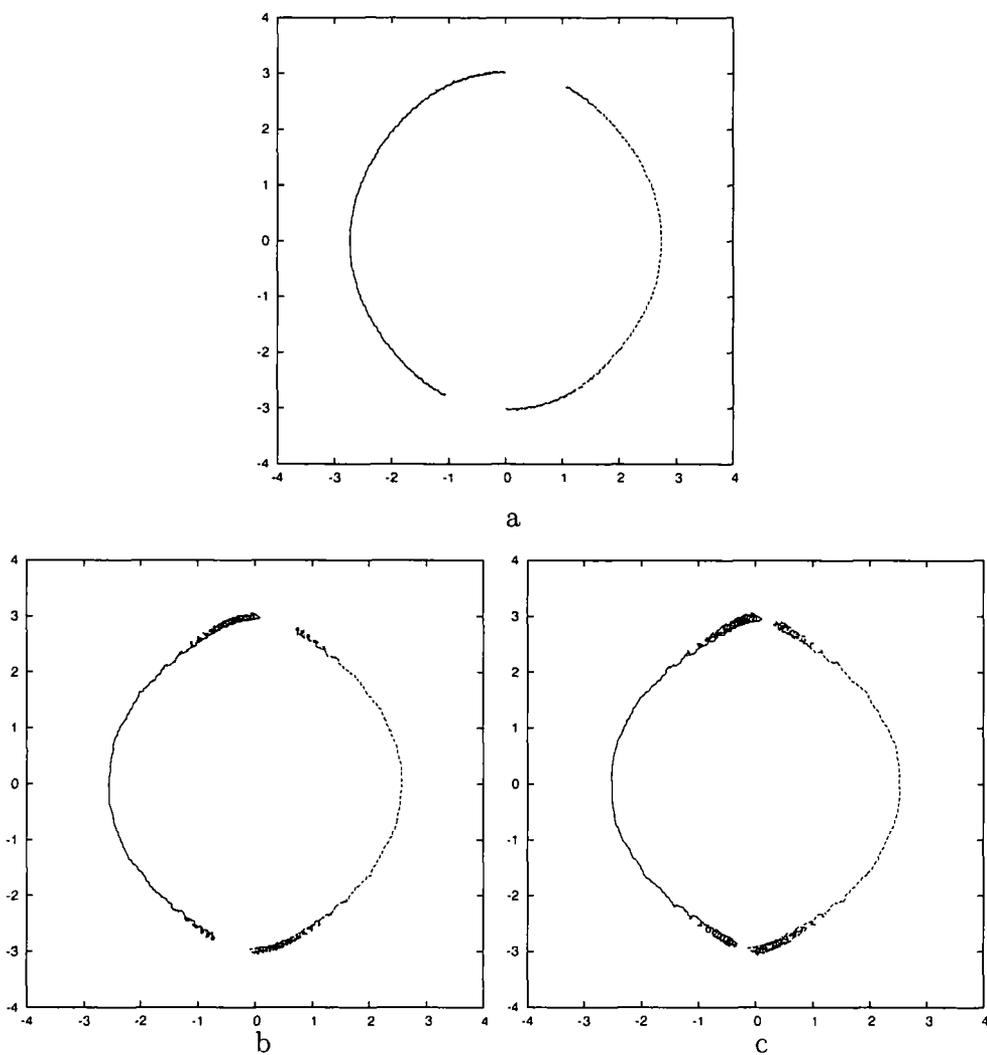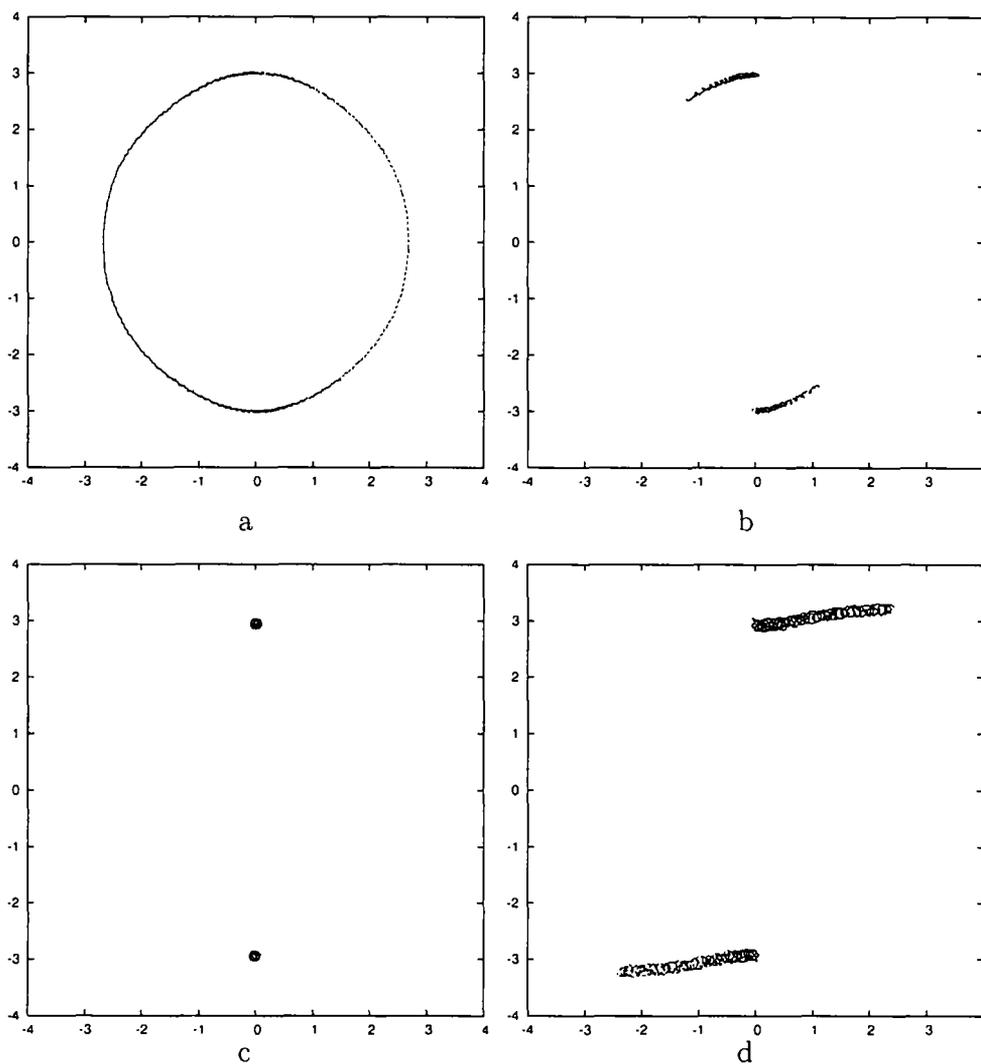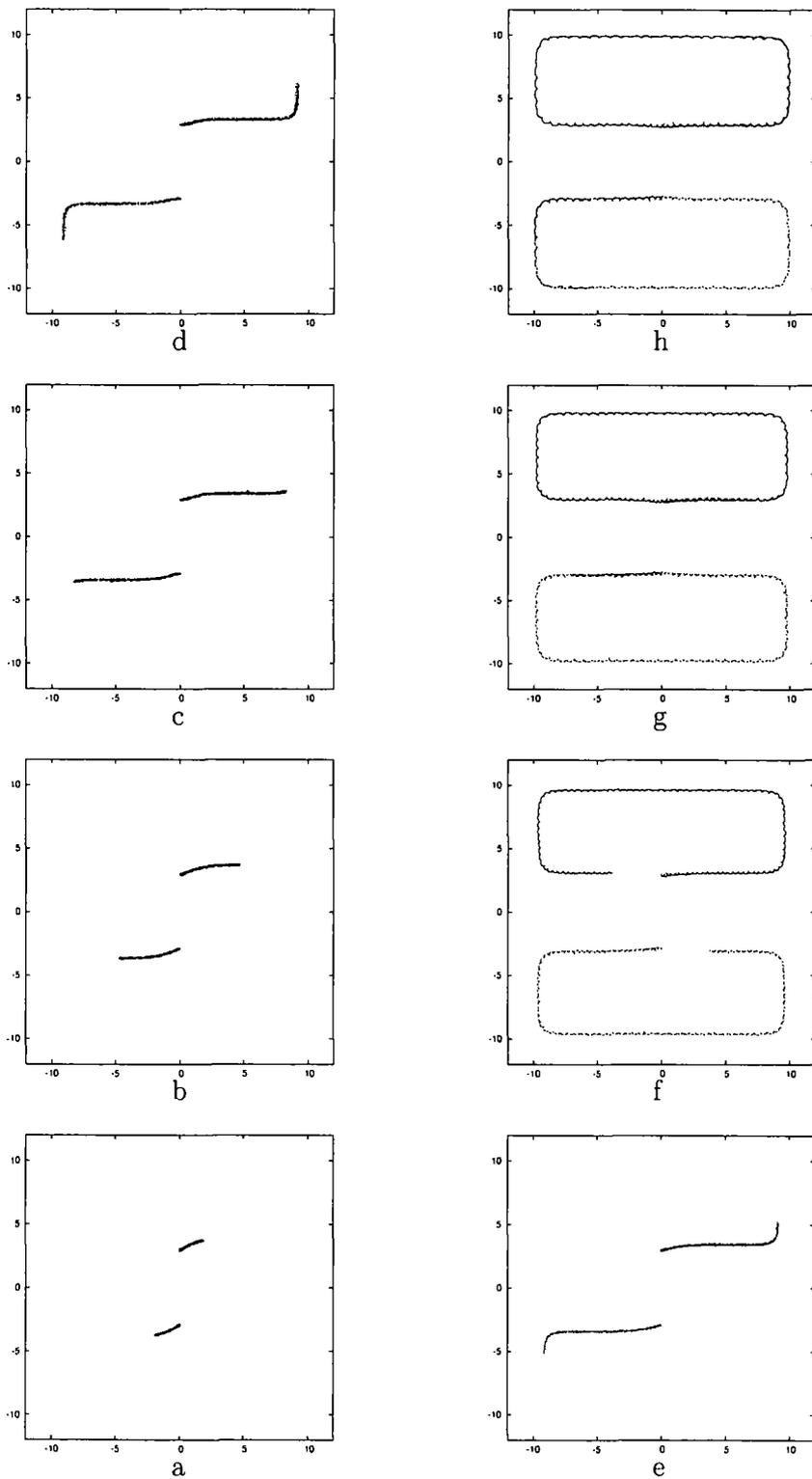
Figure 4.6: Plots of the trajectories of the upper and lower skyrmions for a $d = 6$ skyrmion configuration interacting with a potential barrier of width $b = 2$ (left) and $b = 3$ (right) for various values of Γ: a)0.37, b)0.4, c)0.45, d)0.5, e)0.21, f)0.3, g)0.35, h)0.4, where the horizontal axis represents the x coordinate and the vertical axis the y coordinate.

4.2 Angular momentum

In this section we present the explanation of our results based on the study of the total angular momentum J. The orbital angular momentum l and the total magnetization in the third direction m were calculated through all the simulations using the definitions given by (1.28) and (1.29), defined in Chapter 1. Fig. 4.7 shows a plot of l, m and J for a $d = 6$ two-skyrmion configuration interacting with a potential barrier of width $b = 2$ and $\Gamma = 0.25$. It is clear that $\dot{m} = 0$ throughout but that l and J are not conserved in time.

Figure 4.7: Plots of the orbital angular momentum, l, total magnetization, m, and total angular momentum, $J = l + m$, with time for a potential barrier of width $b = 2$ and $\Gamma = 0.25$, in units of 8π.

In systems involving a two-skyrmion configuration the guiding centre coordinate $\underline{R}$, defined in Chapter 1, corresponds to the centre of the configuration. A calculation of $\underline{R}$ during the barrier simulations has indeed shown that $\underline{R} = 0$. This is expected since the trajectories of the skyrmions in the system are always symmetric with respect to a reflection through the origin and so the centre of the configuration always lies at this point. Considering the definition of the average size of the skyrmions, r, from (1.36), with $\underline{R} = 0$, we note that the orbital angular momentum l and the average size of the skyrmions r are now directly related to each other in this system

by:

$$r^2 = \frac{l}{2\pi Q}.$$ (4.8)

Fig. 4.8 shows a plot of the average skyrmion radius as a function of time for a potential barrier system of width $b = 2$ and $\Gamma = 0.25$. The points at which $r(t)$ approaches its minimum corresponds to the skyrmions traversing the barrier. The point at which they have reached the maximum of the barrier corresponds to the minimum of $r(t)$. Thus as the skyrmions traverse the barrier their average size decreases from its starting value by around 20%. Since the tail of the skyrmion is exponentially localised and this localisation is governed by the potential coefficient parameter γ_3, it is expected that due to the inhomogeneity in γ_3 their size would decrease in the region of larger γ_3, explaining the observed behaviour in l.
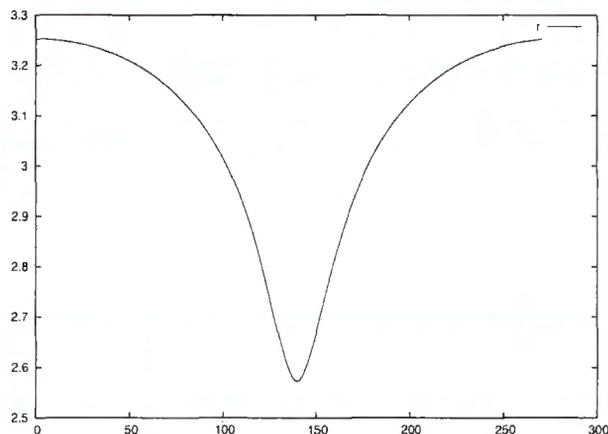
Figure 4.8: Plot of the average skyrmion radius as a function of time for a potential barrier with $b = 2$ and $\Gamma = 0.25$.

Fig. 4.9 shows a plot of l, m and J for a $d = 6$ two-skyrmion configuration interacting with a potential hole of width $b = 2$ and $\Gamma = 0.25$. Again it is clear that $\dot{m} = 0$ throughout but l and J are not conserved in time, analogous to what was seen in the system involving a potential barrier. The guiding centre coordinate, $\underline{R}$, for this system can also be shown to vanish and thus (4.8) is valid also in systems with potential holes. Using this, we can therefore plot $r(t)$ for a potential hole. Fig. 4.10

shows a plot of the average skyrmion radius as a function of time for a potential hole system of width $b = 2$ and $\Gamma = -0.25$. It is clear from the plot that as the skyrmions approach the boundary, asymptotically along the edge of the hole, the average size of the skyrmion increases continually to approximately 3 times its initial size. This is due to the tail of the skyrmions. The skyrmion cannot penetrate the hole, as explained in the previous sections, but its tail can. The exponential localisation of the skyrmions, as explained earlier, is governed by the potential coefficient γ_3. In the region of reduced γ_3, their average size is able to grow and so it continues to increase until they reach the boundary of the system, where they get reflected. In our simulations we saw that following this reflection the skyrmion's size decreased back to its starting value as the system tends to its starting point.

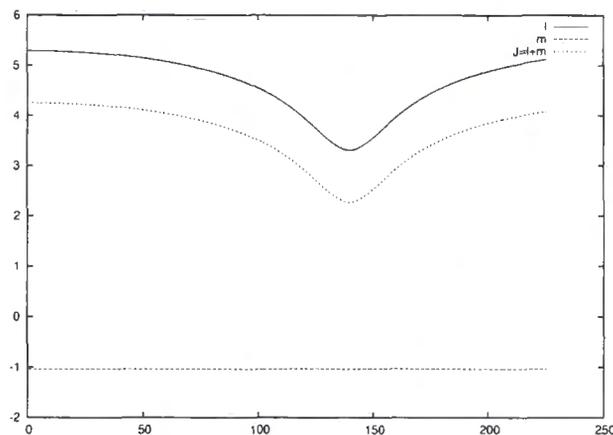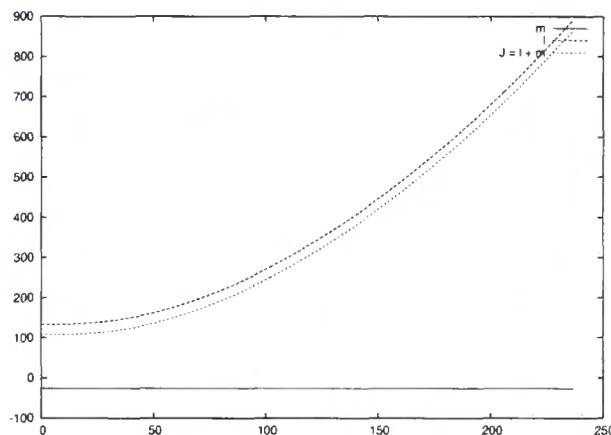Figure 4.9: Plots of the orbital angular momentum, l, total magnetization, m, and total angular momentum, $J = l + m$, with time for a potential hole with b=2 and $\Gamma = -0.25$.

4.3 Further discussion of Angular Momentum

Here we discuss further the apparent non-conservation of J. Assuming the definitions of l, m and hence of J are valid and shown to be true in the free system, we
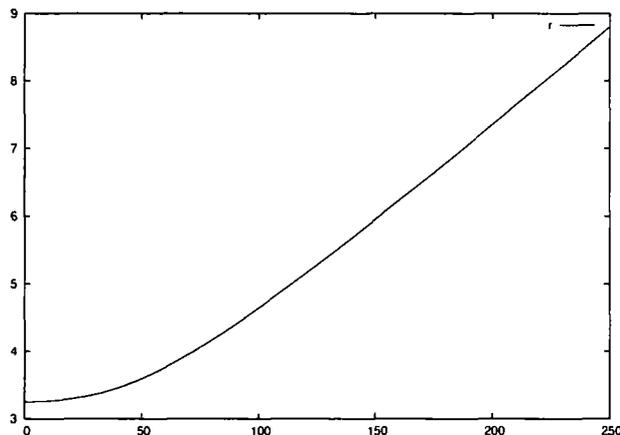
Figure 4.10: Plot of the average skyrmion radius as a function of time for a potential hole with $b = 2$ and $\Gamma = -0.25$.

ask ourselves can we explain this more qualitatively? Let us consider the behaviour of J. The form of $l(t)$ from Fig. 4.7 indicates that $\dot{l} \neq 0$ and hence $\dot{J} \neq 0$. The calculation of l includes only the contribution of the fields but clearly this may, for systems involving obstructions, not be sufficient. We can consider adding an external contribution due to the potential obstruction and see whether this restores J-conservation. How the potential obstructions affect, if at all, the orbital angular momentum needs to be considered. The symmetric obstructions can be written as a contribution to the potential term $V(\phi)$ in terms of Heaviside functions. The potential term and this inhomogeneity, expressed in terms of Heaviside functions, can be written as:

$$V(\phi) = \frac{1}{2}\gamma_3 \left(1 - \phi_3^2\right) + \frac{1}{2}\Gamma \left(1 - \phi_3^2\right) \left[\Theta(y + y_0) - \Theta(y - y_0)\right]. \qquad (4.9)$$

Using the above definition of $V(\phi)$, one can compute the contribution made to l in addition to the fields already computed from (1.28). One needs to construct $\dot{q}$ from its constituent parts as shown in (1.31). Using the properties of the Heaviside functions and their relations to the δ-function, one can show that the potential obstruction's contribution to $\dot{q}$ is given by:

$$\dot{q} = \phi_3 \partial_x \phi_3 \Gamma \left[\delta(y + y_0) - \delta(y - y_0))\right].$$

With this expression for $\dot{q}$ we can evaluate the total rate of change of the orbital angular momentum due to the obstruction:

$$
\begin{aligned}
\dot{l} &= \frac{1}{2} \int_{\mathbb{R}^2} d^2x \, \underline{x}^2 \dot{q} \\
&= \frac{\Gamma}{2} \int_{-\infty}^{\infty} dx \int_{-\infty}^{\infty} \underline{x}^2 \partial_x (\frac{1}{2} \phi_3^2) \left[\delta(y + y_0) - \delta(y - y_0) \right] dy \\
&= \frac{\Gamma}{2} \int_{-\infty}^{\infty} dx \underline{x}^2 \partial_x (\frac{1}{2} \phi_3^2) \Bigg|_{y=y_0}^{y=-y_0} .
\end{aligned}
\tag{4.10}
$$

The integrals in (4.10) have been calculated during each simulation. Fig. 4.11 shows the numerically computed integral contributions due to the obstruction and the numerically calculated derivative of the orbital angular momentum from Fig. 4.7 plotted with respect to time, for a potential barrier with $b = 2$ and $\Gamma = 0.25$.
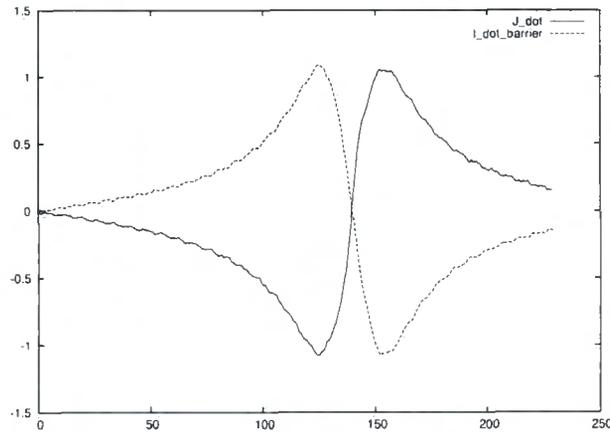
Figure 4.11: Plots of the numerically calculated time derivative of the total angular momentum, $J = l + m$, and the contribution of the barrier to $\dot{l}$ for b=2 and $\Gamma = 0.25$.

It can be seen from the plot that the time evolution of the integral contributions exactly matches that of $\dot{l}$ due to the fields, so that we have:

$$
\begin{aligned}
\dot{l} &= \dot{l}_{fields} + \dot{l}_{barrier} \\
&= \frac{d}{dt} \left[\frac{1}{2} \int_{\mathbb{R}^2} d^2x \, \underline{x}^2 \dot{q} \right] + \frac{\Gamma}{2} \int_{-\infty}^{\infty} dx \, (x^2 + y^2) \, \partial_x (\frac{1}{2} \phi_3^2) \Bigg|_{y=y_0}^{y=-y_0} \\
&\simeq 0.
\end{aligned}
$$

Due to discretisation effects and numerical inaccuracies, the result is not exact but the qualitative features of the integral contributions makes this a very consistent result.
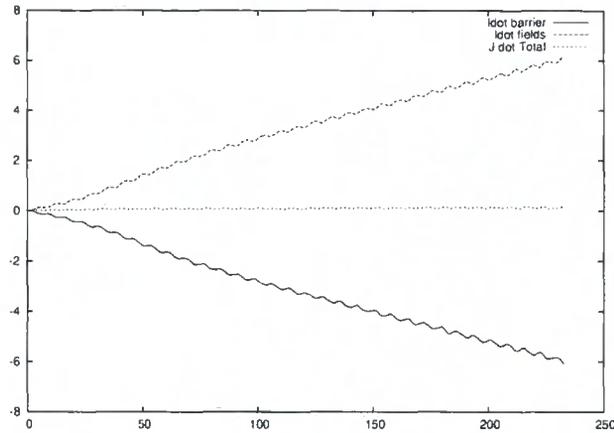
Figure 4.12: Plots of the numerically calculated time derivative of the total angular momentum, $J = l + m$, for the fields and the contribution of the hole to $\dot{l}$ for b=2 and $\Gamma = -0.25$.

Fig. 4.12 shows the numerically computed integral contributions due to the obstruction and the numerically calculated derivative of the orbital angular momentum from Fig. 4.9 plotted with time, for a potential hole with $b = 2$ and $\Gamma = -0.25$. It is clear from these plots that the conservation of the total angular momentum J is restored by the introduction of the terms corresponding to the potential obstructions' contribution to $\dot{l}$.

Chapter 5

Asymmetric Potential

Obstructions

In the previous chapter we presented the results of our investigations into the scattering properties of a skyrmion configuration off various symmetric potential obstructions. We can ask ourselves, how many of the properties of that system are indicative of its symmetric nature? In other words, if the symmetric nature of the system was to disappear, will the dynamics of the skyrmions be greatly changed? Hence in this section we shall discuss the results and analysis of the same skyrmion configuration used in the previous chapter, in the presence of an asymmetric potential obstruction of width b and height or depth Γ. The asymmetric obstruction is introduced into the system in the same manner as the symmetric obstruction where $\gamma_3(x, y)$ of (4.3) in this system can be written as:

$$\gamma_3(x, y) = 1 + \Gamma\Big\{\Theta(-x + x_0)\big[\Theta(y + y_0) - \Theta(y - y_0)\big]\Big\},$$

where $y_0 = b/2$ and $x_0 = 0$. The sign of the additional potential term's coefficient, Γ, determines whether the obstruction is a hole, $\Gamma < 0$, or a barrier, $\Gamma > 0$.

5.1 Potential barrier

In this section we shall illustrate some of the results seen in the potential barrier system for various values of Γ and the barrier width b. The physically interesting
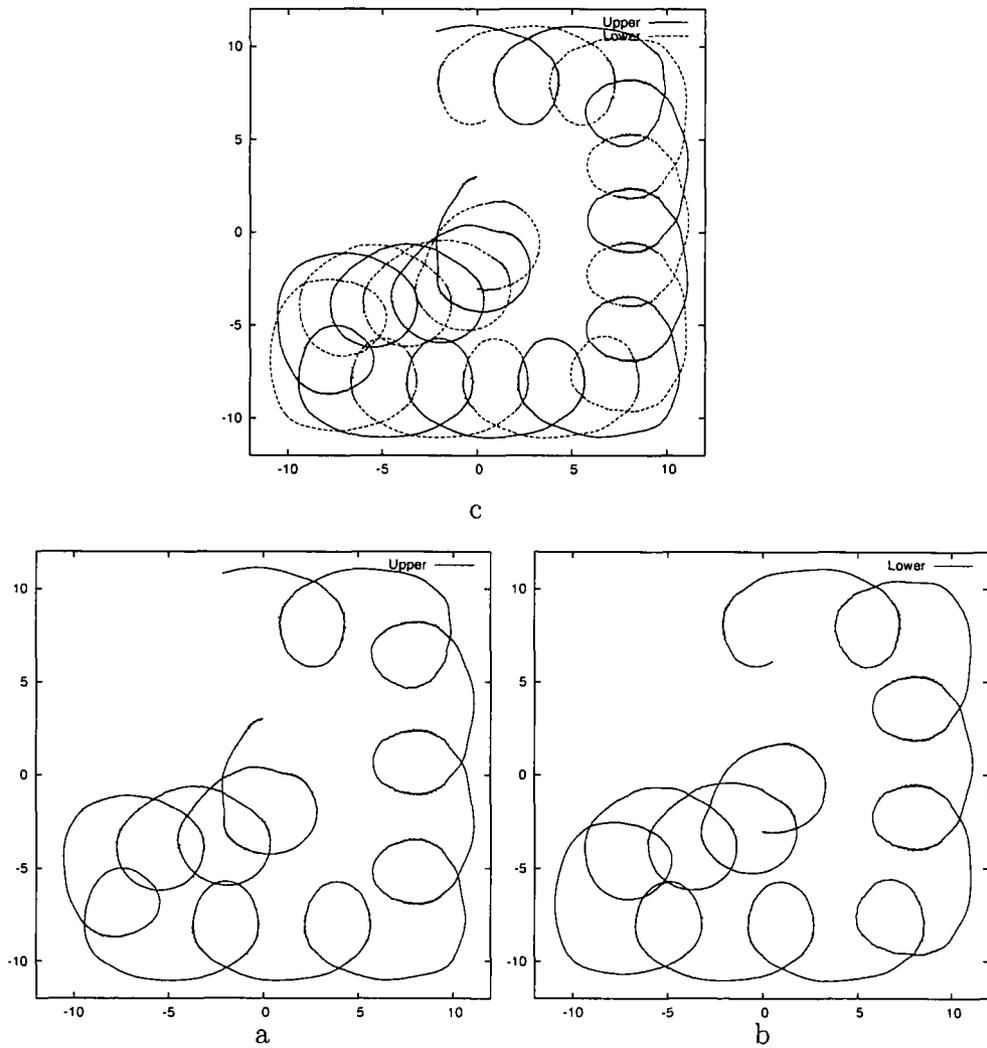
Figure 5.1: Plots of the trajectories of the upper (a) and lower (b) skyrmions in a system with an asymmetric potential barrier of width $b = 2$ and height $\Gamma = 0.25$, where the horizontal axis represents the x coordinate and the vertical axis the y coordinate.

Γ	$E_2/8\pi$	$E_1/8\pi$	$E_B/8\pi$
0.1	2.1298	1.0700	-0.0102
0.2	2.1319	1.0706	-0.0093
0.3	2.1340	1.0713	-0.0086
0.4	2.1361	1.0719	-0.0077
0.5	2.1382	1.0725	-0.0068
1.0	2.1487	1.0757	-0.0027
1.1	2.1508	1.0763	-0.0018
1.2	2.1529	1.0770	-0.0011
1.3	2.1550	1.0776	-0.0002
1.4	2.1571	1.0782	+0.0007
1.5	2.1592	1.0789	+0.0014

Table 5.1: Table showing the variation in the total energy and binding energy for a $d = 6$ two skyrmion configuration interacting with a potential barrier of width $b = 2$ for various values of Γ .

part of these systems is the initial phase of the dynamics, when the skyrmions are alternating between moving 'on' and 'off' the barrier. The motion here is very similar to that seen in the symmetric system. Due to the asymmetry of the system the skyrmions no longer execute a symmetric path about the obstruction. Once the skyrmions have drifted away from the potential barrier they move along the boundary of the system. This element of the dynamics is covered in a separate section 5.1.2.

5.1.1   Initial phase

The analysis of the skyrmion scattering in the barrier system is divided into the sections where the skyrmions are far from the obstruction and when they are executing their circular motion 'on' or near the barrier. The initial phase of the dynamics corresponds to the latter of these two sections. Fig. 5.1 shows multiple plots of a $d = 6$ skyrmion configuration interacting with an asymmetric barrier of width $b = 2$ and depth $\Gamma = 0.25$. The skyrmions centres are initially located at $(0, \pm 3)$ where we refer to the skyrmion initially placed at $(0, 3)$ as the upper skyrmion and $(0, -3)$ as the lower one. Fig. 5.1a and b show the trajectories of the upper and lower skyrmions over a time length of 3500 secs. Fig. 5.1c shows the two trajectories plotted together. It can be seen from the first two plots that initially the two skyrmions try to execute their normal circular motion around each other. As the skyrmions approach the obstruction, their path is deformed due to the barrier. The trajectory of the skyrmions in this system suggests that the skyrmions still form a bound state, for these values of Γ and d. The binding energy of a two-skyrmion configuration in the presence of a potential obstruction is denoted by E_B and was defined in the previous chapter in (4.5). Table 5.1 shows the variation in the binding energies for various values of Γ for a $d = 6$ skyrmion configuration, interacting with a potential barrier of width $b = 2$. Here for $\Gamma = 0.25$ the binding energy of the skyrmions $E_B < 0$ and thus the skyrmions still form a bound state, which the plots in Fig. 5.1 confirm.

In the absence of any obstructions the skyrmions form a bound state. The strength of the bound state is dependent upon the separation between the two

skyrmions. For $d = 6$ the skyrmions are reasonably well separated and the skyrmions are not tightly bound. As the size of the barrier increases the potential obstruction can break the bound state between the skyrmions, for a sufficiently large height. This is evident in table 5.1 where for $\Gamma = 1.4$ the skyrmions are unbound. The breaking of the skyrmion bound state by the potential barrier will be discussed in a later section, 5.1.3. Fig. 5.2 shows the plot of the initial phase of the above system, up to 1500 secs, with a set of labels A-K and 1-3. The labels A-K are reference points used to examine the motion and speed of the skyrmions during this initial phase. The labels 1-3 refer to the different times the skyrmions traverse the barrier. The potential obstruction's position is outlined by the dotted lines appearing on the plot of Fig. 5.2. Although the barrier has been defined in section 5, the lines have been continued for $x > 0$ and for $y > y_0$, $y < -y_0$ for purely illustrative purposes. In order to identify the times at which the skyrmions have entered the barrier region, we have further plotted $x(t)$ and $y(t)$ for the upper skyrmion shown in Fig. 5.3. These plots are labelled with A-K accordingly.

The initial path of the upper skyrmion as it approaches the barrier is A-B. The distance of A-B and the distance of the path over the barrier B-C are comparable. However, the time taken for the skyrmion to travel A-B is $\sim$ 100 secs, whereas to traverse B-C it is $\sim$ 30 secs. If we examine the gradient of $y(t)$ for the upper skyrmion, we can see that the gradient rapidly increases and then decreases as the skyrmions traverse the barrier. The speeding up of the skyrmions as they traverse a potential barrier was seen in the analysis of systems with a symmetric potential obstruction. In the further two scattering paths the times taken to traverse the barrier is $\sim$ 30 secs for F-G, and $\sim$ 30 secs for J-K. Fig. 5.4 shows a plot of the trajectory of the lower skyrmion with the labels A-L and 1-3, where the labels illustrate the same key points as Fig. 5.2. It can be shown that the lower skyrmion traverses the barrier in similar times as the upper skyrmion, for paths 1, 2 and 3. There exists only one discrepancy; the I-J path, where the time take is $\sim$ 35 secs. We believe that this small increase in time is due to an edge effect caused by the barrier.

Fig. 5.5 shows a plot of the skyrmion separation as a function of time, $d(t)$, for
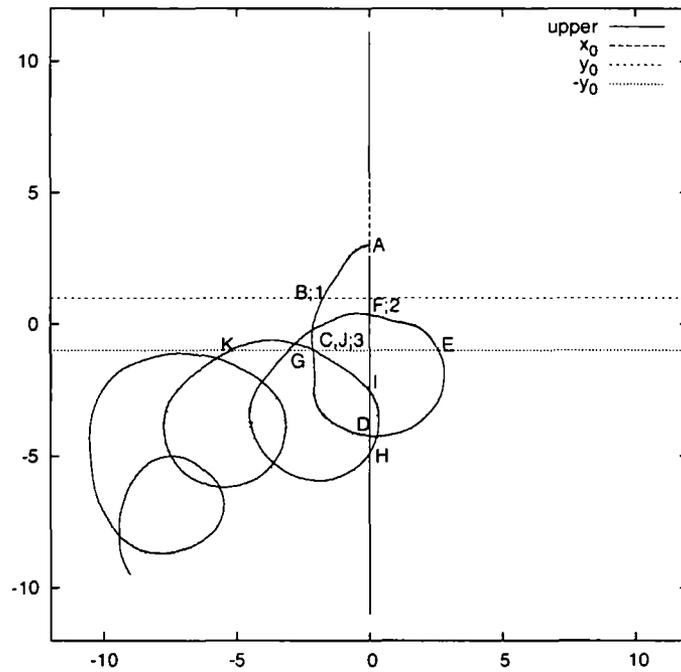
Figure 5.2: Plot of the trajectory for the upper skyrmion of a $d = 6$ configuration interacting with an asymmetric potential barrier of width $b = 2$ and $\Gamma = 0.25$, where the horizontal axis represents the x coordinate and the vertical axis the y coordinate.

the first 1500 secs, with an initial separation of $d = 6$. As the skyrmions move 'on' and 'off' the barrier, the distance of separation decreases and increases accordingly. The minima of $d(t)$ correspond to the times when one of the skyrmions is on the barrier. The skyrmions, initially placed in the attractive channel, compensate for the increase in potential energy by reducing their distance of separation. Once off the barrier the skyrmion configuration returns to its initial state and the skyrmions separate once again. This process repeats with each of the different paths 1-3.

5.1.2 Away from the barrier

Another interesting feature of this system is the way the skyrmions avoid the boundary and potential obstruction after the initial phase described previously. After the transient period where the skyrmions traverse the barrier, they eventually settle down to a steady state where the skyrmion configuration moves about the grid

a

b
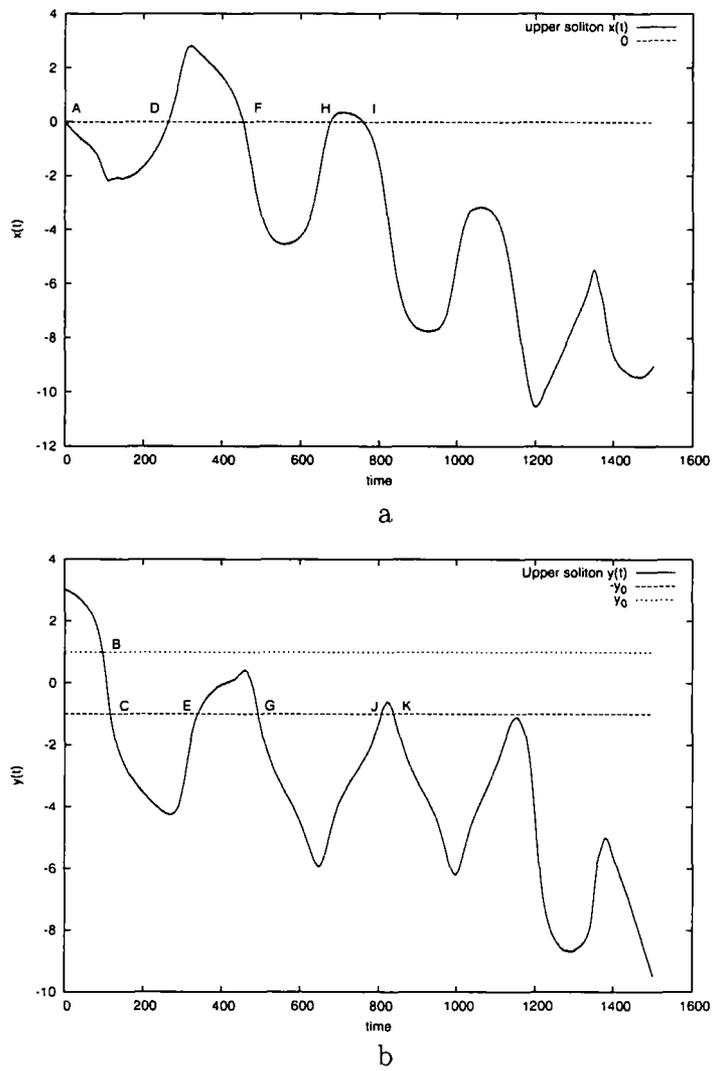
Figure 5.3: Plot $x(t)$ and $y(t)$ for the upper skyrmion in a system with an asymmetric potential barrier of width $b = 2$ and $\Gamma = 0.25$.
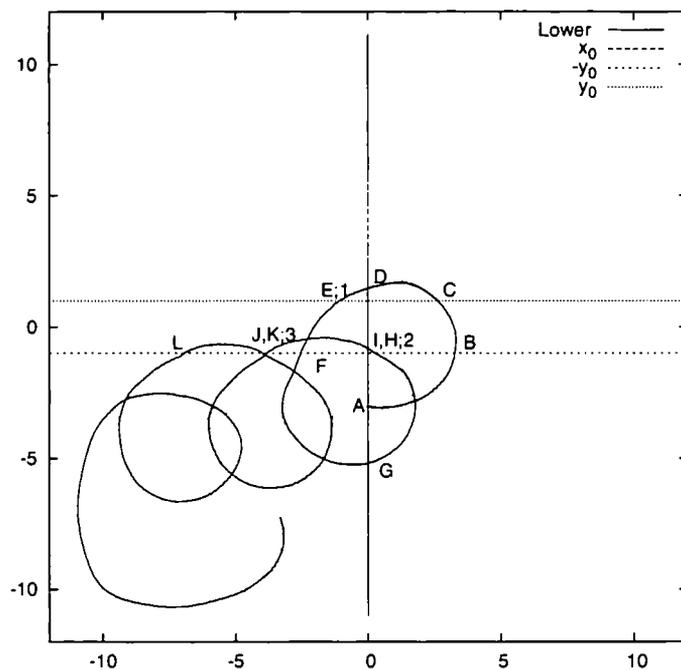
Figure 5.4: Plot of the trajectory for the lower skyrmion of a $d = 6$ skyrmion configuration interacting with an asymmetric potential barrier of width $b = 2$ and $\Gamma = 0.25$, where the horizontal axis represents the x coordinate and the vertical axis the y coordinate.

avoiding the barrier and the boundary. During this steady state the skyrmions continue to execute the circular motion about the configuration centre, when they are close enough to interact. The skyrmions have a strong repulsion from the boundary and keep a certain distance from it. The skyrmions motion in this phase is determined by the boundary. If we increase the size of the boundary, after performing a similar initial phase, the skyrmions continue to move around the edge of the boundary. This is illustrated in Fig. 5.6 which shows the upper skyrmion of the same system of $b = 2$ and $\Gamma = 0.25$, plotted with an identical upper skyrmion in a system with the same values of b and Γ but with a grid size of 291 $\times$ 291 points. The boundary of the two different grid sizes is also shown on Fig. 5.6. The larger grid means that the boundary of the system is further away than for the system with a smaller grid size. This plot confirms that the skyrmions trajectory away from the
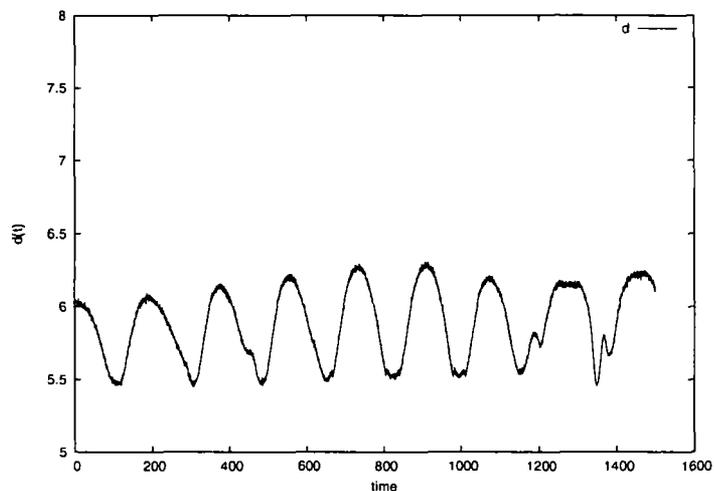
Figure 5.5: Plots of the distance of separation, d, between two skyrmions in a system with an asymmetric potential barrier of width $b = 2$ and $\Gamma = 0.25$.

barrier is dependent upon the boundary. Thus the physically relevant part of the dynamics i.e. the phase unique to the problem of interest, is the initial phase before the skyrmions drift along the boundaries edge. The movement of the skyrmions along the boundaries edge and during its initial interaction with the barrier can be seen in the simulation of the $d = 6$, $b = 2$ and $\Gamma = 0.25$ asymmetric barrier system on the accompanying Cd.

5.1.3   The dynamics variation with Γ and d

In the previous sections we described the general system of a bound skyrmion configuration interacting with a potential barrier. This system was chosen because it illustrated many of the generic features of the skyrmions motion in these systems either in the region near the obstruction or away from it. However, there are a few additional features which exist for only certain values of the barrier height, Γ and distance of skyrmion separation, d and shall be presented here.

In the $d = 6$, $\Gamma = 0.25$ barrier system, we observed that the skyrmions were still bound due to value of the binding energy. This was also reflected in the trajectories
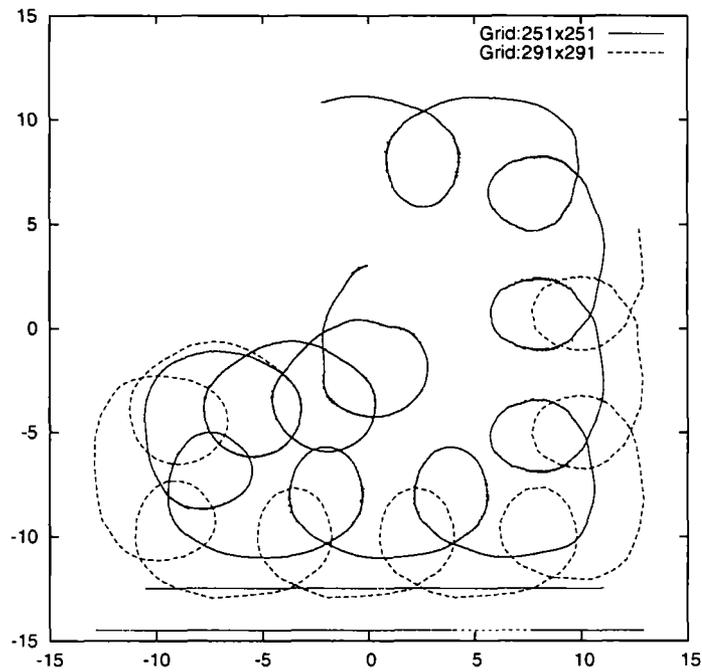
Figure 5.6: Plot of the trajectories of the upper skyrmions, where both skyrmions are initially at $(0, 3)$, in a system with an asymmetric potential barrier of width $b = 2$ and $\Gamma = 0.25$ for grid sizes 251 ×251 and 291 × 291 with the boundary of different grid size shown. The horizontal axis represents the x coordinate and the vertical axis the y coordinate.

of the skyrmions in that system. The skyrmion configurations when $d < 6$, due to the attractive channel, are more tightly bound than the $d = 6$ skyrmions. In systems with small values of Γ, the skyrmions exhibit bound behaviour in both the binding energy and trajectories. Away from the barrier they orbit the boundary of the system as usual. This behaviour is evident in Fig. 5.7 which shows the plots of the trajectories for a skyrmion configuration with $d = 4$ and $d = 5$ for various values of the barrier height Γ. The skyrmions in these systems orbit each other much faster than the looser bound $d = 6$ system. The trajectories of the skyrmions in the $d = 4, 5$ systems are slowly distorted as they execute their motion, identical to the system analysed in section 5.1.1. As the value of Γ increases the distortion of the skyrmion trajectory becomes more pronounced.

For large values of Γ however, the binding energy of these skyrmion configurations can increase and the bound state can be broken. As the barrier height gets larger, the skyrmions are unable to overcome it. In Chapter 4, in the barrier's transition dynamics, it was seen that the skyrmions cannot distinguish between the boundary of the system and very large barriers. We showed that the skyrmions scatter at an angle α relative to the barrier's edge. This angle $\alpha \rightarrow 0$ as Γ gets larger. In the asymmetric system for a sufficiently large barrier, which the skyrmions cannot traverse, the skyrmions begin to move at this angle α. Initially the upper skyrmion starts to move in the direction away from the obstruction but due to the asymmetry of the system it is able to interact with the lower skyrmion and sling shot around the edge of the barrier. This unusual motion can be seen in the simulation of the $d = 6$, $b = 2$ and $\Gamma = 1.5$ barrier system on the accompanying Cd.

The breaking of the bound state between two skyrmions is much more difficult to detect in the asymmetric system than in the symmetric one. In the symmetric system the unbound skyrmions, after being repelled from the barrier, were unable to move into the lower or upper semi-planes because the obstruction was placed over the whole x range. In the asymmetric system the skyrmions are able to move into these semi-planes, as seen in the previous simulation. Thus in the symmetric system the trajectory of an unbound configuration was clearly defined. When two skyrmions are close enough to interact they will perform their usual circular mo-

Figure 5.7: Plots of the trajectories for the upper skyrmions of a system with an asymmetric potential barrier of width $b = 2$ for various values of Γ and d : a) $\Gamma = 0.3$ and $d = 4$, b) $\Gamma = 0.5$ and $d = 4$, c) $\Gamma = 0.5$ and $d = 5$ and d) $\Gamma = 0.8$ and $d = 5$, where the horizontal axis represents the x coordinate and the vertical axis the y coordinate.

tion about the configuration centre. It is difficult therefore to distinguish between states that are unbound or those that are not. The only way one is certain the skyrmions are unbound is to observe states for a sufficiently large values of Γ. In those cases, after the skyrmions have moved around the the obstructions, we observe the skyrmions moving about the boundary of the system singly. Periodically, the skyrmion configuration undergoes the circular motion, when the skyrmions are close enough to interact. This behaviour is evident in the simulation of the $d = 6$, $b = 2$, and $\Gamma = 1.5$ barrier system on the accompanying Cd.

5.2 Potential hole

In Chapter 4 it was observed that the dynamics of the skyrmion configuration interacting with a potential hole was largely dependent upon whether the skyrmions were bound or not. When the skyrmions were unbound they were free to separate from each other. During the separation the skyrmions moved along the edge of the potential hole. This movement continued until the skyrmions reached the physical boundary of the system. It is here that both skyrmions underwent reflection at right angles to the boundary, traversing the hole and then executing an identical trajectory along the opposite edge of the the hole. The skyrmions motion continued back to the starting points where the system looked the same, with just an exchange of the two skyrmions. In the system of an asymmetric obstruction we would expect the previously mentioned symmetric trajectories to no longer persist. As indicated in previous sections, the hole exists on only half of the plane and hence the dynamics in this system should differ from the symmetric system. However, we expect that the factor determining the form of the dynamics should be the same as in the symmetric system, namely, the binding energy, E_B, defined in (4.5). In the following three sections we shall present and discuss the results of a two-skyrmion configuration interacting with a potential hole of varying widths and depths, for a number of different skyrmion separations, d. The different sections are categorised according to whether the skyrmion dynamics is bound, unbound or in between.

$|\Gamma|$	$E_2/8\pi$	$E_1/8\pi$	$E_B/8\pi$
0.1	1.9189	1.0662	-0.2135
0.2	1.9117	1.0630	-0.2143
0.3	1.9046	1.0598	-0.2150
0.4	1.8975	1.0566	-0.2157
0.5	1.8904	1.0534	-0.2164

Table 5.2: Table showing the variation in the total energy and binding energy for a $d = 4$ two-skyrmion configuration interacting with a potential hole of width $b = 2$ for various values of Γ.

5.2.1 Bound dynamics

The skyrmions are initially set up in an attractive channel, which means that for close distances they form a bound state. Thus the states that one would presume to exhibit bound-like behaviour are those corresponding to small distances of separation and small hole depths. This natural observation turns out to be correct and the skyrmions, for small values of the hole depth Γ and distance of skyrmion separation d, do behave as a bound state. Tables 5.2 and 5.3 demonstrate the variation in the binding energy for the skyrmion configuration with the hole depth, for a fixed value of the width $b = 2$. The data shows that as the hole depth gets larger, the binding energy increases. As we will discuss in the later sections, this method of analysis does not include the effect of the hole on the skyrmion during its motion. Moreover, the binding energy is more of a dynamic quantity. Skyrmions are extended objects and in an asymmetric system one of the skyrmions feels the effect of the hole more than the other. Although the energy of each skyrmion can vary, for small values of Γ and d the static binding energy provides a good explanation of the behaviour of the skyrmions.

Fig. 5.8 shows the trajectories of the upper skyrmion of a $d = 4$ configuration interacting with a potential hole for various values of the hole depth Γ. The trajectories show that the skyrmions are still bound, as was suggested by the binding energy analysis. Each plot was taken for a time length of 1000 secs. The behaviour
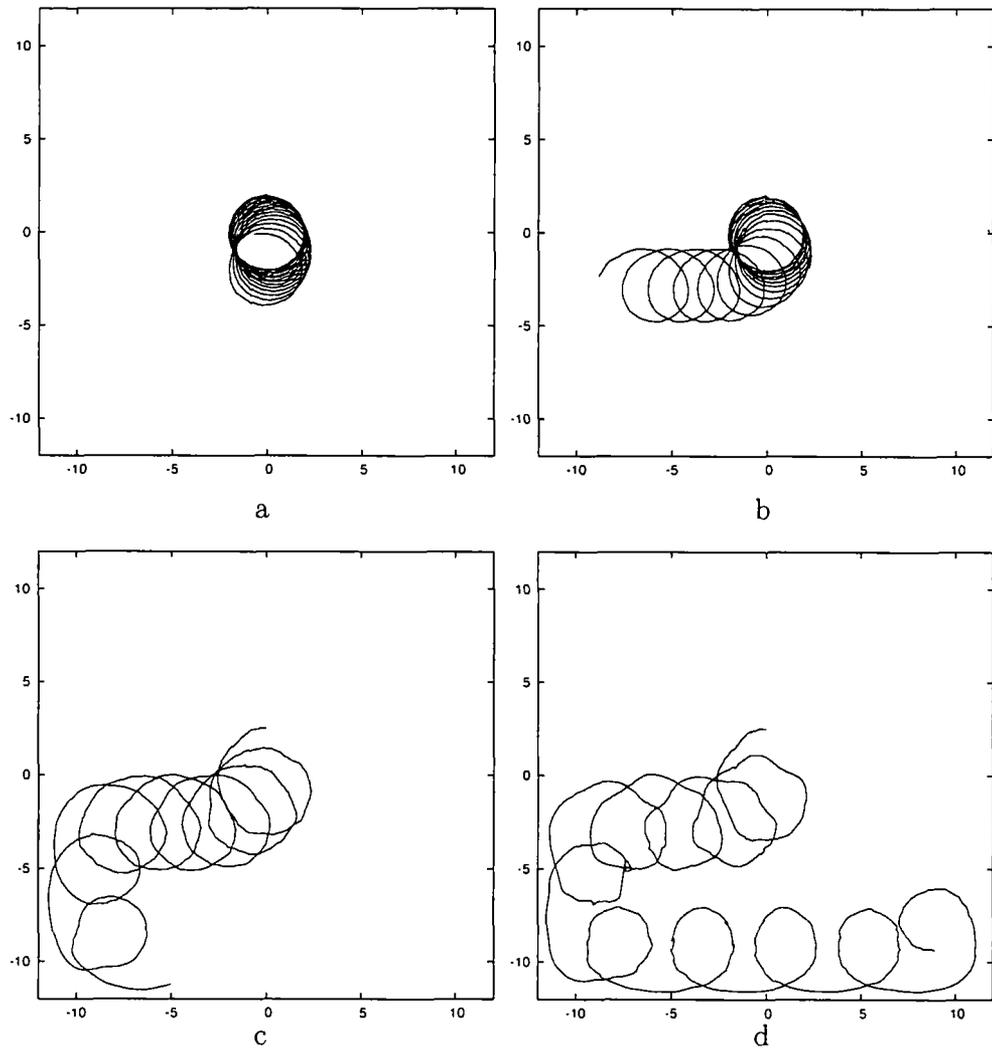
Figure 5.8: Plots of the trajectories for the upper skyrmions in a system with an asymmetric potential hole of width $b = 2$ with $d = 4$ for various values of Γ: a) $\Gamma = -0.1$, b) $\Gamma = -0.2$, c) $\Gamma = -0.4$ and d) $\Gamma = -0.5$, where the horizontal axis represents the x coordinate and the vertical axis the y coordinate.

Figure 5.9: Plot of the trajectories of the upper skyrmions in a system with an asymmetric potential hole of width $b = 2$ with $d = 5$ for various values of Γ: a) $\Gamma = -0.1$, b) $\Gamma = -0.3$, c) $\Gamma = -0.5$ and d) $\Gamma = -0.8$, where the horizontal axis represents the x coordinate and the vertical axis the y coordinate.

$\lvert\Gamma\rvert$	$E_2/8\pi$	$E_1/8\pi$	$E_B/8\pi$
0.1	2.0572	1.0678	-0.0784
0.2	2.0501	1.0661	-0.0821
0.3	2.0429	1.0645	-0.0861
0.5	2.0286	1.0613	-0.094
0.8	2.0072	1.0564	-0.1056
0.9	2.0000	1.0548	-0.1096
1.0	1.9929	1.0532	-0.1164

Table 5.3: Table showing the variation in the total energy and binding energy for a $d = 5$ two-skyrmion configuration interacting with a potential hole of width $b = 2$ for various values of Γ.

of the skyrmions in this system is reminiscent of a sling-shot type motion. Due to the small value of d, the skyrmions are tightly bound. When the skyrmions initially try to execute the normal circular motion, the upper skyrmion, s_1, is moving towards the hole and the lower, s_2, is moving into the space away from the hole. As s_1 approaches the hole its energy is reduced due to its tail interactions with the hole. To conserve the total energy of the system the skyrmions separate a little from each other. This separation increases as s_1 gets into the hole. In the meantime s_2 moves further away from the hole as s_1 approaches it. Classically we know that objects in a conserved system should speed up as they traverse a potential hole. Thus as s_1 enters the hole it quickly traverses it. The interaction between the two skyrmions during this period results in s_2 being sling shot around the hole towards the boundary at infinity. Once both skyrmions are out of the hole the normal motion can resume and the distance between the skyrmions corrects itself, resulting in s_2 being kept to the left of the hole, as we observe it. This motion continues as the skyrmions move along the edge of the hole. The plots corresponding to larger values of $\lvert\Gamma\rvert$ show that the skyrmions have travelled further than for the smaller values of $\lvert\Gamma\rvert$, over the same time length. This is due to the hole depth, where for a larger value of $\lvert\Gamma\rvert$ the skyrmions move faster across the hole, resulting in the increase in the distance travelled in the same amount of time.

Fig. 5.9 shows the trajectories for a $d = 5$ skyrmion configuration interacting with a potential hole of width $b = 2$ for various values of the hole depth Γ. We note the differences between these trajectories and those of the Fig. 5.8. In Fig. 5.9 the skyrmions, although still executing circular motion about the configuration centre, follow a trajectory that is more distorted than the skyrmions of Fig. 5.8. The skyrmions in this system are also able to penetrate the hole more than the skyrmions in the $d = 4$ case. If we examine the skyrmions of both systems during the initial phase, where the upper skyrmion approaches the hole, it can be seen that the ability to penetrate the hole is due to the skyrmions' binding energy. As before, let s_1 be the upper skyrmion and s_2 the lower. The skyrmions try to execute their normal circular motion but as s_1 approaches the hole its energy decreases. It was seen before that the initial binding energies for the $d = 4$ and $d = 5$ system are largely different due to the attractive channel in which they were created. As the energy of one skyrmion decreases the skyrmions separate from each other to conserve energy. Consequently, the binding energy or the interaction between the skyrmions, is reduced. In the system for $d = 4$, the skyrmions do not separate as much from each other as in the $d = 5$ case due to the tightness of the bound state. In the $d = 5$ state the point at which s_1 is in the hole corresponds to the initial maximum separation between the skyrmions. The weak interaction between the skyrmions slows down the distorted rotation about the configuration centre. Thus in Fig. 5.9 as s_1 reaches the hole it moves slower going through it than we would expect it to, since it is a classical object. In comparison with the trajectories of Fig. 5.8, we see that the skyrmions' rate of rotation is not as reduced by the hole as in the $d = 5$ system. Since the skyrmions are much more tightly bound at the start, the effect of the hole upon the interaction between the skyrmions is much less pronounced. Therefore the skyrmion trajectory is less distorted and the skyrmions move faster while traversing the hole.

5.2.2 Transition dynamics

In this section we describe the transition from the bound systems described in the previous section to one in which the skyrmions behave as if they were unbound,
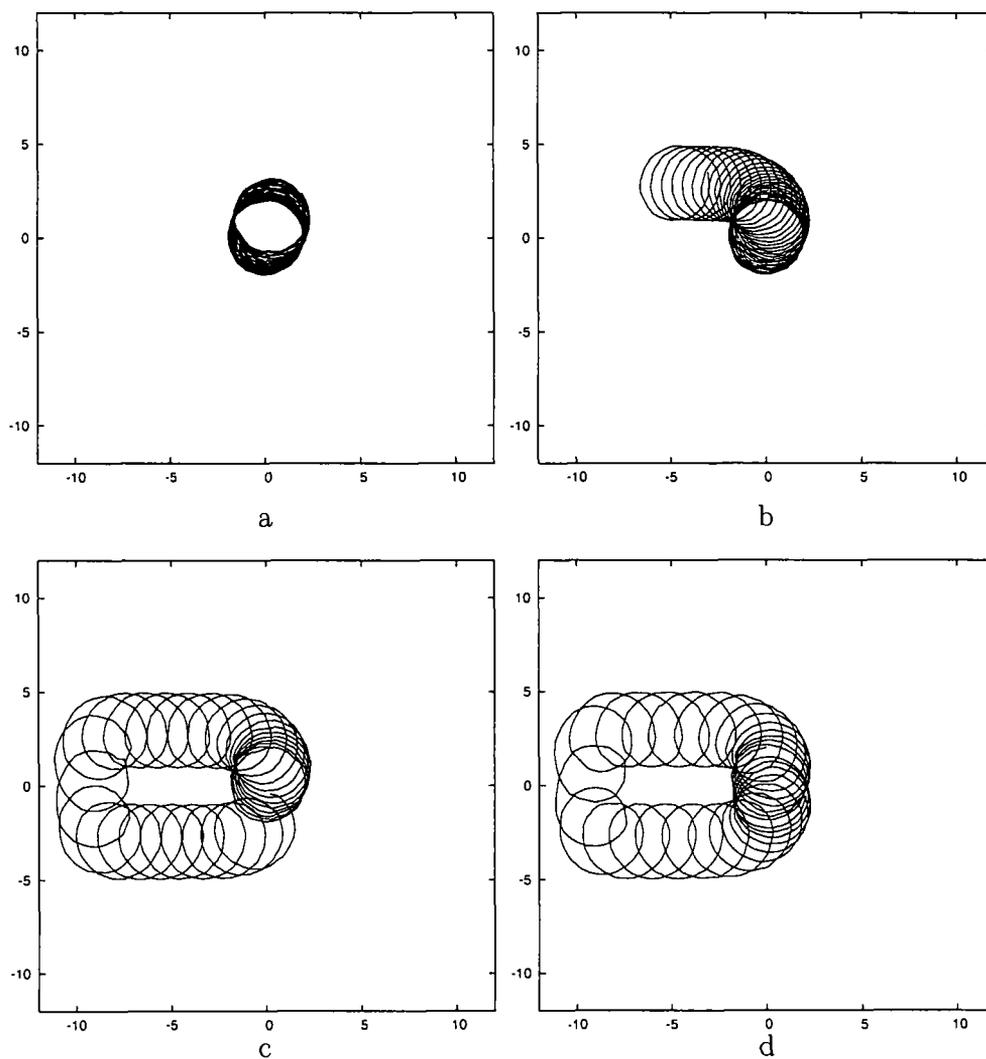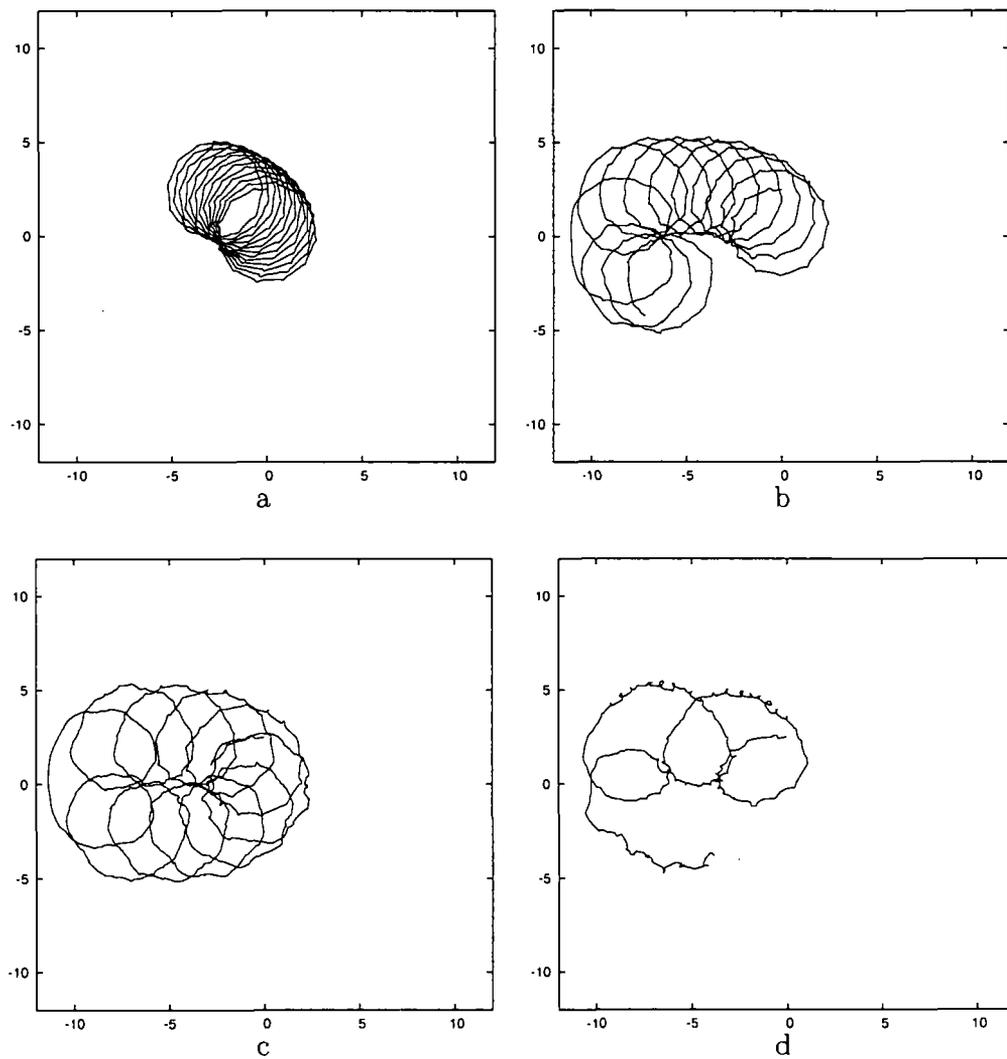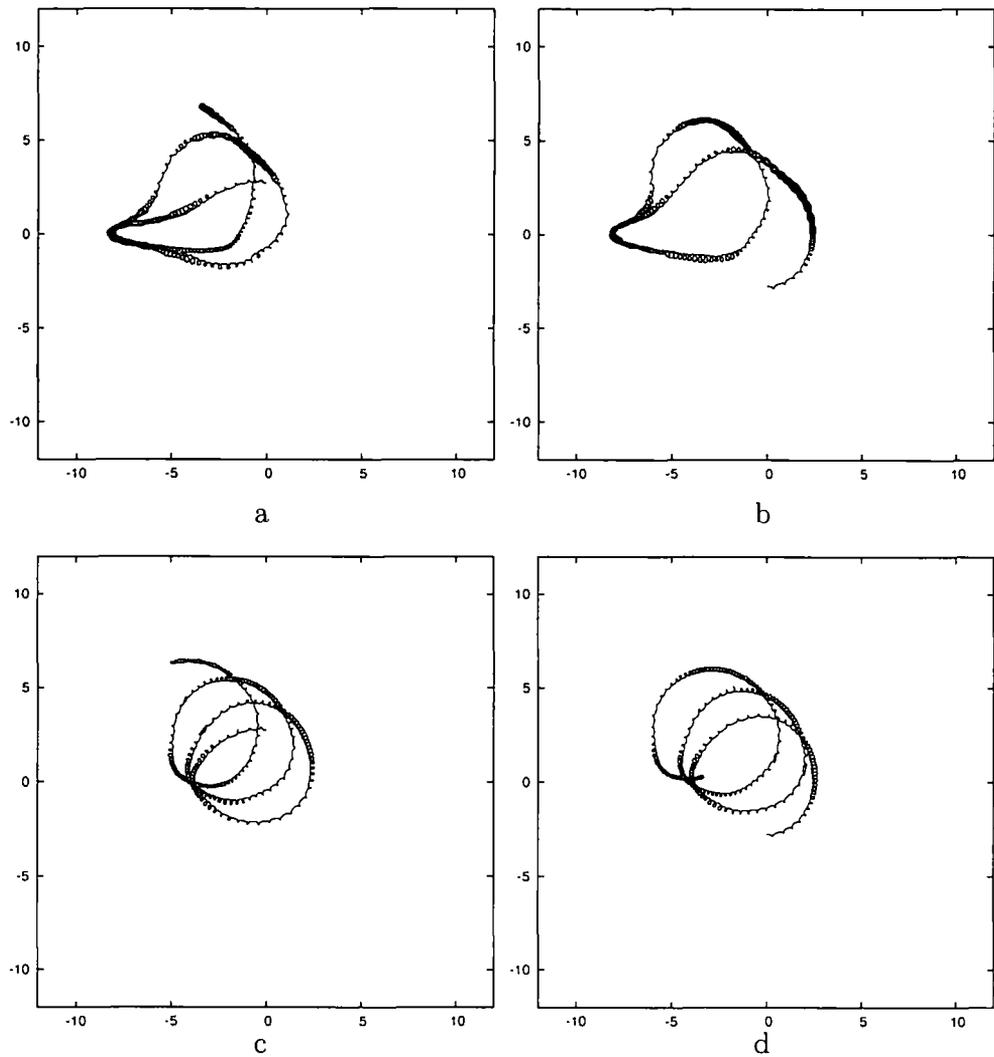
Figure 5.10: Plots of the trajectories for the upper and lower skyrmions of a system with an asymmetric potential hole of width $b = 2$ with $d = 5.5$ for various values of Γ: a) $\Gamma = -0.3$, upper skyrmion , b) $\Gamma = -0.3$, lower skyrmion, c) $\Gamma = -0.2$, upper skyrmion and d) $\Gamma = -0.2$, lower skyrmion, where the horizontal axis represents the x coordinate and the vertical axis the y coordinate.
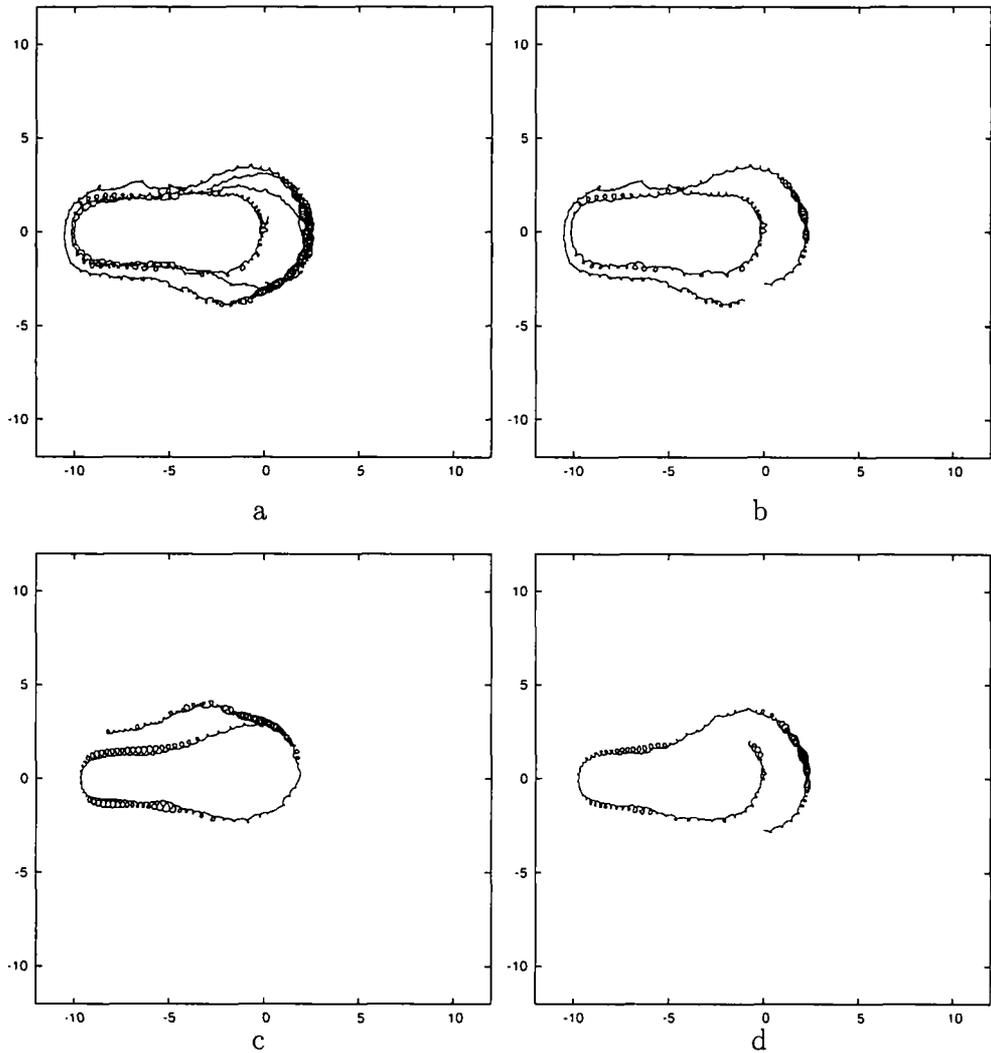
Figure 5.11: Plots of the trajectories for the upper and lower skyrmions of a system with an asymmetric potential hole of width $b = 2$ with $d = 5.5$ for various values of Γ: a) $\Gamma = -0.5$, upper skyrmion, b) $\Gamma = -0.5$, lower skyrmion, c) $\Gamma = -0.4$, upper skyrmion and d) $\Gamma = -0.4$, lower skyrmion, where the horizontal axis represents the x coordinate and the vertical axis the y coordinate.

$|\Gamma|$	$E_2/8\pi$	$E_1/8\pi$	$E_B/8\pi$
0.1	2.1099	1.0683	-0.0267
0.2	2.1058	1.0673	-0.0288
0.3	2.1017	1.0663	-0.0309
0.4	2.0977	1.0652	-0.0327
0.5	2.0936	1.0642	-0.0348

Table 5.4: Table showing the variation in the total energy and binding energy for a $d = 5.5$ two-skyrmion configuration interacting with a potential hole of width $b = 2$ for various values of Γ.

similar to the dynamics seen in the symmetric system of Chapter 4. The transition state is best observed through the variation in Γ for the $d = 5.5$ system. It can be seen from the trajectories in Fig. 5.10 that the skyrmions for $\Gamma = -0.2$ still form a bound state. However, as we increase the hole depth from $\Gamma = -0.2$ to $\Gamma = -0.3$ and further to $\Gamma = -0.5$, the dynamics is no longer bound and the skyrmion trajectories are uncorrelated, as seen in Fig. 5.11. In Fig. 5.10a and b the skyrmions are able to penetrate the hole more than in other previous systems. As one skyrmion penetrates the hole the other remains stationary outside. The skyrmions in this state are just on the point of being broken up by the hole. The skyrmions still remain bound after the upper skyrmion comes out of the hole and this is evident in the trajectory. In the case of $\Gamma = -0.4, -0.5$, the skyrmions behave differently. Here one of the skyrmions moves along the axis of the hole after a small initial circular motion. The other comes to rest after this initial movement. The other skyrmion continues along its path until it reaches the boundary, where it gets reflected and moves back towards the stationary skyrmion. When they get close to each other, the skyrmions violently oscillate due to their mutual interaction. This oscillation is evident in the simulations of the $d = 5.5$ and $\Gamma = -0.3, 0.5$ skyrmion systems on the accompanying Cd and is discussed in section 5.3.

Let us consider the binding energy, E_B, defined in (4.5) to be a function of D, the distance a single skyrmion is from the asymmetric hole in (4.5). By examining the binding energy for the skyrmions in these systems as a function of D, it can

$|\Gamma|$	$E_2/8\pi$	$E_1/8\pi$	$E_B/8\pi$
0.1	2.1256	1.0687	-0.0118
0.2	2.1235	1.0681	-0.0127
0.3	2.1214	1.0675	-0.0136
0.4	2.1292	1.0668	-0.0044
0.5	2.1172	1.0662	-0.0152

Table 5.5: Table showing the variation in the total energy and binding energy for a $d = 6$ two-skyrmion configuration interacting with a potential hole of width $b = 2$ for various values of Γ .

be seen how the skyrmions become unbound as they get close to the hole. Tables 5.2, 5.3, 5.4 and 5.5 provide information on how the single skyrmion energy varies with D. The energies of the two-skyrmion configuration in the presence of a hole of depth $\Gamma = -0.4$ is $E_2 = 2.0977/8\pi$ and for $\Gamma = -0.5$ is $E_2 = 2.0936/8\pi$. Tables 5.6 and 5.7 show how the binding energy of the skyrmion configuration varies when one of the skyrmions approaches the hole. It is clear that when the skyrmions, in the case of $\Gamma = -0.4$, get near $D = 1$ the binding energy of their configuration becomes positive and the skyrmions are no longer bound. Thus as the skyrmion approaches the hole, after the initial circular motion, its starts to feel the effect of the hole. To conserve energy the skyrmions must increase their distance of separation. In order to do this, the upper skyrmion moves along the edge of the hole. The more the skyrmion feels the hole the more the configuration separates. As the binding energy increases the skyrmions interact less and the upper skyrmion is free to move along the edge of the hole towards the boundary. After the reflection from the boundary the skyrmion speeds up traversing the obstruction, moving towards the opposite edge of the hole. This process then repeats itself; when the skyrmion reaches the stationary one it interacts with it causing the the stationary skyrmion to begin moving. The previously moving skyrmion now comes to rest.

The initial distance of closest approach of the upper skyrmion can be estimated from our dynamic binding energy arguments. In the $\Gamma = -0.4$ system, the closest distance the skyrmion reaches, based upon the trajectory, is approximately $D = 1.3$.

D	$E_1/8\pi$	$E_B/8\pi$
2.5	1.0623	-0.0269
2.0	1.0566	-0.0155
1.5	1.0503	-0.0029
1.0	1.0458	+0.0061
0.5	1.0432	+0.0072

Table 5.6: Table showing the variation in the binding energy for a $\Gamma = -0.4$ hole of width $b = 2$ for various values of the single skyrmion distance from the hole D.

D	$E_1/8\pi$	$E_B/8\pi$
2.5	1.0613	-0.029
2.0	1.0534	-0.0132
1.5	1.0455	+0.0026

Table 5.7: Table showing the variation in the binding energy for a $\Gamma = -0.5$ hole of width $b = 2$ for various values of the single skyrmion distance from the hole D.

Comparing this with table 5.6, we can see that the transition point occurs between $D = 1.5$ and $D = 1$. Based upon the numerical values of each, the transition point is closer to 1.5 than 1. In the $\Gamma = -0.5$ case, the closest distance is about $D = 1.75$, based upon the trajectory. Estimating this distance from the energetics, we see that the transition point occurs between $D = 2$ and $D = 1.5$, with it being nearer to 1.5. Thus from just energetic arguments we have a reasonable estimate of the closest distance the skyrmion can initially get to the hole.

5.2.3   Unbound dynamics

It was evident in the previous section that as $|\Gamma|$ increases, for a given value of d, the skyrmions' trajectories change. The skyrmions cease to behave as a bound state and the behaviour of the two skyrmions becomes uncorrelated. Here we discuss the dynamics of the skyrmion configurations for which the given value of Γ and d result in a strongly unbound set of skyrmions. Fig. 5.12 presents the plots of the trajectories of the upper and lower skyrmions in a system with an asymmetric potential hole of width $b = 2$ and depth $\Gamma = -0.25$, for an initial skyrmion separation of $d = 6$. Similar dynamics have already been seen for the larger values of $|\Gamma|$ in the $d = 5.5$ system. According to the static binding energy the skyrmions are initially bound. As they approach the hole they become unbound due to their interaction with the hole. The upper skyrmion, s_1, moves asymptotically along the edge of the hole. The lower skyrmion, s_2, comes to rest after the initial movement. As the skyrmions separate from each other some internal modes of the skyrmions become excited. The excitation of these internal modes and the oscillations persist until the skyrmions reach a critical distance of separation. Beyond this critical distance the skyrmions cease to oscillate but the stationary skyrmion, s_2, proceeds to have an internal motion about its centre. The energy density of the skyrmion can be best described as an inverted cone. The energy gained by s_2 due to the separation of the skyrmions, results in motion along the edge of the cone. A small lump of energy is seen to move about the rim of the cone during the simulations. Once s_1 is reflected from the boundary and moves back along the axis of the hole towards s_2, there exists another critical distance where the skyrmions begin to undergo similar,
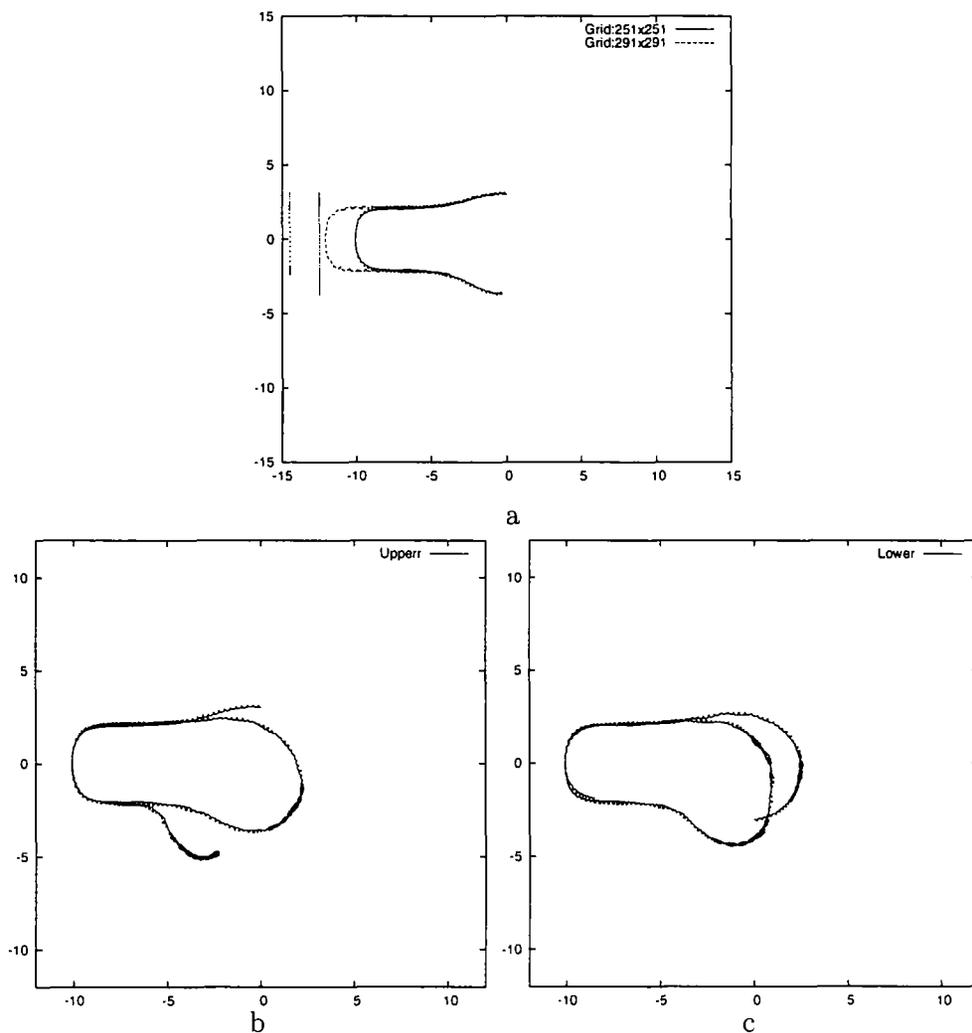
Figure 5.12: Plots of the trajectories of the upper and lower skyrmions in for a $d = 6$ configuration interacting with an asymmetric potential hole of width $b = 2$ and $\Gamma = -0.25$. The upper plot is that of the same system, plotted over a smaller time scale showing the upper skyrmions in system of grid size 251×251 and 291×291 with the boundary of each different grid size shown. The horizontal axis represents the x coordinate and the vertical axis the y coordinate.

if not identical, oscillations. An example of such skyrmion oscillations can be seen in the simulations of the $d = 5.5$ and $\Gamma = -0.5$ system and in also the $d = 6$ and $\Gamma = -0.25$ system on the accompanying Cd.

In the section on the potential barrier system we examined the effect of increasing the bounding box of the simulation. It was found that the skyrmions trajectory away from the obstruction was uniquely determined by the boundary. In the potential hole system the boundary once again determines the dynamics of the skyrmions. The skyrmions in such a system often reach the boundary where they get reflected. If identical skyrmions are put into a system with a larger grid, the skyrmions undergo a reflection from the boundary at a later time than for a system of a smaller grid. This is evident from Fig. 5.12, where the upper plot shows the skyrmions in identical systems for two different grid sizes, where the boundary of the two different grid sizes is shown on the plot.

5.3 Angular Momentum

In this chapter we have considered the scattering of a skyrmion configuration off an asymmetric obstruction, similar to the symmetric obstructions of Chapter 4, except now the obstruction no longer exists for $x > 0$. In this section we shall derive the contributions the potential obstructions make to the derivative of the orbital angular momentum l. We shall also discuss the trends seen in the data obtained for the orbital angular momentum, l. It will be seen that the time variation in l can be decomposed into the behaviour of the average size of the skyrmions, r, and the modulus of the skyrmion guiding centre, $\underline{R}$, both defined in Chapter 2. It was noted in potential hole section that the simulations of the skyrmions in the transition dynamics exhibit oscillations in the energy density. Here we shall show that these oscillations play a significant role in the conservation of the orbital angular momentum.

5.3.1 Asymmetric potential obstructions contribution to l

The potential obstructions are introduced as an inhomogeneity in the potential term's, $V(\underline{\phi})$, coefficient γ_3. The obstructions can be defined more concisely if they are written using Heaviside functions defined previously. In this formalism we can rewrite the approximation of the obstruction as:

$$V(\underline{\phi}) = \frac{1}{2}\left(1 - \phi_3^2\right) + \frac{1}{2}\Gamma\left(1 - \phi_3^2\right)\left\{\Theta(-x + x_0)\left[\Theta(y + y_0) - \Theta(y - y_0)\right]\right\}.$$

We now proceed, as in Chapter 4, to calculate the contribution the obstruction makes to $\dot{q}$:

$$
\begin{aligned}
\dot{q}_{obs} &= -\epsilon_{ij}\partial_i\left(\frac{\delta V(\underline{\phi})}{\delta\underline{\phi}}\cdot\partial_j\underline{\phi}\right) \\
&= -\epsilon_{\mu\nu}\partial_\mu\left(-\phi_3\partial_\nu\phi_3\left(1 + \Gamma\Theta(-x + x_0)\left[\Theta(y + y_0) - \Theta(y - y_0)\right]\right)\right).
\end{aligned}
$$

Using the properties of the Heaviside functions and noticing some cancellations, the above can be rewritten as:

$$
\begin{aligned}
\dot{q}_{obs} &= -\phi_3\partial_y\phi_3\left(\Gamma\delta(-x + x_0)\left[\Theta(y + y_0) - \Theta(y - y_0)\right]\right) \\
&\quad + \phi_3\partial_x\phi_3\left(\Gamma\Theta(-x + x_0)\left[\delta(y + y_0) - \delta(y - y_0)\right]\right)
\end{aligned}
$$

The time derivative of the orbital angular momentum is defined in Chapter 2 by (1.33). If the above is inserted into (1.33), then an expression for the contribution that the asymmetric potential obstruction makes to l can be found:

$$
\begin{aligned}
\dot{l}_{obs} &= \frac{1}{2}\int_{\mathbb{R}^2} d^2x\,\underline{x}^2\dot{q}_{obs} \\
&= -\frac{\Gamma}{2}\int_{\mathbb{R}^2} d^2x\,\underline{x}^2\partial_y(\frac{1}{2}\phi_3^2)\left(\delta(-x + x_0)\left[\Theta(y + y_0) - \Theta(y - y_0)\right]\right) \\
&\quad + \frac{\Gamma}{2}\int_{\mathbb{R}^2} d^2x\,\underline{x}^2\partial_x(\frac{1}{2}\phi_3^2)\Theta(-x + x_0)\delta(y + y_0) \\
&\quad - \frac{\Gamma}{2}\int_{\mathbb{R}^2} d^2x\,\underline{x}^2\partial_x(\frac{1}{2}\phi_3^2)\Theta(-x + x_0)\delta(y - y_0).
\end{aligned}
$$

Where we can define:

$$\dot{l}_y = -\frac{\Gamma}{2}\int_{\mathbb{R}^2} d^2x\underline{x}^2\partial_y(\frac{1}{2}\phi_3^2)\left(\delta(-x + x_0)\left[\Theta(y + y_0) - \Theta(y - y_0)\right]\right). \tag{5.1}$$

and:

$$
\dot{l}_x \;=\; \frac{\Gamma}{2}\int_{\mathbb{R}^2} d^2x\, \underline{x}^2 \partial_x(\tfrac{1}{2}\phi_3^2)\Theta(-x+x_0)\delta(y+y_0)
$$
$$
-\; \frac{\Gamma}{2}\int_{\mathbb{R}^2} d^2x\, \underline{x}^2 \partial_x(\tfrac{1}{2}\phi_3^2)\Theta(-x+x_0)\delta(y-y_0). \tag{5.2}
$$

Performing the integrals over the delta functions in (5.1) gives:

$$
\dot{l}_y = -\frac{\pm\Gamma}{2}\int_{-\infty}^{\infty} dy\, \underline{x}^2 \partial_y(\tfrac{1}{2}\phi_3^2)\big[\Theta(y+y_0)-\Theta(y-y_0)\big]\Big|_{x=x_0}.
$$

The Heaviside step functions provide a condition on the lower limits of the integrals in $\dot{l}_y$ of $\pm y_0$, such that:

$$
\dot{l}_y = \frac{\Gamma}{2}\int_{y_0}^{\infty} dy\, \underline{x}^2 \partial_y(\tfrac{1}{2}\phi_3^2)\Big|_{x=x_0} - \frac{\Gamma}{2}\int_{-y_0}^{\infty} dy\, \underline{x}^2 \partial_y(\tfrac{1}{2}\phi_3^2)\Big|_{x=x_0}.
$$

Applying the same analysis to (5.2) provides an upper bound on both integrals, namely $x=x_0$

$$
\dot{l}_x \;=\; \frac{\Gamma}{2}\int_{-\infty}^{x_0} dx\, \underline{x}^2 \partial_x(\tfrac{1}{2}\phi_3^2)\Big|_{y=-y_0} - \frac{\Gamma}{2}\int_{-\infty}^{x_0} dx\, \underline{x}^2 \partial_x(\tfrac{1}{2}\phi_3^2)\Big|_{y=y_0}.
$$

Combining both of these expressions, $\dot{l}_x$ and $\dot{l}_y$, the overall contribution of the asymmetric obstruction to $\dot{l}$, is given by:

$$
\begin{aligned}
\dot{l}_{obs} &= \dot{l}_x + \dot{l}_y \\
&= \frac{\Gamma}{2}\int_{-\infty}^{x_0} dx\, \underline{x}^2 \partial_x(\tfrac{1}{2}\phi_3^2)\Big|_{y=-y_0} - \frac{\Gamma}{2}\int_{-\infty}^{x_0} dx\, \underline{x}^2 \partial_x(\tfrac{1}{2}\phi_3^2)\Big|_{y=y_0} \\
&\quad + \frac{\Gamma}{2}\int_{y_0}^{\infty} dy\, \underline{x}^2 \partial_y(\tfrac{1}{2}\phi_3^2)\Big|_{x=x_0} - \frac{\Gamma}{2}\int_{-y_0}^{\infty} dy\, \underline{x}^2 \partial_y(\tfrac{1}{2}\phi_3^2)\Big|_{x=x_0} \\
&= \frac{1}{2}\int_{\mathbb{R}^2} d^2x\, \underline{x}^2 \dot{q}_{obs}.
\end{aligned} \tag{5.3}
$$

5.3.2 Examination of J and $\dot{J}$

In any system the total angular momentum, $J = l + m$, should be conserved. However, it was discovered in Chapter 4 that for scattering processes in Landau-Lifshitz models the total angular momentum, as defined by (1.28), is not conserved. On further examination it was found that throughout all the simulations, the total

magnetization in the third direction, m, is well conserved and it is the orbital angular momentum, l, which is not conserved with time. In the asymmetric system such a situation presents itself again, where the total angular momentum is not conserved due to the non-conservation of the orbital angular momentum (1.28), denoted l_{fields}. The non-conservation of J is apparent in the plots of Fig. 5.13. Both of these plots show the total angular momentum, $J = l + m$ and its components, for a $d = 6$ skyrmion configuration, interacting with a potential hole or barrier with $\Gamma = \pm 0.25$. Here it is evident that for either a hole or a barrier the total angular momentum is not conserved due to the non-conservation of l, since m is well conserved throughout. Before analysing this apparent non-conservation of J we shall firstly discuss the general behaviour of l and hence J, during the simulations.

The time evolution of l, as formulated by Papanicolaou and Tomaras [26], provides us with an insight into the behaviour of the skyrmions during the simulations. It was already seen in Chapters 2 and 4 that the average skyrmion size, r and the guiding centre coordinate, $\underline{R}$, can be related to the orbital angular momentum, l, by :

$$r^2 = \frac{l}{2\pi Q} - \underline{R}^2,$$

or

$$l = 2\pi Q\{r^2 + \underline{R}^2\}.$$

The guiding centre coordinate, $\underline{R}$, for a single skyrmion system provides the location of the skyrmion centre. In the case of a two-skyrmion configuration, $\underline{R}$ provides the position of the centre of the configuration. The initial placement of the skyrmions results in the centre of the configuration nearly positioned at (0,0). In the case of a hole or barrier, the asymmetry of the system results in the position of the configuration centre becoming a function of time. How it varies during the simulation depends on the system. In the case of a potential barrier the skyrmions collectively move about the system. Therefore as the skyrmions begin to move, $\underline{R}$ deviates from $(0,0)$ and $|\underline{R}|$ steadily increases. $|\underline{R}|$ continues to increase until the skyrmions reach the boundary of the system. As the skyrmions orbit the boundary, $|\underline{R}|$ slowly increases and decreases as the skyrmions move towards and away from the boundary. If we consider the behaviour of l as corresponding to the dual behaviour
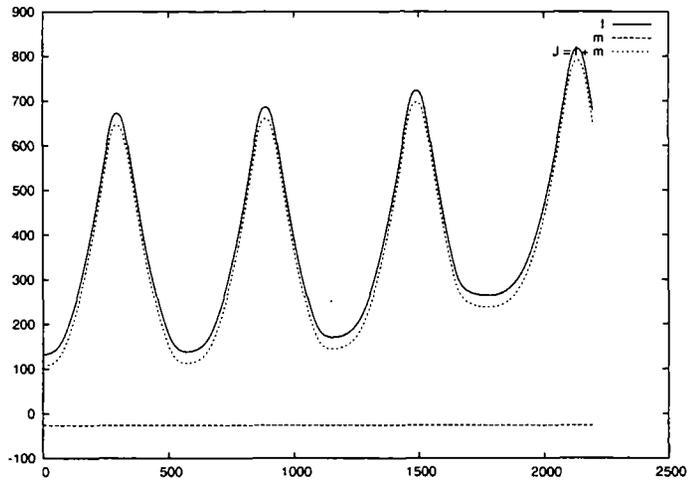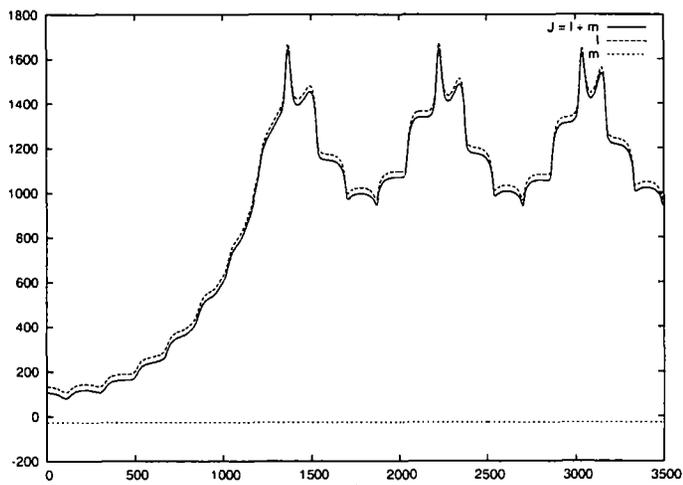
Figure 5.13: Plots of the total angular momentum, $J = l + m$, and its components as a function of time for a $d = 6$ skyrmion configuration interacting with a potential hole or barrier for $\Gamma = \pm 0.25$: a) hole and b) barrier.

of the quantities r and $\underline{R}$, then as $|\underline{R}|$ steadily increases, so does l. This overall trend in $|\underline{R}|$ is evident in Fig. 5.13a which clearly shows l steadily increasing with time. In the case of a potential hole we can use similar analysis. Fig. 5.13b shows a plot of the orbital angular momentum for potential hole with $\Gamma = 0.25$. Here the increase in l, is much larger than in the case of the barrier system. In this particular system, the configuration centre moves much more than the barrier system and is periodic. This is evident if we recall the dynamics of the skyrmions in this system. Here one of the skyrmions moves along the edge of the hole while the other remains stationary. Thus the centre of the configuration moves away from $(0,0)$ as the skyrmion approaches the boundary. After the skyrmion is reflected, $\underline{R}$ begins to approach $(0,0)$ once again. However, due to the dynamics $\underline{R}$ does not reach $(0,0)$ again. This periodic increase and decrease in $|\underline{R}|$ matches the behaviour of l for the potential hole.

It was noted in Chapter 4 that the behaviour of the orbital angular momentum, with $\underline{R} = 0$, could be understood exactly in terms of the behaviour of r. The skyrmions tail is governed by value of the potential coefficient, γ_3 and the regions where this is modified means the skyrmion tails become modified. As the skyrmion moves into a region for which $\gamma_3 \rightarrow 1 + \Gamma$, its tail contracts or expands. This continued shrinking and expansion, as the skyrmion moves on and off the potential obstructions, results in a time oscillation of r^2. In Fig. 5.13a the behaviour of r is evident in the time dependence of l. The periodic small oscillations occurring in l, correspond to the time variation of r. It was seen in the symmetric barrier system that as the skyrmion configuration is 'on' the obstruction, the skyrmions reduce their distance of separation. In the asymmetric barrier system the small oscillations in l are caused by this behaviour. The interplay between the time oscillation in r^2 and the gradual increase in $\underline{R}^2$ sufficiently accounts for the observed behaviour of the angular momentum.

It has already been noted that the total angular momentum, J, is not conserved. It was discovered in Chapter 4 that by examining how the potential obstructions were constructed, an analytical expression for the contribution the potential obstructions make to the time derivative of the orbital angular momentum, $\dot{l}$, was found. These expressions were in the form of two integrals which were calculated

during the simulations. When the contribution of the potential obstructions was included in the expression for $\dot{J}$, the conservation of total angular momentum was restored. These same integrals, for the asymmetric obstruction, were computed in section 5.3.1 and were calculated throughout the simulations. The contribution the obstruction makes to the derivative of the total angular momentum, $\dot{J}_{tot}$, is denoted $\dot{l}_{obs}$. The contribution to $\dot{J}_{tot}$ from the fields, given by (1.28), is denoted $\dot{l}_{fields}$. Therefore the overall conservation of the total angular momentum can be written:

$$\dot{J}_{tot} = \dot{l}_{obs} + \dot{l}_{fields},$$

where there is no contribution due to the total magnetization in the third direction, m, since throughout $\dot{m} = 0$. Fig. 5.14 shows the plots of the total angular momentum, $\dot{J}_{tot} = \dot{l}_{obs} + \dot{l}_{fields}$ for two different systems. In Fig. 5.14a, $\dot{l}_{obs}$, $\dot{l}_{fields}$ and $\dot{J}_{tot}$ are plotted for a $d = 6$ skyrmion configuration interacting with a potential barrier of width $b = 2$ and height $\Gamma = 0.25$. It can seen from the plot that the overall behaviour of $\dot{l}_{fields}$ and $\dot{l}_{obs}$ match, resulting in $\dot{J}_{tot}$ being well conserved in time. It can be seen in the latter stages of the plot that this conservation is slightly destroyed. The skyrmions at this point start to appreciably interact with the boundary of the system. It is due to these boundary effects that $\dot{J}_{tot} \neq 0$ at these points. Fig. 5.14b shows the corresponding plot for a $d = 5$ skyrmion configuration interacting with potential hole of depth $\Gamma = -0.5$. It is evident here, that the behaviour of $\dot{l}_{fields}$ and $\dot{l}_{obs}$ is again nearly identical, resulting in the overall conservation of $\dot{J}_{tot}$. We note again that there exist regions in Fig. 5.14 where $\dot{J}_{tot}$ is not conserved. In this particular system these regions correspond to the points when one of the skyrmions is reflected from the boundary and constitute another boundary effect.
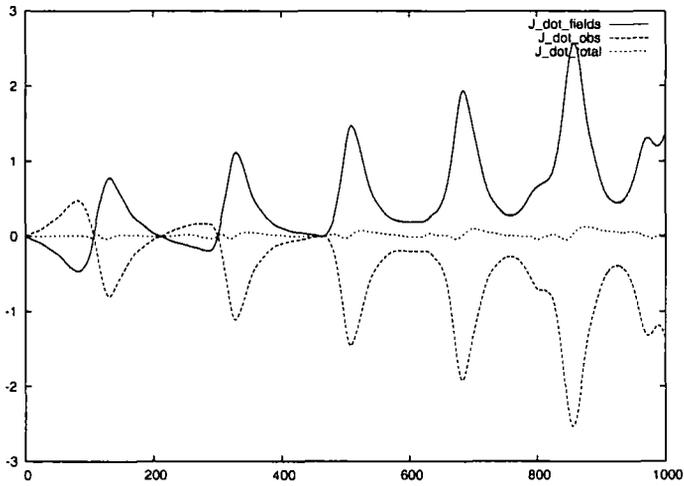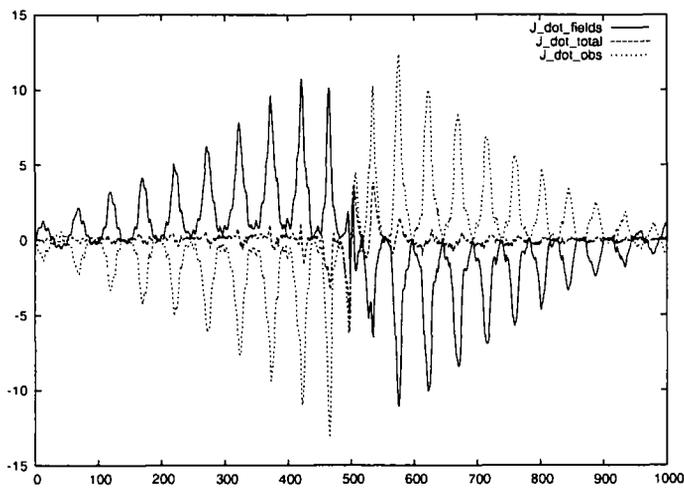
Figure 5.14: Plots of the time derivative of the total angular momentum, $\dot{J}_{tot}$ and its components $\dot{l}_{fields}$ and $\dot{l}_{obs}$ as a function of time for a two different systems: a) $d = 6$ skyrmion configuration with $b = 2$ for $\Gamma = 0.25$ and b) $d = 5$ skyrmion configuration with $b = 2$ for $\Gamma = -0.5$

5.3.3 Skyrmion oscillations

It was seen in the previous section that the total angular momentum, J_{tot}, for the asymmetric system is well conserved, just as it was for the symmetric system. There were regions where this conservation was temporarily destroyed and we have noted that such effects arise due to the skyrmions interaction with the boundary of the system. However for critical values of Γ and d, during the interaction of a skyrmion configuration with a potential hole, there exists regions where J_{tot} is not conserved. Here it shall be seen that the regions where $\dot{J}_{tot} \neq 0$ do not arise due to to boundary effects but are due to an important physical process.

Fig. 5.15a shows a plot of the different angular momentum components for a $d = 5.5$ skyrmion configuration interacting with a potential hole of width $b = 2$ and hole depth, $\Gamma = -0.3$. The plot shows the derivative of the total angular momentum due to the fields, $\dot{l}_{fields}$, given by time derivative of (1.28) and the negative of the contribution from the potential obstruction to the time derivative of orbital angular momentum, $-\dot{l}_{obs}$. Examining the plot, it is evident that there are many regions along the curve where $\dot{J}_{tot} = \dot{l}_{fields} + \dot{l}_{obs} \neq 0$. One such region has been expanded upon in Fig. 5.15b. Initially in the system $\dot{J}_{tot} = 0$. After some time $\dot{J}_{tot}$ starts to deviate from zero. The curves appreciably deviate for t=95 secs, this is denoted by the point P. The difference between the two curves and hence the magnitude to which $\dot{l}_{fields} + \dot{l}_{obs} \neq 0$, becomes larger with time. The difference continues to increase, yet around the point Q, t=495 secs, the curves re-converge for a small period of time. After this period of re-convergence, the two curves deviate once again. The difference between the two curves grows until they re-converge at the point R, t=865 secs. In the latter parts of the plot the curves are seen to match exactly. The time periods of the non-conservation of J_{tot} are approximately equal. We now wish to find the analogous points P,Q and R on the trajectories of the two skyrmions.

Fig. 5.16 shows a plot of $y(t)$ for the upper skyrmion and the variation in the distance of separation between the two skyrmions, $d(t)$. The points P, Q and R can be identified from these plots. The points P and R correspond to the times at which the upper skyrmion's centre has reached the upper and lower edges of the
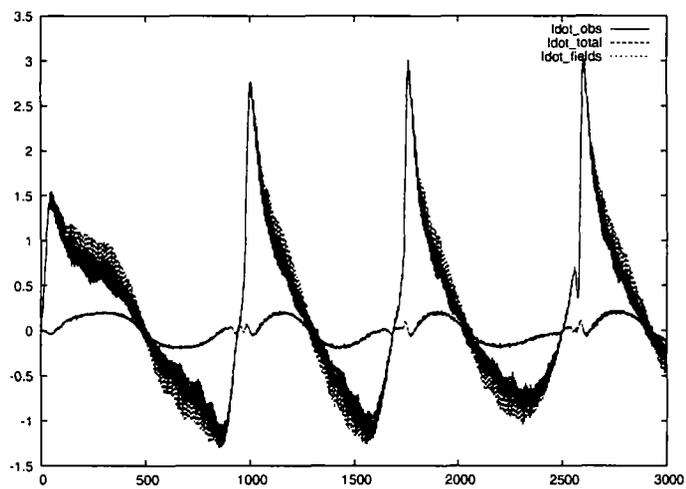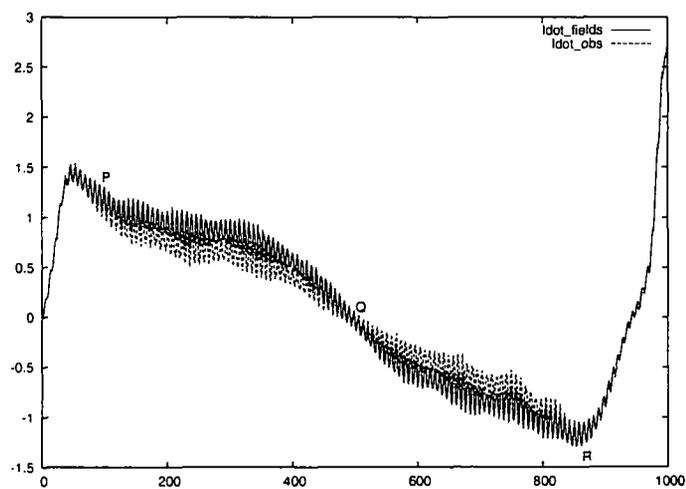
Figure 5.15: Plots of the time derivative of the total angular momentum, $\dot{J}_{tot}$ and its components $\dot{l}_{fields}$ and $-\dot{l}_{obs}$ as a function of time for a $d = 5.5$ skyrmion configuration, interacting with a potential hole with $b = 2$ for $\Gamma = -0.3$.
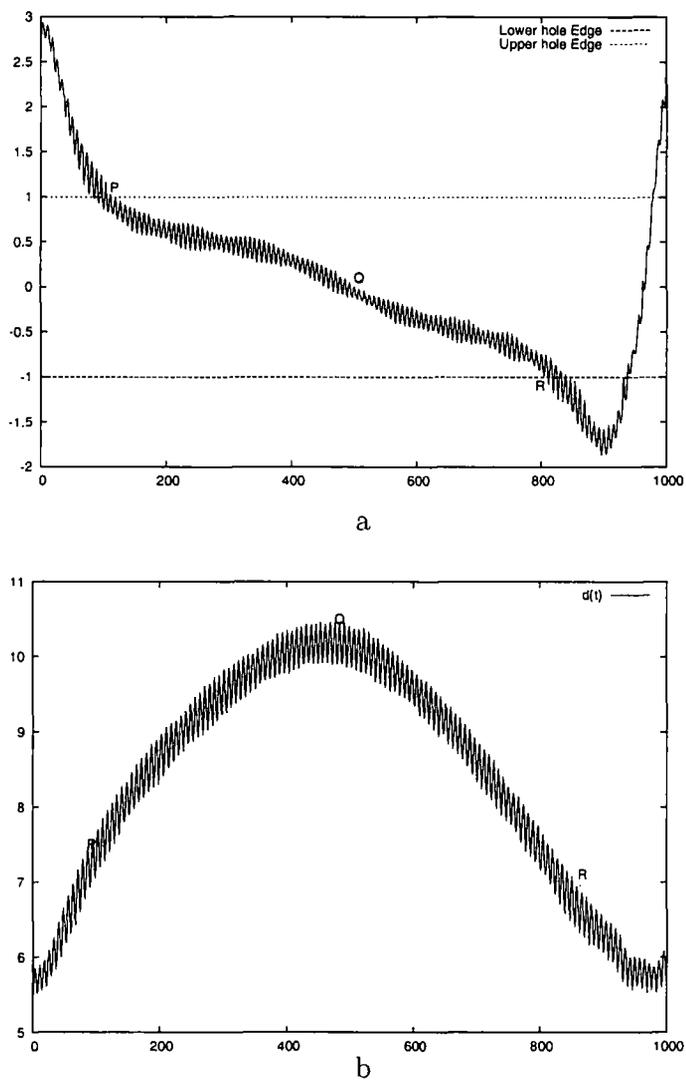
Figure 5.16: Plot $y(t)$ and $d(t)$ for the upper skyrmion in a system with an asymmetric potential hole of width $b = 2$ and $\Gamma = -0.3$.

hole. The plot of $d(t)$ illustrates that the region of maximal skyrmion separation corresponds to the region Q. We must therefore ask ourselves, what distinguishing features are present as the upper skyrmion approaches the hole, that are absent as the skyrmions have reached their peak distance of separation? To do this one needs to examine the simulation of the $d = 5.5, \Gamma = -0.3$ system on the accompanying Cd. In such a system one can see the skyrmions undergo small oscillations during their motion. The oscillations begin once the upper skyrmion's centre has entered the boundary of the the hole. The skyrmion's energy density is seen to slowly pulse up and down, with the stationary skyrmion exhibiting a rotational motion about its centre. Upon entering the hole, the skyrmion is seen to decrease and increase in height repeatedly during its transition through the hole. There exists a point in the hole where the oscillations in the skyrmion's energy density have ceased. As the skyrmion exists the hole the oscillations briefly halt. Due to the skyrmion interaction, the other skyrmion begins to penetrate the hole. It is at this point that the skyrmion's oscillations commence again. The points P and R correspond to the points at which the upper skyrmion has entered and exited the hole and thus when the oscillations have begun and ended. The region Q coincides with the time when the skyrmion has ceased to oscillate. There therefore appears to be a direct link between the non-conservation of angular momentum in these systems and the skyrmion oscillations.

There exists another example of these skyrmion oscillations. In the system of $d = 5.5$ and $\Gamma = -0.5$, the skyrmions also oscillate. The simulation of this system is also on the accompanying Cd. However, for this set of values, the oscillation is much more violent. Fig. 5.18 shows the plot of $\dot{J}_{tot}$ for these values of d and Γ. The trajectories of the skyrmions in this system are plotted in Fig. 5.17 over the period of time $t = 500 - 1000$ secs. This period corresponds to the same period in Fig. 5.18, when the large spike in $\dot{J}_{tot}$ is observed. The points P,Q and R of Fig. 5.18 can be found by examining Fig. 5.19, which show plots of $y(t)$ for both the upper and lower skyrmions. The locations of the upper and lower skyrmions for the points P,Q and R are shown on the trajectory in Fig. 5.17 and are given the subscript 1 and 2 to identify the upper and lower skyrmions respectively. During the periods
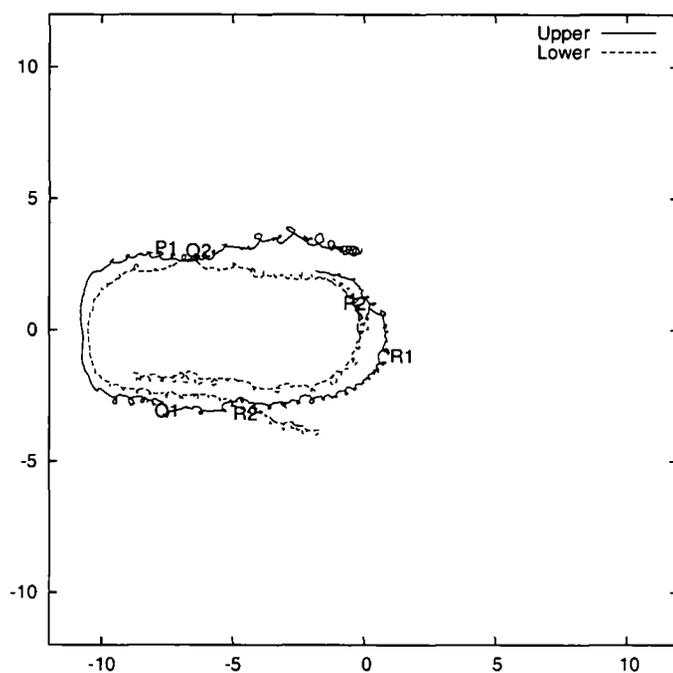
Figure 5.17: Trajectory of both skyrmions for a $d = 5.5$ configuration interacting with a potential hole of width $b = 2$ and depth $\Gamma = -0.5$, plotted over the time range $500 - 1000$, where the horizontal axis represents the x coordinate and the vertical axis the y coordinate.
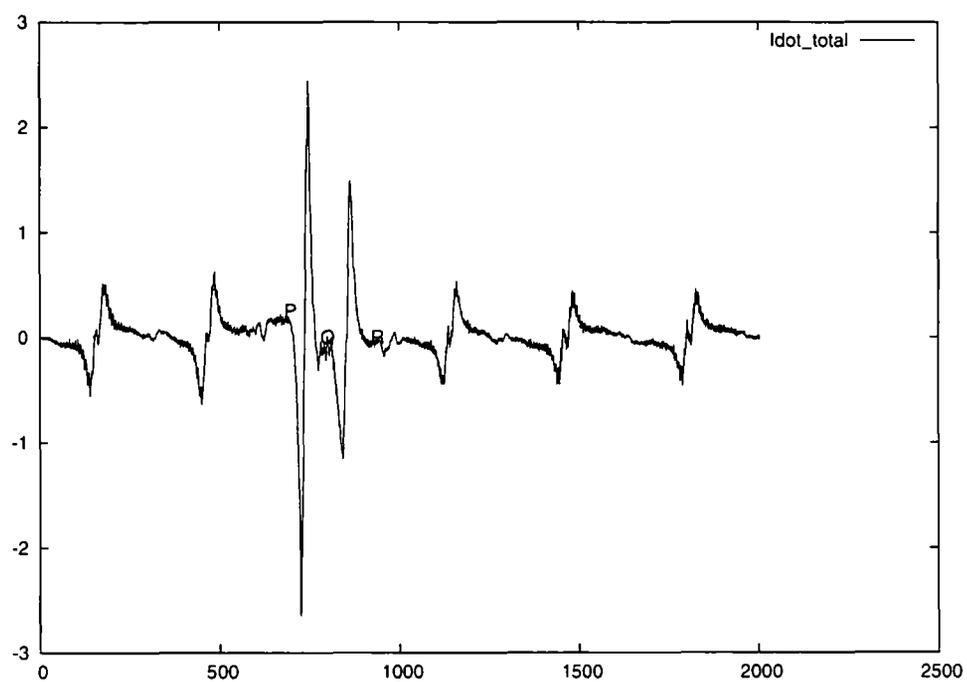
Figure 5.18: Plot of the derivative of the total angular momentum, $\dot{J}_{tot} = \dot{l}_{fields} + \dot{l}_{obs}$ for a $d = 5.5$ two-skyrmion configuration interacting with a potential hole of width $b = 2$ and $\Gamma = -0.5$.
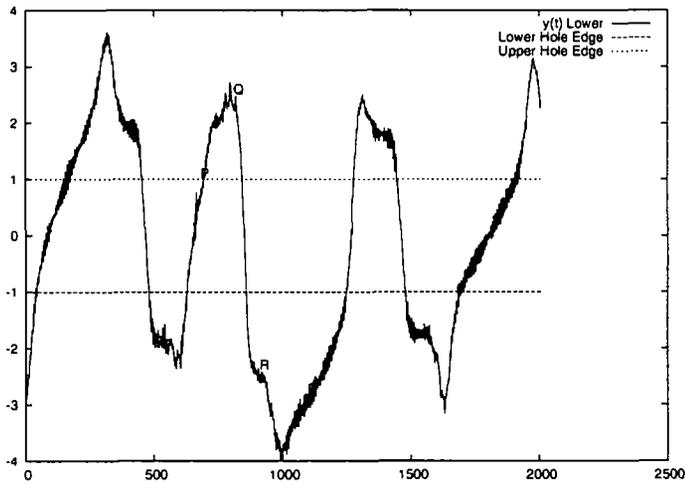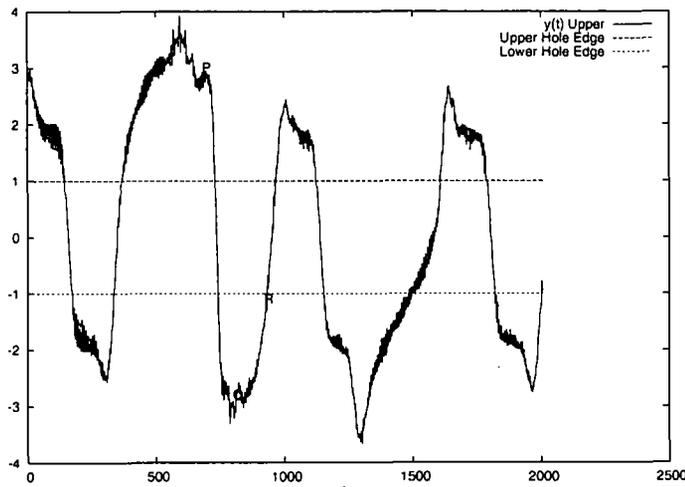
Figure 5.19: Plots of $y(t)$ for the upper (b) and lower (a) skyrmions in a system with an asymmetric potential hole of width $b = 2$ and $\Gamma = -0.5$.

of P-Q and Q-R, $\dot{J}_{tot}$ undergoes a rapid change. Over the same time length both the skyrmions have traversed the hole, firstly the upper skyrmion, s_1, and then the lower, s_2. In the path, P1-Q1, s_1 traverses the hole while s_2 starts to move along the edge of the hole. In the next path, Q1-R1, s_1 now moves along the lower edge of the hole and begins to execute circular motion after its interaction with s_2. The path Q2-R2 coincides with s_2 traversing the hole. In the simulation of this system, s_1 traverses the hole during the initial 500 secs. After s_1 traverses the hole for a second time, the skyrmions undergo a violent oscillation in their energy densities. Their energy densities dramatically pulse before the skyrmions continue with their motion around the edge of the hole. The first of these oscillations occur during the period P-Q and the skyrmions are subsequently seen to undergo another oscillation, during the period Q-R. The large change in the energy densities, causes the observed spike in Fig. 5.18. This second piece of data confirms the earlier observation relating the non-conservation of J_{tot} and skyrmion oscillations in Landau-Lifshitz models.

Chapter 6

Conclusions

Our studies have shown that the scattering of baby skyrmions in our model, off potential obstructions, for which the dynamics is governed by the Landau-Lifshitz equation, exhibits some non-trivial results. We have studied two different types of obstructions: a symmetric and an asymmetric obstruction. Both of the geometries of these obstructions have been defined in Chapters 4 and 5. The dynamics of each of the two systems is similar although for particular values of the hole depth and the skyrmion distance of separation, the two systems differ. There have been some notable discoveries during these simulations regarding the binding energy between the two skyrmions and its dependence upon the potential obstructions' size and depth. The conservation laws of the system were well observed as expected but the angular momentum as defined by Papanicolaou and Tomaras, required some modification in order for it to be conserved with time.

In the symmetric system it has been possible to effectively understand the observed scattering properties of our skyrmions, despite their seemingly non-intuitive behavior. In the case of a potential hole the skyrmions, initially placed at the points $(0, \pm d/2)$, were unable to penetrate the hole and so moved parallel to the 'x'-axis at a distance y_{max}^s from the hole. The energy considerations have shown that the skyrmions, in systems involving a potential hole, became unbound as they approached the hole and so could and did move away from each other. In the barrier systems the skyrmions were able to traverse the barrier. Our simulations have shown that as the skyrmions traversed the barrier their distance of separa-

tion d decreased to overcome this increase in potential energy. At the same time the skyrmions sped up as they climbed the barrier. The transition dynamics have shown that there exists a threshold value of binding energy in the barrier systems $E_B \simeq -0.05/8\pi$. By comparison, in the absence of any potential obstructions, the binding energy of the two skyrmions is $E_B = -0.11/8\pi$. Therefore this threshold binding energy is roughly half the binding energy, if there is no barrier. Above this value the skyrmions behave as a bound state and below this value they can separate from each other. Our intuition and reasoning has led us to the conclusion that the tail-tail interaction between the skyrmions is reduced due to the attenuation of the skyrmion tail by the barrier.

In the asymmetric barrier system the skyrmions behave similarly to the skyrmions observed in the symmetric barrier system. The bound skyrmions perform the normal circular motion about the configuration centre moving on and off the barrier during their evolution. The distance of separation of the skyrmions increases and decreases with time. The maximum separation between the two skyrmions corresponds to the times when one or both of the skyrmions is off the obstruction. The minimum separation corresponds to times when both the skyrmions are interacting appreciably with the barrier. This change in the distance of separation between the skyrmions results in the distortion of their path as they traverse the obstruction. In this same system the skyrmions are able to move into the upper and lower semi-planes. In the symmetric system they could not do this due to the obstruction existing over the whole x range. When the skyrmions have moved away from the obstruction they orbit the boundary of the system. It was noted that this phase of the dynamics is uniquely determined by the boundary of the system. If the skyrmions are placed in an identical system, with a larger grid, after initially executing similar trajectories as the skyrmions for the system of a smaller grid, the skyrmions move in a near identical motion about the boundary of the system, except they are further from the obstruction than the skyrmions of a smaller grid. The binding energy in the barrier system also plays an important role. The bound state formed by two skyrmions can be broken by a potential barrier. The breaking point in the asymmetric system is much more difficult to observe than in the symmetric system. In the symmetric sys-

tem the geometry of the potential obstructions uniquely determines the trajectories of the unbound skyrmions. The unbound skyrmions in the asymmetric system move almost independently of each other about the system. Periodically the skyrmions, when they are close enough to interact due to the confinement of the boundary, execute circular motion about their centre.

In the system of a potential hole the skyrmions behave completely differently from the skyrmions observed in the symmetric system. Here the binding energy plays a crucial role in categorising the different phases of the dynamics; bound, unbound or in between the two. The skyrmions, for tightly bound configurations, orbit each other as they traverse the edge of the hole. These bound states occur for small distances of separation and hole depth. As the hole depth or the distance of separation increases, the binding energy of the skyrmions increases. However, as the skyrmions approach the point at which the bound state is broken, the dynamics of the skyrmion configuration changes. The skyrmions in these 'in between states' are able to penetrate the hole. They behave as bound skyrmions in the sense that their trajectory could be described as a very distorted circular path but they behave as unbound skyrmions since they separate appreciably during the simulation. In a potential hole system, as was noted in the analysis on the symmetric system, the binding energy becomes a dynamic quantity. As the skyrmions approach the hole the binding energy or the interaction energy between the skyrmions, changes. The skyrmions are extended objects. When one of the skyrmions approaches the hole, the energy of the skyrmion decreases due to the tail interactions with the hole. Due to the asymmetry of the system, one of the skyrmions can feel the effect of the hole more than the other. Energy conservation allows the skyrmions to separate. The more a skyrmion approaches the hole the more they can separate and thus the skyrmion bound state is broken by the potential hole. This process is sensitive to the hole depth, Γ. In the transition state dynamics, $d = 5.5$, increasing the value of Γ results in a complete change in the behaviour of the skyrmions. This is largely due to the binding energy as the skyrmion initially approaches the hole. In the case of large values of Γ, the skyrmions are unbound when they are further from the hole and begin to execute dynamics reminiscent of the skyrmions for a symmetric potential

hole. When Γ is slightly smaller, due to E_B, the skyrmion is able to penetrate the hole and there is still an appreciable interaction with the other skyrmion. This allows the skyrmion to escape the hole and a pseudo-bound state behaviour to resume. Our examination of the dynamic behaviour of the binding energy led us to a reasonably accurate estimate for the closest initial distance of approach of the upper skyrmion during the transition dynamics. We thus believe that the subsequent analysis regarding the binding energy and the skyrmions' dynamics dependence upon it, is a valid and a good representation of the details of these complicated systems.

The system of unbound skyrmions in the potential hole system also shows some unusual properties, some of which were seen in the transition dynamics. The unbound skyrmions occur for large values of the distance of skyrmion separation and large hole depths. The skyrmions of these system behave, as was alluded to previously, similarly to the skyrmions in the symmetric potential hole system where both skyrmions moved along the axis of the hole. Here, due to geometry of the hole, only one of the skyrmions moves along the edge of the hole, while the other, after the initial motion, comes to rest. During the initial period of separation both of the skyrmions' energy densities are seen to oscillate. This oscillation continues until the skyrmions reach a critical distance of separation, where it ceases. These oscillations surface again after the skyrmion is reflected from the boundary, when it has reached another critical distance from the stationary skyrmion. These oscillations are rather peculiar and the only other system to bear such oscillations is the transition dynamics. In the transition dynamics for $\Gamma = -0.4$ and -0.5, the skyrmions' energy densities undergo violent oscillations. These oscillations are the result of the excitation of one or more of the internal modes of the skyrmions due to the energetics during the skyrmion separation. We would expect that any of the excited modes would be of the lowest order. Piette et al [27] have previously undertaken an analysis of the excited modes of the skyrmions of the new baby skyrme model, in the fully relativistic system. In [27] the modes of a single skyrmion and a two-skyrmion configuration during a scattering process were analysed. It would be interesting to see how the excited modes of the skyrmions observed in our simulations compare with the excited modes seen in their work.

One of the most interesting observations of our simulations was the apparent non-conservation of the total angular momentum J (given its usual definition). This non-conservation of J was due to the non-conservation of the orbital angular momentum, l, as we have found that in all of the simulations the total magnetization in the third direction, m, was well conserved in time. At the same time we showed that $\dot{l} \neq 0$. Thinking about this further we showed that when a system involves potential obstructions, these obstructions made a significant contribution to $\dot{l}$. Hence one has to modify the conventional definition of l. We have found and calculated this missing contribution. In all of the simulations of the skyrmions in both the symmetric and asymmetric systems we have shown that its change compensates $\dot{l}$. This results in the overall conservation of l and J for the full system. However, there were a few systems studied that didn't adhere to the above statement. In the transition dynamics in the asymmetric system, there were regions where the angular momentum due to the fields, $\dot{l}_{fields}$, and the angular momentum due to the obstruction, $\dot{l}_{obs}$, did not sufficiently cancel each other out, in order for total angular momentum conservation. However, when comparing the size for which $\dot{J} \neq 0$ in such regions, with the total angular momentum as a whole, these regions of non-conservation are brief and the magnitude in most of the cases is small. In some systems, where the non-conservation of J was larger, we noted that this was due to boundary effects.

An examination of the times when there was an appreciable discrepancy in $\dot{l}_{fields} + \dot{l}_{obs} \neq 0$, provided a direct link between the skyrmion oscillations and the non-conservation of J. Initially J is well conserved but as the oscillations begin to increase this conservation is destroyed. There reaches a point when the J conservation is restored. It is at these points that the skyrmion oscillations have ceased. In many of the cases these oscillations reappear again and again during the skyrmions dynamics and each time the conservation of J is destroyed. The size of the oscillation and the magnitude to which $\dot{J} \neq 0$ are also correlated. In the transition dynamics the large spike observed in the $\Gamma = -0.5$ plot of $\dot{l}_{fields} + \dot{l}_{obs}$ system corresponds to the violent oscillation during the dynamics of the skyrmions. Conversely in the system with $\Gamma = -0.3$ smaller oscillation are apparent in that system, resulting in a smaller spike in $\dot{l}_{fields} + \dot{l}_{obs}$. The regions where $\dot{J}_{tot} \neq 0$ suggest that the inclusion of

an additional term is required for the overall exact conservation of the total angular momentum, J, for skyrmion scattering in a Landau-Lifshitz model. Any term or terms that are included must have a direct correspondence with the oscillations of the skyrmions observed in these systems.

6.1 Discussion and final thoughts

We believe that most of the results presented here form a generic basis for the description of the scattering of baby skyrmion configurations in Landau-Lifshitz models. This is primarily due to the conservation laws of the Landau-Lifshitz model, as constructed by Papanicolaou and Tomaras [26] and the observation that the potential obstructions contribute to the conservation laws of the system. There is also the important detail that the skyrmion configurations used throughout the work are those set up in the attractive channel. This has been an important detail since the majority of our energetic arguments have centred upon this fact. Here I would like to discuss some modifications we could have made in our work and avenues for further research.

The skyrmions used in all of these simulations were, as previously stated, initially constructed in the attractive channel. This means that for reasonable distances of separation the skyrmions form a bound state. The binding energy, or interaction energy, between the two skyrmions becomes modified when the potential obstructions are introduced into the system. Therefore, we believe that these simulations show generically what happens when a bound state interacts with a potential obstruction in a Landau-Lifshitz model. Thus we believe that an attractive configuration will behave in the same manner as the skyrmions have done in this system. The only times when one could anticipate something different to happen are when two skyrmions get close enough to sufficiently overlap. In Chapter 2 we discussed the various different baby Skyrme models. In two of the models, the old and new baby Skyrme model, the skyrmions possess exponential localisation, whereas in the holomorphic model they only have polynomial localisation. All of the skyrmions undergo 90° scattering when sent at a sufficiently high velocity towards each other. However,

the behaviour of the skyrmions at short distances and low velocities is largely different. It was seen that the skyrmions of the holomorphic model do not form bound states. In the work of [29] a two-skyrmion configuration was constructed based upon the known analytic solution to the holomorphic model. When this model was used as an initial condition for a Landau-Lifshitz model it was seen that the skyrmions orbited on deformed circular trajectories. In the paper the authors also calculated the interaction energy between the two skyrmions and saw that for all distances of separation the force was repulsive. Thus if this skyrmion configuration was used as an initial condition in one of our simulations, with either a symmetric or an asymmetric potential obstruction, what would be seen to happen? We may expect the skyrmions in the barrier system, if they are able to traverse the barrier, to separate from each other as they traverse it. In the hole system the repulsive force may allow the skyrmions to traverse the hole, unlike skyrmions in the attractive channel. In the case of the old baby skyrme model the skyrmions can form bound states. However, it was noted that the skyrmions do not like to be on top of each other and so are repulsive at short distances. This skyrme model is in between the new baby skyrme model we have been investigating and the holomorphic model: attractive for large distances but repulsive when they are close together. The balance between these forces as the skyrmions interact with the potential obstructions would be difficult to predict. These different systems would present interesting problems to be studied, since the interplay between the attractive channel and repulsive points should provide some interesting results.

Instead of investigating the dynamics of skyrmions of a different baby Skyrme model in the Landau-Lifshitz system, with the same potential obstructions, one could also investigate new and more complicated versions of the system we have already examined. We could easily conceive constructing a system which involved multiple holes or barriers for different sizes and differing geometries. We could also construct a system with holes and barrier in it. The binding energy of the skyrmion configurations in any of these systems is modified by the presence of a potential obstruction. Therefore the effect of the obstructions, which modify the binding energy in different ways, would present a fascinating problem. The Landau-Lifshitz

model is an idealised version of the continuum limit of the classical spin model for a ferromagnetic system. In a more realistic system there exists the Landau-Lifshitz-Gilbert equation, which includes the effect of dissipation in the system. Introducing such dissipation into our system would dramatically change the freedom of the skyrmions during the evolution. The dissipation would provide a more difficult problem to solve, although it could potentially provide more realistic results for those interested in the correlations between baby skyrmions and the experimentally observable magnetic bubbles.

Bibliography

[1] J. Al-Alawi and W. Zakrzewski 2007, Q-ball scattering on barriers and holes in one or two dimensions, arxiv: 0902.4358

[2] J. Al-Alawi and W. Zakrzewski 2008, Scattering of topological solitons on barriers and holes in deformed sine-Gordon models, *J. Phys. A* **41** 315206.

[3] J. Al-Alawi and W. Zakrzewski 2007, Scattering of topological solitons on barriers and holes in two $\lambda\phi^4$ models, *J. Phys. A* **40** 11319-11332.

[4] A. Bobeck and Della Torre 1975, *Magnetic bubbles* (Selected topics in Solid State Physics, North-Holland publishing company).

[5] J.Brand, B.Piette and W.Zakrzewski 2005, Scattering of topological solitons on holes and barriers, *J. Phys. A* **38**, 10403-10412.

[6] S. Coleman 1985, Q balls, *Nuc. Phys. B* **262**, 263.

[7] J. Collins and W. Zakrzewski 2009, Scattering of a two skyrmion configuration on potential holes or barriers in model Landau-Lifshitz equation, *J. Phys. A* **42** 165102.

[8] G.H. Derrick 1964, Comments on nonlinear wave equations as models for elementary particles, *J.Maths.Phys* **5** 1252.

[9] P. Eslami, M. Sarbishaei and W. Zakrzewski 2000, Baby Skyrme models for a class of potentials, *Nonlinearity* **13** 1867-1881.

[10] D. Foster 2009, Baby Skyrmion chains, arXiv:0904.3846v1

115

[11] D. Foster and P. Sutcliffe 2009, Baby Skyrmions stabilised by vector mesons, arXiv:0901.3622v1.

[12] C. Gerald and P. Wheatly, *Applied Numerical Analysis* 3rd Ed. Addison-Wesley Publishing Company.

[13] N. Hitchin, G. Segal and R. Ward 1999, *Integrable Systems* Oxford Science Publications.

[14] A. Kudryavtsev, B.Piette, and W.Zakrzewski 1998, Skyrmions and domain walls in (2+1) dimensions, *Nonlinearity* **11**, 783-795.

[15] S. Komineas and N. Papanicolaou 1998, Vortex dynamics in 2D anti-ferromagnet, *Nonlinearity* **11** 265.

[16] S. Komineas and N. Papanicolaou 1998, Topology and dynamics in ferromagnetic media, *Physica D* **99** 81-107.

[17] F. de Leeuw 1980, R van den Doel and U. Enz, Dynamic properties of magnetic domain walls and magnetic bubbles,

Rep. Prog. Phys. **vol 43**.

[18] R. Leese 1991, Q-lumps and their interactions, *Nuc. Phys. B* **366**, 283-311.

[19] R. Leese, M. Peyrard and W.Zakrzewski 1990, Soliton stability in the $O(3)\sigma$-model in (2+1) dimensions, *Nonlinearity* **3**, 387-412.

[20] R.A. Leese, M. Peyrard and W.Zakrzewski 1990, Soliton scatterings in some relativistic models in (2+1) dimensions, *Nonlinearity* **3**, 773-807.

[21] N. Manton and P. Sutcliffe 2004, *Topological Solitons* Cambridge University Press.

[22] O'Dell T 1974 *Magnetic bubbles* (The Macmillan Press Ltd.).

[23] R. Palais 1979, The principle of symmetric criticality, *Commun. Math. Phys.* **69** 19.

[24] B.Piette, B. Schroers and W. Zakrzewski 1995, Multi-solitons in a two-dimensional Skyrme model, *Zeitschrift feur Physik C* **65**, 165.

[25] B.Piette, B. Schroers and W.Zakrzewski 1995, Dynamics of baby Skyrmions, *Nuc. Phys. B* **439**, 205-235.

[26] N. Papanicolaou and T. Tomaras 1991, Dynamics of magnetic vortices, *Nuc. Phys. B* **360** 425-462.

[27] B. Piette and R. Ward 2005, Planar skyrmions: vibrational modes and dynamics, *Physica D* **201**, 45-55.

[28] B.Piette and W.Zakrzewski 1998, Numerical integration of (2+1) dimensional PDEs for S^2 valued functions, *J. Comp. Phys.* **145**, 359-381.

[29] N. Papanicolaou and W. Zakrzewski 1996, Dynamics of magnetic bubbles in skyrme model, *Phys.Lett. A* **210** 328-336.

[30] N. Papanicolaou and W. Zakrzewski 1995, Dynamics of interacting magnetic vortices in a model Landau-Lifshitz equation, *Physica D* **80** 225-245.

[31] R. Rajaraman 1982, *Solitons and Instantons* North-Holland Publishing.

[32] T. Skyrme 1961, A non-linear field theory, *Proc. R. Soc. Lond. A* **260** 127.

[33] J.M. Speight 2006, Sigma models on curved space and bubble refraction in doped anti-ferromagnets, *Nonlinearity* **19** 1565-1579.

[34] P. Sutcliffe 1991, The interaction of Skyrme-like lumps in (2+1) dimensions, *Nonlinearity* **4** 1109-1121.

[35] T. Weidig 1999, The baby Skyrme models and their multi-skyrmions, *Nonlinearity* **12** 1489-1503.

[36] Y. Yang 2001, *Solitons in Field Theory and Nonlinear Analysis* Springer.

Appendix A

Simulations

In this section the details of the simulations submitted along with this thesis are given. The simulations were created using open dx by piecing together snapshots of the energy density at particular time intervals. The time interval used is varied depending upon the system investigated. The length of the simulation also varies from system to system. In most of the simulations the points of interest happen over a smaller time frame than others. There are certain systems that were run for much longer times in order to aid a better understanding. It is recommended that these simulations are viewed using VLC media player. This is because VLC has a facility which allows you to reduce the speed of the simulations and therefore obtain a better view of the processes occurring during the simulations.

The following table lists the different files according to the type of obstruction and shows their respective time intervals and the length of the simulation.

Type of obstruction	d	Γ	b	Simulation length in secs	Time Interval
none	6	0	0	850	10
symm	6	+0.25	2	850	10
symm	6	-0.25	2	850	10
asymm	6	+0.25	2	5000	10
asymm	6	+1.5	2	1500	5
asymm	4	-0.5	2	100	5
asymm	5.5	-0.3	2	3000	10
asymm	5.5	-0.5	2	1500	10
asymm	6	-0.25	2	2000	10